Ph.D. Thesis

Effective Hamiltonian theory of anomalous optical responses induced by spin-orbit interaction

スピン軌道相互作用による特異な光学応答現象の有効理論（英文）

Hideo Kawaguchi
川口　秀雄

Department of Physics,
Graduate Scool of Science and Engineering,
Tokyo Metropolitan University
首都大学東京大学院　理工学研究科　物理学専攻

2018

Abstract

Spin-orbit interaction arising from the breaking of spatial-inversion symmetry induces electromagnetic cross-correlation effects, resulting in anomalous optical responses. In present Thesis, we theoretically study anomalous light propagation induced by cross-correlation effects in spin-orbit systems by effective Hamiltonian approach based on a microscopic ground.

First, we investigate nonreciprocal directional dichroism in the magnetic Rashba conductor by deriving an effective Hamiltonian based on an imaginary-time path-integral formalism. We show that the effective Hamiltonian representing the directional dichroism in the magnetic Rashba conductor is written in terms of toroidal and quadrupole moments as in insulator multiferroics. The toroidal-moment term consists of the vector coupling between toroidal moment and Poynting vector, resulting in the directional dichroism irrespective of the light polarization due to the Doppler shift. We also see that the quadrupole-moment term also induces directional dichroism for linearly-polarized waves. Furthermore, we discuss difference between optical responses of magnetic Rashba conductor and that of 3+1 dimensional Weyl semimetal in context of the effective Hamiltonian.

Next, we examine optical properties of a Weyl spin-orbit system having quadratic dispersion by deriving an effective Hamiltonian of electromagnetic fields. We demonstrate that an optical chirality order parameter introduced by Lipkin appears in the effective Hamiltonian, and that the optical chirality order parameter indeed leads to natural optical activity from the viewpoint of the effective Hamiltonian.

Contents

List of Figures

Chapter 1

Introduction

First of all, we briefly introduce electromagnetic cross-correlation effects and optical responses in spin-orbit systems without spatially-inversion symmetry in Chapter 1. Especially, we focus on effects of Rashba spin-orbit interaction and that of Weyl spin-orbit interaction in medium. We summarize the organization of this Thesis in the last section.

1.1 Electromagnetism and spintronics

Lows of electromagnetism that couple electricity to magnetism were discovered by James Clerk Maxwell and Michael Faraday about 150 years ago [1]. Conversion between electric signals and magnetic information plays an important role in the development of currently available information technologies from that time on. Such conversions were first performed using classical laws of electromagnetism, such as Faraday's law and Ampére's law as shown below.

$$\boldsymbol{\nabla} \times \boldsymbol{E} = -\frac{\partial \boldsymbol{B}}{\partial t}, \tag{1.1}$$

$$\boldsymbol{\nabla} \times \boldsymbol{B} = \mu_0 \boldsymbol{j} + \mu_0 \epsilon_0 \frac{\partial \boldsymbol{E}}{\partial t}, \tag{1.2}$$

where $\boldsymbol{E}$ and $\boldsymbol{B}$ are electric and magnetic fields, respectively. Here, $\boldsymbol{j}$ is the charge-current density, and ϵ_0 and μ_0 are the electric permittivity and magnetic permeability of the vacuum, respectively. In magnetic devices such as a cassette tape and a hard disk drive, Faraday's law, Eq. (1.1), was used to read out information while Ampére's law, Eq. (1.2), is applied to write in information by magnetization flip [2].

However, these classical mechanisms have not been able to sufficiently meet the recent technological requirements of fast processing of large amounts of information and high-density storage; hence, they have been gradually replaced by solid-state mechanisms such as spin-transfer torque [3, 4]. The interaction Hamiltonian describing the spin-transfer effect in magnets is

$$H_{\rm st} = \int \mathrm{d}^3 r \frac{\hbar P}{2e}(1 - \cos\theta)(\boldsymbol{j} \cdot \nabla)\phi, \tag{1.3}$$

where θ and ϕ are the polar coordinates representing the direction of a magnetization, P is the spin polarization of conduction electrons, $\hbar$ is the Planck constant divided by 2π, and e is the electron charge. Spin-transfer torque induced by an applied electric current in ferromagnetic metals is a crucially important effect in the context of current-induced magnetization reversal in spintronics. In fact, we see that the spin torque by the electric current, $\boldsymbol{\tau}_{\rm st} \equiv -\frac{\delta H_{\rm st}}{\delta \boldsymbol{n}} = -\frac{P}{2e}(\boldsymbol{j}\cdot\boldsymbol{\nabla})\boldsymbol{n}$, acts on a magnetization, where $\boldsymbol{n}$ is a unit vector representing the direction of the magnetization; hence the magnetization reversal can be induced by the spin-polarized electric current (spin current) described as $\boldsymbol{j}_{\rm s} \equiv P\boldsymbol{j}$. The idea of the spin-transfer effect was first proposed theoretically by Berger [5] in the case of a domain wall motion and by Slonczewski [3] and Berger [4] in the case of the uniform magnetization of thin films. The spin-transfer effect arises from the transfer of spin angular momentum from conduction electrons to localized spins which induce the magnetization. The effect is caused by an *sd* exchange interaction, and the angular momentum transfer occurs owing to the angular momentum conservation [3].

In resent years, the effect arising from spin-orbit interaction attracts the interest of researchers in this context. One example is the magnetization reversal using an effective magnetic field induced by a spin-orbit interaction, called Rashba interaction (Ref. [6]). In the case of a strong *sd* interaction, i.e., adiabatic limit, the interaction describing the magnetization reversal is given by [7–10]

$$H_{\rm st,R} = -\int {\rm d}^3 r (\boldsymbol{B}_{\rm eff,R}\cdot\boldsymbol{n}), \tag{1.4}$$

with

$$\boldsymbol{B}_{\rm eff,R} \equiv \frac{m}{e\hbar}(\boldsymbol{\alpha}_{\rm R}\times\boldsymbol{j}_{\rm s}), \tag{1.5}$$

where m is electron mass and $\boldsymbol{\alpha}_{\rm R}$ is the Rashba field along z-axis representing the strength of the Rashba interaction. It was reported that the effective magnetic field induced by the Rashba interaction such as Eq. (1.5) plays a key role in pining for domain wall motion under the electric current [11]. Refs. [12, 13] have been argued optical magnetization reversal induced by inverse Faraday effect, which is a nonlinear effect with respect to an incident electric field in the presence of the Rashba interaction.

1.2 Spin-orbit interaction

Spin-orbit interaction, which couples the orbital motion of an electron to its spin via a relativistic effect, plays an important role in the context of a mixing of electric and magnetic degrees of freedom. Originally, spin-orbit interaction is derived directly from the Dirac equation as a relativistic effect [14]. Under the effect of electromagnetic fields, the Dirac equation is given by

$$\left[\sum_{\mu}\gamma^{\mu}\left(i\frac{\partial}{\partial x_{\mu}} - \frac{q}{c}A_{\mu}\right) - mc\right]\psi = 0, \tag{1.6}$$

where we set $\hbar = 1$, γ^μ is gamma matrices, c is light speed, m is rest mass of Dirac electron, q is the charge of Dirac electron, and ψ is the Dirac field having 4-components. Here, $A_\mu \equiv (\phi, \boldsymbol{A})$ is a gauge field being 4-vector whose time component is a scalar potential and whose spatial component is a vector potential. Using the 4×4 matrices, $\alpha^i \equiv \gamma^0\gamma^i$ and $\beta \equiv \gamma^0$, Eq. (1.6) reads

$$i\frac{\partial}{\partial t}\psi = \mathcal{H}_{\rm Dirac}\psi, \tag{1.7}$$

with

$$\mathcal{H}_{\rm Dirac} \equiv \left[c\boldsymbol{\alpha}\cdot\left(\boldsymbol{p} - \frac{q}{c}\boldsymbol{A}\right) + mc^2\beta + q\phi\right], \tag{1.8}$$

where $\boldsymbol{p} \equiv -i\boldsymbol{\nabla}$ is a linear momentum of Dirac electron and $\mathcal{H}_{\rm Dirac}$ is the Dirac Hamiltonian being 4 ×4. In non-relativistic limit, Eq. (1.8) up to the second order in $\boldsymbol{p}$ reduces to the 2×2 Hamiltonian such as

$$\mathcal{H} \simeq \frac{\boldsymbol{p}^2}{2m} - q\phi - \frac{q}{2mc}(\boldsymbol{B}\cdot\boldsymbol{\sigma}) - \frac{q}{16m^2c^2}(\boldsymbol{\nabla}\cdot\boldsymbol{E}) + \mathcal{H}_{\rm SOI}, \tag{1.9}$$

with

$$\mathcal{H}_{\rm SOI} \equiv -\lambda_{\rm so}\boldsymbol{E}\cdot(\boldsymbol{p}\times\boldsymbol{\sigma}), \tag{1.10}$$

where $\boldsymbol{\sigma}$ is the vector of Pauli matrices, $\lambda_{\rm so} \equiv \frac{q}{4m^2c^2}$ and $\boldsymbol{E} \equiv -\boldsymbol{\nabla}\phi$ and $\boldsymbol{B} \equiv \boldsymbol{\nabla}\times\boldsymbol{A}$ are electric and magnetic fields, respectively. In Eq. (1.9), the first term is kinetic energy of the charged particle. The second term is the interaction between the particle charge and the scalar potential. The third term is Zeeman interaction describing the coupling between the magnetic field and the particle's spin. The fourth term is called Darwin term. The term $\mathcal{H}_{\rm SOI}$ is spin-orbit interaction that couples particle motion to it's spin and $\lambda_{\rm so}$ is the coupling constant of the spin-orbit interaction in vacuum.

1.3 Electromagnetic cross-correlation effect induced by Rashba spin-orbit interaction

Recent studies have shown that spin-orbit interaction becomes prominent for surfaces and interfaces containing heavy metals as it significantly modifies their electric and magnetic properties as a consequence of inversion symmetry breaking [15]. The most typical spin-orbit interaction lacking inversion symmetry is the Rashba interaction [6], whose Hamiltonian is as shown below.

$$\mathcal{H}_{\rm R} = -\boldsymbol{\alpha}_{\rm R}\cdot(\boldsymbol{p}\times\boldsymbol{\sigma}), \tag{1.11}$$

where $\boldsymbol{p}$ is a linear momentum of electron, $\boldsymbol{\sigma}$ is the vector of Pauli matrices, and $\boldsymbol{\alpha}_{\rm R}$ is the Rashba field representing the strength and direction of the Rashba spin-orbit interaction. This form of interaction is derived directly from the Dirac

equation as a relativistic effect as was shown in section 1.2, but its magnitude can be significantly enhanced for solids containing heavy elements as compared to that for the vacuum case.

Of particular current interest is electromagnetic effects induced by such strong spin-orbit interaction because the effects are qualitatively different from conventional electromagnetic responses like in Ohm's law and Curie's law as shown below.

$$\begin{aligned} \boldsymbol{j} =& \sigma_{\mathrm{B}} \boldsymbol{E}, \\ \boldsymbol{M} =& \chi \boldsymbol{B}, \end{aligned} \tag{1.12}$$

where $\boldsymbol{j}$ is an electric current, $\boldsymbol{M}$ is a magnetization, σ_{B} is the Boltzmann conductivity, and χ is the magnetic susceptibility. A direct consequence of the Rashba interaction is electromagnetic cross-correlation effects where a magnetization and an electric current are induced by external electric and magnetic fields, $\boldsymbol{E}$ and $\boldsymbol{B}$, as

$$\boldsymbol{M}_{\mathrm{E}} = \gamma_{ME}(\boldsymbol{\alpha}_{\mathrm{R}} \times \boldsymbol{E}), \tag{1.13}$$

$$\boldsymbol{j}_{\mathrm{IE}} = \gamma_{jB}(\boldsymbol{\alpha}_{\mathrm{R}} \times \boldsymbol{B}), \tag{1.14}$$

where γ_{ME} and γ_{jB} are coefficients that generally depend on frequency. The Rashba field induces a tangential electron spin texture on Fermi surface depicted in Fig. 1.1, resulting in effects described by Eqs. (1.13) and (1.14). The emergence of spin accumulation from the applied electric field, mentioned in Ref. [6], was studied in detail by Edelstein [17]; hence, this effect is sometimes referred to as the Edelstein effect. Experimentally, the magnetization by Edelstein effect is observed using Kerr effect at interface between Cu, Ag and Bismuth oxide [18]. The generation of electric current by a magnetic field or magnetization, called the inverse Edelstein effect [19], was recently observed in a multilayer structure consisting of Ag, Bi, and a ferromagnet [20]. In Appendixes A.1 and A.2, we confirm that the the Edelstein and inverse Edelstein effects arise from the spin polarization induced by Rashba interaction through the microscopic calculation in the long-wave region [21, 22].

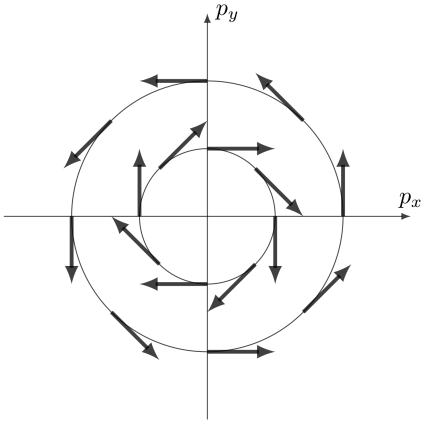

Figure 1.1: Schematic illustration of the electron spin configuration on Fermi surface induced by the Rashba interaction. Black arrows denote the direction of the electron spin. The tangential spin configuration was optically detected in bulk Rashba conductor such as BeTeI [16].

1.4 Optical responses in Rashba conductor

1.4.1 Birefringence and softening of plasma frequency in non-magnetic Rashba conductor

Recent studies (Refs. [21, 22]) showed that the cross-correlation effects of the Rashba spin-orbit interaction lead to anomalous optical properties in bulk Rashba conductor. From Eqs. (1.13), we obtain a magnetization current induced by the Edelstein effect as

$$\begin{aligned} \boldsymbol{j}_{\mathrm{E}} &\equiv \boldsymbol{\nabla} \times \boldsymbol{M}_{\mathrm{E}} \\ &= i\gamma_{ME}[(\boldsymbol{\alpha}_{\mathrm{R}} \cdot \boldsymbol{k})\boldsymbol{E} - (\boldsymbol{k} \cdot \boldsymbol{E})\boldsymbol{\alpha}_{\mathrm{R}}], \end{aligned} \tag{1.15}$$

where $\boldsymbol{k}$ is the wave vector of electromagnetic waves. Using Faraday's law ($\boldsymbol{\nabla} \times \boldsymbol{E} = -\frac{\partial \boldsymbol{B}}{\partial t}$) and the Onsager's reciplocal relation ($\gamma_{jB} = i\omega\gamma_{ME}$, where ω is angular frequency of electromagnetic waves), Eq. (1.14) is rewritten as

$$\boldsymbol{j}_{\mathrm{IE}} = i\gamma_{ME}[(\boldsymbol{\alpha}_{\mathrm{R}} \cdot \boldsymbol{E})\boldsymbol{k} - (\boldsymbol{\alpha}_{\mathrm{R}} \cdot \boldsymbol{k})\boldsymbol{E}]. \tag{1.16}$$

We thus get the electric current including the cross-correlation effects as

$$j_{\mathrm{EE-IE},\mu} \equiv j_{\mathrm{E},\mu} + j_{\mathrm{IE},\mu} = \sum_{\nu} \sigma_{\mu\nu}^{\mathrm{EE-IE}} E_{\nu}, \tag{1.17}$$

with

$$\sigma_{\mu\nu}^{\mathrm{EE-IE}}(\omega) = i\gamma_{ME}(k_{\mu}\alpha_{\mathrm{R},\nu} - \alpha_{\mathrm{R},\mu}k_{\nu}), \tag{1.18}$$

where $\sigma_{\mu\nu}^{\mathrm{EE-IE}}$ is an electric conductivity tensor being liner in $\boldsymbol{k}$. Above equation indicates that Edelstein and inverse Edelstein effects give rise to an antisymmetric

component of the electric conductivity tensor, resulting in an anomalous optical response for linearly-polarized waves such as birefringence [21, 22]. In fact, from Maxwell's equations and Eq. (1.18), we obtain the dispersion relation of light describing extraordinary waves where the direction of Poynting vector and that of the wave vector differ,

$$k = \omega\left[c^2 - \left(\frac{\gamma_{ME}\alpha_{\rm R}}{\epsilon_0}\right)^2\right]^{-\frac{1}{2}}, \tag{1.19}$$

where c is the light velocity in vacuum.

Furthermore, it was pointed out that a strongly anisotropic light propagation arises from the electric current induced by a direct coupling between Edelstein effect and inverse Edelstein effect defined as

$$\boldsymbol{j}_{\rm EIE} \equiv \gamma_{ME}(\boldsymbol{\alpha}_{\rm R} \times \boldsymbol{M}_{\rm E}). \tag{1.20}$$

The anisotropic contribution arising from the Rashba field is written by diagonal components of the electric conductivity tensor as shown below [21, 22]. (see Appendix A.3 for details of the derivation.)

$$\sigma^{\rm EIE}_{\mu\nu}(\omega) = \frac{ie^2}{\omega + i0}\frac{n_{\rm e}}{m}\left[\delta_{\mu\nu}[1 + C(\omega)] - \hat{\alpha}_{{\rm R},\mu}\hat{\alpha}_{{\rm R},\nu}C(\omega)\right], \tag{1.21}$$

where $\hat{\boldsymbol{\alpha}}_{\rm R} \equiv \boldsymbol{\alpha}_{\rm R}/|\boldsymbol{\alpha}_{\rm R}|$ is a unit vector representing the direction of the Rashba field, 0 is a positive infinitesimal, and $n_{\rm e}$ and $C(\omega)$ are defined in Eq. (A.28) and Eq. (A.13), respectively. Equation (1.21) leads to the softening of plasma frequency due to $C(\omega)$ originated from the current-spin correlation function. As a consequence of the softening of plasma frequency, the dispersion relation being hyperbola for linearly-polarized waves,

$$\frac{\omega^2}{c^2} = \frac{k_x^2}{1 + \epsilon^{\rm EIE}_{zz}} + \frac{k_z^2}{1 + \epsilon^{\rm EIE}_{xx}}, \tag{1.22}$$

can emerge, resulting in a hyperbolic metamaterial [23] that exhibits a negative refraction and a focusing effect, where $\epsilon^{\rm EIE}_{xx} = -\frac{\omega_p^2}{\omega^2}[1 + C(\omega)]$, $\epsilon^{\rm EIE}_{zz} = -\frac{\omega_p^2}{\omega^2}$, and $\omega_p \equiv \sqrt{\frac{e^2 n_{\rm e}^2}{\epsilon_0 m}}$ is the plasma frequency. Here, we used the relation, $\epsilon_{\mu\nu} = \delta_{\mu\nu} + i\frac{1}{\epsilon_0\omega}\sigma_{\mu\nu}$.

1.4.2 Directional dichroism in magnetic Rashba conductor

Until now, we introduce electromagnetic cross-correlation effects and optical responses in the Rshaba system with time-reversal inversion. Refs. [21, 22] also reported anomalous optical responses in magnetic Rashba conductors realized in the Rashba system attached ferromagnet. In such systems, the time-reversal invariance breaking is caused by the *sd* exchange interaction that couples the electron spin to the magnetization, whose Hamiltonian is given by

$$H_{sd} = -J_{sd}\int {\rm d}^3 r(\boldsymbol{M}\cdot\boldsymbol{\sigma}), \tag{1.23}$$

where, $\boldsymbol{M}$ is the magnetization vector, $\boldsymbol{\sigma}$ is the vector of Pauli matrices, and J_{sd} is the strength of the exchange interaction.

If Rashba conductors are magnetic or under the effect of an external magnetic field, directional dichroism, a form of anisotropic wave propagation, has been shown to occur as with insulator multiferroics. An electric conductivity tensor describing optical responses in magnetic Rashba conductors is given by [21, 22]

$$\begin{aligned}\sigma^M_{\mu\nu}(\Omega) =&\sigma^{\rm AHE}(\Omega)\sum_l \epsilon_{\mu\nu l}M^{\parallel}_k \\ &+\sigma^M_1(\Omega)(\boldsymbol{\alpha}_{\rm R}\times\boldsymbol{M})\cdot\boldsymbol{q}[\delta_{\mu\nu}-\hat{\alpha}_{{\rm R},\mu}\hat{\alpha}_{{\rm R},\nu}] \\ &+\sigma^M_2(\Omega)[(\boldsymbol{\alpha}_{\rm R}\times\boldsymbol{M})_\mu q^\perp_\nu+(\boldsymbol{\alpha}_{\rm R}\times\boldsymbol{M})_\nu q^\perp_\mu] \\ &+\sigma^M_3(\Omega)\sum_{\ell m}[M^\perp_\mu\alpha_{{\rm R},\ell}\epsilon_{\nu\ell m}+\epsilon_{\mu\ell m}M^\perp_\nu\alpha_{{\rm R},\ell}]q_m, \end{aligned} \tag{1.24}$$

where $\boldsymbol{q}$ and Ω are the wave vector and angular frequency of electromagnetic waves, respectively, $\boldsymbol{q}^\perp\equiv\boldsymbol{q}-\hat{\boldsymbol{\alpha}}_{\rm R}(\hat{\boldsymbol{\alpha}}_{\rm R}\cdot\boldsymbol{q})$, $\boldsymbol{M}^\parallel\equiv(\boldsymbol{\alpha}_{\rm R}\cdot\boldsymbol{M})\boldsymbol{\alpha}_{\rm R}$, $\boldsymbol{M}^\perp\equiv\boldsymbol{M}-\hat{\boldsymbol{\alpha}}_{\rm R}(\hat{\boldsymbol{\alpha}}_{\rm R}\cdot\boldsymbol{M})$, $\epsilon_{\mu\nu l}$ is a totally antisymmetric tensor, and $\sigma^{\rm AHE}$, σ^M_1, σ^M_2, and σ^M_3 are coefficients depending on the angular frequency. The antisymmetric component being $\boldsymbol{q}^0$ with $\sigma^{\rm AHE}$ on the right-hand side of Eq. (1.24) induces anomalous Hall effect [24] when $\boldsymbol{\alpha}_{\rm R}\cdot\boldsymbol{M}$ is finite, resulting in the magneto-optical effect such as Faraday effect [25] for circularly-polarized waves traveling along in the direction of magnetization. The dispersion relation describing the Faraday effect is

$$\boldsymbol{q}^2=\frac{\Omega^2}{c^2}\left[1\pm\frac{\sigma^{\rm AHE}(\Omega)\alpha^2_{\rm R}(-M)}{\epsilon_0\Omega}\right], \tag{1.25}$$

where $\pm$ stands for the sense of circular polarization. On the other hand, the symmetric terms proportional to $\boldsymbol{q}^1$ on the right-hand side of Eq. (1.24) lead to diagonal components, resulting in directional dichroism depending on the direction of light propagation in the case where $\boldsymbol{\alpha}_{\rm R}\times\boldsymbol{M}$ being finite and $\boldsymbol{q}$ take parallel or antiparallel configuration. In fact, the dispersion relation describing the directional dichroism for linearly-polarized waves is shown to be [21, 22]

$$q=\frac{\Omega}{c}\sqrt{1+\epsilon^{\rm EIE}_{xx}}+\sigma^M_{13}(\Omega)[(\boldsymbol{\alpha}_{\rm R}\times\boldsymbol{M})\cdot\hat{\boldsymbol{q}}], \tag{1.26}$$

where $\sigma^M_{13}\equiv\sigma^M_1+\sigma^M_3$.

The directional dichroism was found to be governed by the relative direction of the wave vector and another vector $\boldsymbol{\mathcal{A}}_{\rm R}\equiv\boldsymbol{\alpha}_{\rm R}\times\boldsymbol{M}$ depicted in Fig. 1.2. The latter vector is known to be an effective gauge field coupled with the electron's spin (Rashba-induced spin gauge field), which generates a spin current [26–28]. From the symmetry point of view, the Rashba field $\boldsymbol{\alpha}_{\rm R}$ is equivalent to an electric polarization $\boldsymbol{P}$ (Ref. [29]); hence, the vector $\boldsymbol{\mathcal{A}}_{\rm R}$ works as a toroidal moment $\boldsymbol{t}\equiv\boldsymbol{P}\times\boldsymbol{M}$. The toroidal moment has been reported to act as an effective vector potential for light in the case of multiferroics [30]; however, microscopic justification for the same has not been provided. The study in Refs. [21, 22] further discussed that the effective theory describing magnetic Rashba conductors is similar to the one describing insulator multiferroics.

In Chapter 2, we examine the propagation of electromagnetic waves in magnetic Rashba conductors based on an effective Hamiltonian analysis on a microscopic ground. We show that the effective Hamiltonian describing the directional dichroism consists of two terms, one representing the Doppler shift and the other denoting the cross-correlation effect induced by a quadrupole moment [31]. The results of our study confirm with those of Refs. [21, 22] obtained by calculating an optical conductivity.

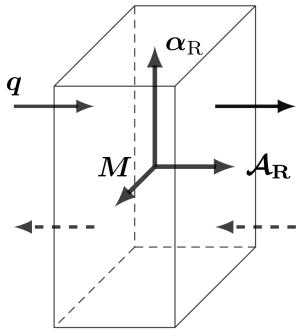

Figure 1.2: Schematic illustration of the directional dichroism in the magnetic Rashba conductor. When the toroidal moment (Rashba-induced spin gauge field) $\boldsymbol{\mathcal{A}}_{\mathrm{R}} \equiv \boldsymbol{\alpha}_{\mathrm{R}} \times \boldsymbol{M}$ is finite, the directional dichroism is caused by the coupling between the toroidal moment and the wave vector of light.

1.5 Spin gauge fields

In this section, we introduce two spin gauge fields. First one is the Volovik's spin gauge field, and second one is the Rashba-induced spin gauge field which plays an important part in argument about the directional dichroism in magnetic Rashba conductors. Rewriting the spin-transfer interactions shown in Sec. 1.1 in terms of the spin gauge fields, we see that these fields generate the spin current.

1.5.1 Volovik's spin gauge field

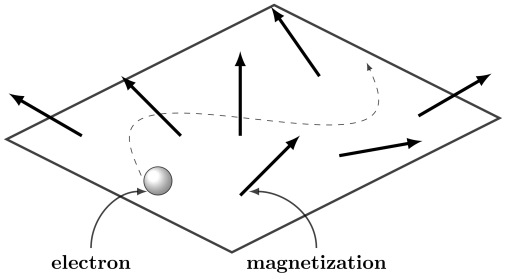

Figure 1.3: Schematic illustration of ferromagnetic metals with inhomogeneous magnetization texture. Electrons travel in the metals under the effect of the strong *sd* exchange interaction.

In ferromagnetic metals without the Rashba interaction depicted in Fig 1.3, an effective electromagnetic field arises from the *sd* exchange interaction described by

$$H_{sd} = -\Delta_{sd} \int \mathrm{d}^3 r (\boldsymbol{n} \cdot \boldsymbol{s}_{\mathrm{e}}), \tag{1.27}$$

where $\Delta_{sd} \equiv J_{sd} M$ is the exchange energy, $M \equiv |\boldsymbol{M}|$, $\boldsymbol{n}$ is a unit vector representing the direction of the magnetization, and $\boldsymbol{s}_{\mathrm{e}}$ is the direction of the conduction electron spin. When this exchange interaction is strong, the conduction electron spin is aligned parallel to the magnetization direction, and this effect results in a quantum mechanical phase attached to the electron spin when the electron moves (see Ref. [32] for details of derivation). The spin part of the electron wave function with the expectation value along $\boldsymbol{n} \equiv \boldsymbol{n}(\boldsymbol{r})$ is $|\boldsymbol{n}\rangle = \cos\frac{\theta}{2}|\uparrow\rangle + \sin\frac{\theta}{2} e^{i\phi}|\downarrow\rangle$, where $\boldsymbol{r}$ means a position, θ and ϕ are the polar coordinates of $\boldsymbol{n}$, and $|\uparrow\rangle$ and $|\downarrow\rangle$ denote the spin states [33].

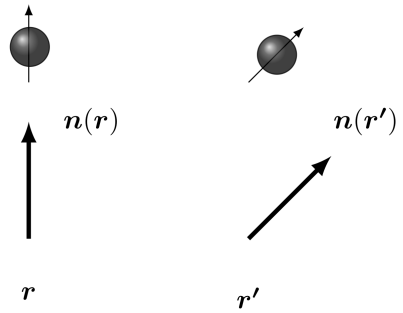

Figure 1.4: Schematic illustration of electron hopping. The strong *sd* interaction changes the direction of the electron spin when the electron travels in the inhomogeneous magnetization texture.

When the electron hops over a small distance $\mathrm{d}\boldsymbol{r} \equiv \boldsymbol{r}' - \boldsymbol{r}$ to a nearby site where the magnetization is along $\boldsymbol{n}' \equiv \boldsymbol{n}(\boldsymbol{r}')$ as is shown in Fig. 1.4, the overlap

of the wave functions is calculated as $\langle \boldsymbol{n}'|\boldsymbol{n}\rangle \simeq e^{\frac{i}{\hbar}e\boldsymbol{A}_{\rm s}^z\cdot {\rm d}\boldsymbol{r}}$, where

$$\boldsymbol{A}_{\rm s}^z = \frac{\hbar}{2e}(1-\cos\theta)\boldsymbol{\nabla}\phi, \tag{1.28}$$

and the factor of $\frac{1}{2}$ is due to the magnitude of the electron spin. The field $\boldsymbol{A}_{\rm s}^z$ is an effective vector potential or an effective gauge field. When the electron's path is finite, the phase becomes $\varphi = \frac{e}{\hbar}\int_C {\rm d}\boldsymbol{r}\cdot\boldsymbol{A}_{\rm s}^z$. The existence of the phase means that there is an effective magnetic field $\boldsymbol{B}_{\rm s}$, as seen by rewriting the integral over a closed path using the Stokes theorem as $\varphi = \frac{e}{\hbar}\int_S {\rm d}\boldsymbol{S}\cdot\boldsymbol{B}_{\rm s}$, where $\boldsymbol{B}_{\rm s}\equiv\boldsymbol{\nabla}\times\boldsymbol{A}_{\rm s}^z$. The time derivative of the phase is equivalent to a voltage, and thus, we have an effective electric field defined by $\dot{\varphi} = -\frac{e}{\hbar}\int_C {\rm d}\boldsymbol{r}\cdot\boldsymbol{E}_{\rm s}$, where $\boldsymbol{E}_{\rm s}\equiv -\dot{\boldsymbol{A}}_{\rm s}^z$. These two fields satisfy Faraday's law, $\boldsymbol{\nabla}\times\boldsymbol{E}_{\rm s}+\dot{\boldsymbol{B}}_{\rm s}=0$. We therefore have effective electromagnetic fields that couple to the conduction electron spin as a result of the *sd* exchange interaction. We call the field a spin electromagnetic field [34]. Using the explicit form of the effective gauge field, Eq. (1.28), we see that the emergent spin electromagnetic fields are

$$\begin{aligned}
\boldsymbol{E}_{{\rm s},i} &= -\frac{\hbar}{2e}\boldsymbol{n}\cdot(\dot{\boldsymbol{n}}\times\nabla_i\boldsymbol{n}),\\
\boldsymbol{B}_{{\rm s},i} &= \frac{\hbar}{4e}\sum_{jk}\epsilon_{ijk}\boldsymbol{n}\cdot(\nabla_j\boldsymbol{n}\times\nabla_k\boldsymbol{n}).
\end{aligned} \tag{1.29}$$

The magnetic component $\boldsymbol{B}_{\rm s}$ is the spin Berry's curvature [35] or scalar chirality. The electric component $\boldsymbol{E}_{\rm s}$, called the spin motive force, is a chirality in the space-time, which arises when the magnetization structure $\boldsymbol{n}$ is time-dependent. The expression Eq. (1.29) was derived by Volovik in 1987 [36]. Experimentally, the spin magnetic field (the spin Berry's curvature) has been observed using the anomalous Hall effect [1] in frustrated ferromagnets [37, 38]. The spin electric field has been measured in the motion of various ferromagnetic structures such as domain walls [41], magnetic vortices [42], and skyrmions [43].

By use of Eq. (1.28), we see that the spin-transfer interaction, Eq. (1.3), is represented as a gauge coupling to the adiabatic spin gauge field (Volovik's spin gauge field) (Refs [2, 44]) as shown below.

$$H_{\rm st} = \int {\rm d}^3r(\boldsymbol{j}_{\rm s}\cdot\boldsymbol{A}_{\rm s}^z), \tag{1.30}$$

where $\boldsymbol{j}_{\rm s}$ is the spin-polarized electric current. Above expression clearly shows that the adiabatic spin gauge field $\boldsymbol{A}_{\rm s}^z$ induces the spin current. In the case of the *sd* interaction having time dependence, it is theoretically shown that non-adiabatic components of an SU(2) spin gauge field intrinsically contribute to the spin current generation in the context of the spin pumping effect [45].

[1] By taking into consideration of vertex corrections due to random impurities, the anomalous Hall effect induced by the non-local component of the scalar chirality is theoretically investigated in the case of a weak *sd* interaction [39, 40].

1.5.2 Rashba-induced spin gauge field

In Ref. [27], the Rashba-induced spin gauge field is derived in the strong *sd* coupling region by calculating a pumped electric current, $\boldsymbol{j}_{\rm pump}$, by magnetization texture and a spin Hall current, $\boldsymbol{j}_{\rm Hall}$, by effective magnetic field based on the microscopic transport theory [28, 46]. These electric currents are given by (see Appendixes C.1 and C.2 for details of derivation)

$$\begin{aligned}\boldsymbol{j}_{\rm pump} =& \boldsymbol{j}^{\rm (A)} + \boldsymbol{j}^{\rm (B)} + \boldsymbol{j}^{\rm (C)} \\ =& -a_1 \frac{\partial}{\partial t}(\boldsymbol{\alpha}_{\rm R} \times \boldsymbol{n}) + b_1 \boldsymbol{\nabla} \times [\boldsymbol{\nabla} \times (\boldsymbol{\alpha}_{\rm R} \times \boldsymbol{n})], \qquad (1.31)\\ \boldsymbol{j}_{\rm Hall} =& \boldsymbol{j}^{\rm (Hall,1)} + \boldsymbol{j}^{\rm (Hall,2)} \\ =& -c_1 \boldsymbol{E} \times [\boldsymbol{\nabla} \times (\boldsymbol{\alpha}_{\rm R} \times \boldsymbol{n})], \qquad (1.32)\end{aligned}$$

where $\boldsymbol{n}$ is a unit vector representing the direction of the magnetization. Contributions for $\boldsymbol{j}_{\rm pump}$ and $\boldsymbol{j}_{\rm Hall}$ at the linear order of the Rashba interaction are diagrammatically shown in Fig. 1.5 and Fig. 1.6, respectively. The coefficients a_1, b_2, and c_3 are defined in Appendixes C.1 and C.2.

From Eq. (1.31), Eq. (1.32), and Maxwell's equation including effective spin electromagnetic fields in medium (Refs. [28, 46]),

$$\boldsymbol{j} = \sigma_{\rm s} \boldsymbol{E}_{\rm s,eff} + \frac{1}{\mu_{\rm s}} \boldsymbol{\nabla} \times \boldsymbol{B}_{\rm s,eff}, \qquad (1.33)$$

with the spin-dependent electric conductivity $\sigma_{\rm s}$ and the spin-dependent magnetic permeability $\mu_{\rm s}$, Rashba-induced spin electric and magnetic fields are obtained as

$$\begin{aligned}\boldsymbol{E}_{\rm R} \equiv& -\dot{\boldsymbol{\mathcal{A}}}_{\rm R} = -\boldsymbol{\alpha}_{\rm R} \times \dot{\boldsymbol{n}} \\ \boldsymbol{B}_{\rm R} \equiv& \boldsymbol{\nabla} \times \boldsymbol{\mathcal{A}}_{\rm R} = \boldsymbol{\nabla} \times (\boldsymbol{\alpha}_{\rm R} \times \boldsymbol{n}), \qquad (1.34)\end{aligned}$$

respectively. These two fields satisfy Faraday's law, $\boldsymbol{\nabla} \times \boldsymbol{E}_{\rm R} + \dot{\boldsymbol{B}}_{\rm R} = 0$. Here,

$$\boldsymbol{\mathcal{A}}_{\rm R} \equiv \boldsymbol{\alpha}_{\rm R} \times \boldsymbol{n} \qquad (1.35)$$

is the Rashba-induced spin gauge fields [27], which is an effective vector potential for electron spin. The spin-dependent electric conductivity, magnetic permeability, and Hall conductivity are given by a_1, b_1^{-1}, and c_1, respectively. Using the above expression, the spin-transfer interaction by the Rashba interaction, Eq. (1.4), is rewritten as a form of gauge coupling as shown below.

$$H_{\rm st,R} = \int {\rm d}^3 r \frac{m}{e} (\boldsymbol{j}_{\rm s} \cdot \boldsymbol{\mathcal{A}}_{\rm R}). \qquad (1.36)$$

Therefore, we see that the Rashba-induced spin gauge fields $\boldsymbol{\mathcal{A}}_{\rm R}$ plays a role of the spin current generation as with the adiabatic spin gauge field suggested by Volovik.

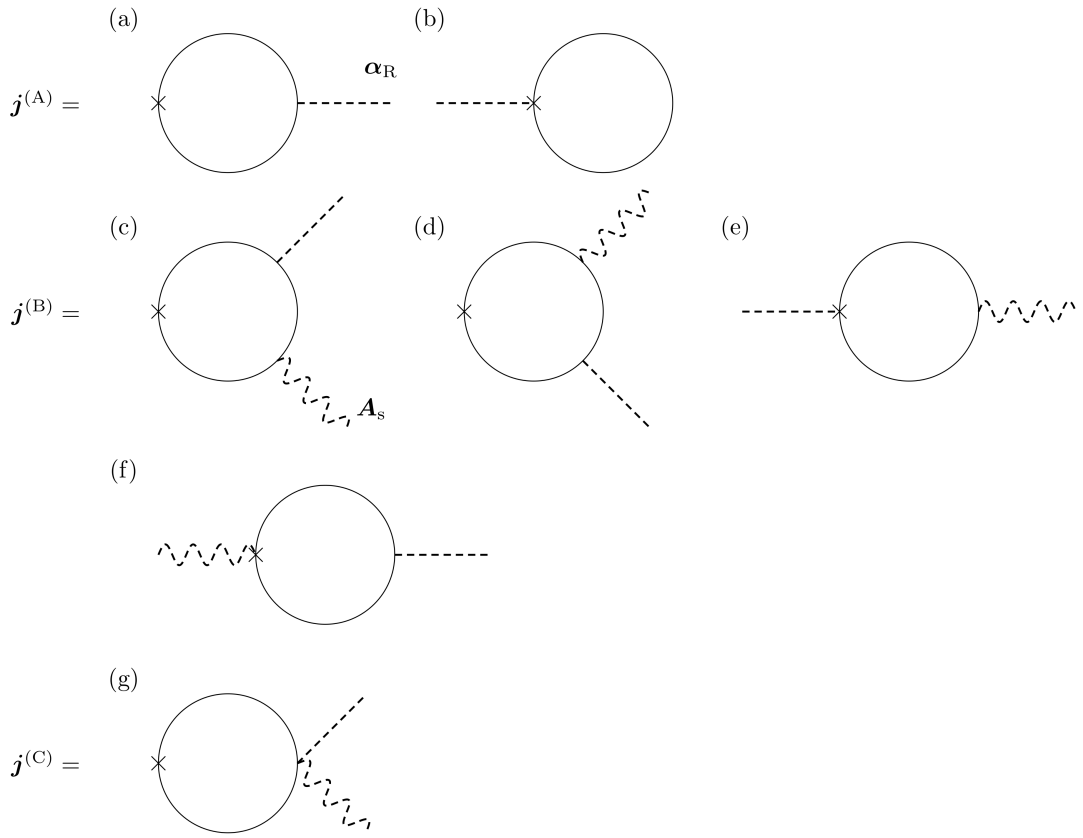

Figure 1.5: The Feynman diagrams for the electric current pumped by non-uniform magnetization texture and the Rashba field. Solid lines represent the conducting electrons' Green's function including the *sd* interaction. The dotted lines and the dotted wavy lines denote the Rashba field $\boldsymbol{\alpha}_{\mathrm{R}}$ and the spin gauge field $\boldsymbol{A}_{\mathrm{s}}$, respectively. Diagrams (a) and (b) are contributions of $\boldsymbol{j}^{(\mathrm{A})}$. Diagrams (c), (d), (e), and (f) are contributions of $\boldsymbol{j}^{(\mathrm{B})}$. Diagram (g) is contribution of $\boldsymbol{j}^{(\mathrm{C})}$. Note that $\boldsymbol{j}^{(\mathrm{C})}$ dose not contribute to the expression for the pumped current in this calculation.

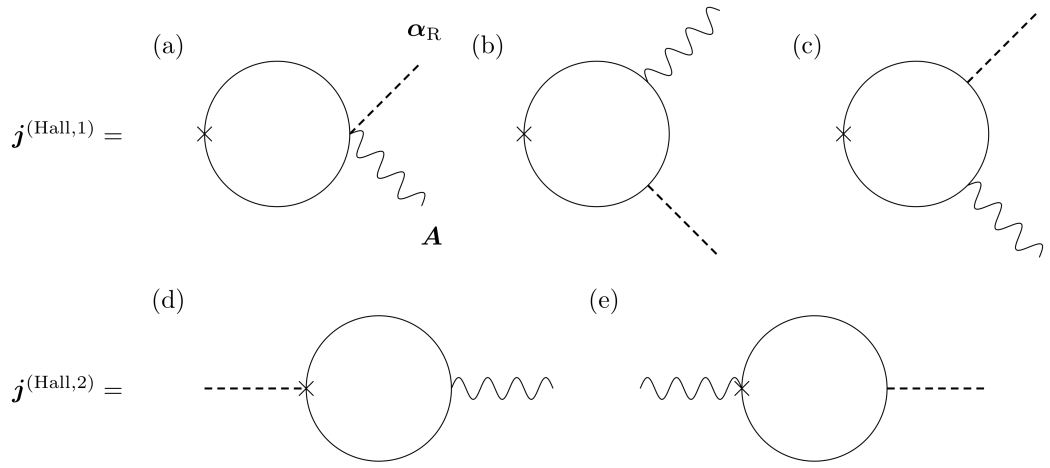

Figure 1.6: The Feynman diagrams for the spin Hall current driven by the Rashba-induced spin magnetic field. Solid lines represent the conducting electrons' Green's function including the *sd* interaction. The dotted lines and the wavy lines denote the Rashba interaction and the gauge field $\boldsymbol{A}$, respectively. Diagrams (a), (b), and (c) are contributions of $\boldsymbol{j}^{(\mathrm{Hall},1)}$. Diagrams (d) and (e) are contributions of $\boldsymbol{j}^{(\mathrm{Hall},2)}$. As was pointed out in Ref. [27], the contribution arising from the spin gauge field $\boldsymbol{A}_{\mathrm{s}}$ is negligibly small in this description. Note that $\boldsymbol{j}^{(\mathrm{Hall},2)}$ does not contribute to the expression for the Hall current in this calculation.

As has been reported by Volovik [36], the original spin gauge field (adiabatic spin gauge field) occurs in the absence of the Rashba interaction in the strong *sd*-coupling regime (Ref. [32]), and induces effective electric and magnetic fields acting on electron spin as was shown in Sec. 1.5.1. Originally, the emergence of the effective electric field from moving magnetic structures was found in 1986 by Berger, where a voltage generated by canting a moving domain wall was calculated [5]. Stern discussed the motive force in the context of the spin Berry's phase and the Aharonov-Bohm effect in a ring, and showed similarity to Faraday's law [47]. The spin motive force was rederived in Ref. [48] in the case of the domain wall motion, and discussed in the context of topological pumping in Ref. [49]. Recenty, a generation mechanism of a spin electric field using a nonlinear effect of non-monochromatic spin-wave excitations was proposed in Ref. [50]. This mechanism is applicable to the case of a uniform magnetization, and it would have a great advantage in applications over common setups using non-coplanar structures. This theoretical considerations call for an experimental verification of the effect. The coupling of adiabatic spin gauge field to electromagnetic field was studied based on the effective Hamiltonian study in Refs. [50,51]. It was found that the spin-transfer effect is described using the linear coupling term of the adiabatic spin gauge field and the electric field [2]. Ref. [54] reported the effect of adiabatic spin gauge field on

[2]It was experimentally confirmed that the spin-transfer effect causes nonreciprocal spin-wave propagation due to the Doppler shift in ferromagnetic metals when the electric current is applied [52]. Recent study (Ref. [53]) theoretically showed that the spin-transfer effect can induce the

nonlinear optical effects and a topological inverse Faraday effect was shown to have occurred from a spin Berry's curvature in the absence of a spin-orbit interaction.

Those works consider only the adiabatic limit, i.e., in the case of a strong *sd* exchange interaction and in the absence of spin-dependent scattering. The idea of the spin motive force has recently been extended to include the spin-orbit interaction [26, 27, 34, 55–58], and it was shown that the spin-orbit interaction modifies the spin electric field. It was also shown that the spin electromagnetic field arises even in the limit of the weak *sd* interaction [28,46], as was shown in Eq. (1.33). The case of the Rashba spin-orbit interaction has been studied in detail recently. It was shown that the spin electric field in this case emerges even from a uniform precession of magnetization [27,34]. This fact suggests that the Rashba interaction at interfaces would be useful in controlling the spin-charge conversion. The Rashba-induced spin electric field induces a voltage in the same direction as in the inverse spin Hall and inverse Edelstein effects [20, 59] driven by the spin pumping effect [60]. It was also pointed out that the spin electromagnetic fields in the presence of spin relaxation satisfy Maxwell's equations with spin magnetic monopoles that are driven dynamically [28].

1.6 Optical responses and cross-correlation effects in Weyl spin-orbit system

Optical responses and cross-correlation effects are qualitatively discussed based on symmetry argument. An optical response for circularly-polarized waves, natural optical activity, is caused by the inversion symmetry breaking which induces an antisymmetric off-diagonal component linear in the wave vector of light in an electric conductivity tensor [61]. Natural optical activity of chiral molecules was phenomenologically discussed in Ref. [62]. It was pointed out that chiral nature leads to the electric flux density and magnetic field strength, $\boldsymbol{D}$ and $\boldsymbol{H}$, given by

$$\begin{aligned} \boldsymbol{D} =& \epsilon \left[\boldsymbol{E} - \frac{g}{\epsilon} \dot{\boldsymbol{B}} \right], \\ \boldsymbol{H} =& \frac{1}{\mu} \left[\boldsymbol{B} - \mu g \dot{\boldsymbol{E}} \right], \end{aligned} \tag{1.37}$$

where $\boldsymbol{E}$ and $\boldsymbol{B}$ are electric and magnetic fields, respectively. ϵ and μ are the electric permittivity and magnetic permeability in the medium, respectively, and the constant g characterizes the breaking of spatial inversion symmetry. It was demonstrated through discussion on a correlation function that g is finite when the inversion symmetry is broken [63].

In the case of electron systems, a typical chiral system is the one with the Weyl spin-orbit interaction (Refs. [64–66]), whose Hamiltonian is given by

$$\mathcal{H}_{\mathrm{W}} = -\lambda (\boldsymbol{p} \cdot \boldsymbol{\sigma}), \tag{1.38}$$

spin-wave-Doppler shift even in antiferromagnets.

where λ stands for the coupling constant of the spin-orbit interaction with broken inversion symmetry. The interaction, Eq. (1.38), breaks mirror symmetry with respect to all the three axes (Ref. [67]), resulting in a radial electron spin texture on Fermi surface [68] depicted in Fig. 1.7. The radial electron spin texture generates magnetization by the electric field in the system having helical structure such as Se or Te [68]. In Chapter 3, we examine natural optical activity in the Weyl spin-orbit system by deriving an effective Hamiltonian for electromagnetic fields.

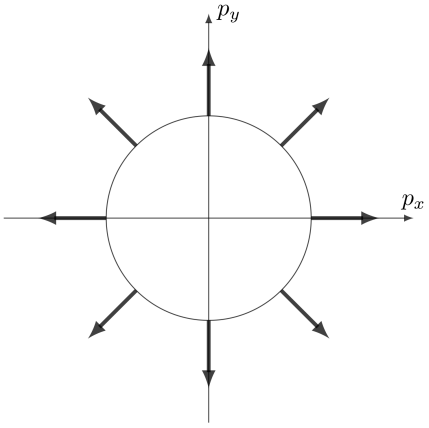

Figure 1.7: Schematic illustration of the electron spin configuration on Fermi surface induced by the Weyl interaction. Black arrows denote the direction of the electron spin.

The Weyl spin-orbit systems, where time-reversal symmetry is kept, are called truly chiral systems [69]. In contrast, quantity which breaks time-reversal invariance besides spatial one is called "false chirality" . A symmetry analysis showed that the truly chiral interaction $\boldsymbol{p} \cdot \boldsymbol{\sigma}$ leads to natural optical activity in chiral molecules [69]. In the case of electromagnetism, quantities with "false chirality" are $\boldsymbol{E} \cdot \boldsymbol{B}$ and $\boldsymbol{E} \times \boldsymbol{B}$. The scaler product $\boldsymbol{E} \cdot \boldsymbol{B}$ appears in an effective Hamiltonian of 3+1-dimensional Weyl semimetal in the form $\mathcal{H}_\theta = \theta(\boldsymbol{r}, t)\boldsymbol{E} \cdot \boldsymbol{B}$ [70, 71], where $\theta(\boldsymbol{r}, t)$ is a topological field depending on space $\boldsymbol{r}$ and time t. The effective Hamiltonian leads to topological electromagnetic cross-correlation effects such as chiral magnetic effect and anomalous Hall effect [72]. The vector product form $\boldsymbol{E} \times \boldsymbol{B}$ appears in magnetic Rashba conductors [31] or insulator multiferroics [73]. The effective Hamiltonian in this case is $\mathcal{H}_u = \boldsymbol{u} \cdot (\boldsymbol{E} \times \boldsymbol{B})$ with a constant vector $\boldsymbol{u}$ representing an intrinsic flow and it could cause directional dichroism [31], as is shown in Chapter 2.

1.7 Overview of this Thesis

This Thesis is structured as follows. In Chapter 2, we examine an anisotropic light propagation, directional dichroism, in magnetic Rashba conductors in terms of an effective Hamiltonian for electromagnetic fields. By deriving the effective Hamiltonian based on an imaginary-times path-integral formalism, we show

that the directional dichroism in magnetic Rashba conductors is described by the toroidal-moment term and the quadrupole moment term like in insulator multiferroics. From the result, the directional dichroism is interpreted as Doppler shift of light. Furthermore, we discuss optical responses in relativistic spin-orbit systems such as 3+1-dimensional Weyl semimetals. This work was reported in Ref. [31]. In Chapter 3, we investigate optical properties of a Weyl spin-orbit system with quadratic dispersion by deriving an effective Hamiltonian of electromagnetic fields. We show that an optical chirality order parameter appears in the effective Hamiltonian, and describes natural optical activity in a typically chiral system. This work was reported in Ref. [74].

Chapter 2

Theory of nonreciprocal directional dichroism in magnetic Rashba conductor

Rashba spin-orbit interaction leads to a number of electromagnetic cross correlation effects by inducing a mixing of electric and magnetic degrees of freedom as mentioned in Introduction. In this Chapter, we investigate the optical properties of a magnetic Rashba conductor by deriving an effective Hamiltonian based on an imaginary-time path-integral formalism. We show that the effective Hamiltonian can be described in terms of toroidal and quadrupole moments, as has been argued in the case of insulator multiferroics [31]. The toroidal moment turns out to coincide with the spin gauge field induced by the Rashba field. It causes Doppler shift by inducing intrinsic electric current, resulting in anisotropic light propagation (directional dichroism) irrespective of the polarization. In addition, we see that the quadrupole moment contributes to the linear dichroism for linearly-polarized waves.

2.1 Phenomenological argument: Doppler-shift picture

In this section, we discuss an effective Hamiltonian for electromagnetic fields in magnetic Rashba conductors with breaking of both spatial-inversion symmetry and time-reversal invariance from the symmetry point of view.

In the case of electromagnetism in vacuum, the effective Hamiltonian density of electromagnetic fields induced by charged particles (electrons) is restricted to [75]

$$\mathcal{H} = \frac{1}{2}\left(\epsilon_0|\boldsymbol{E}|^2 + \frac{1}{\mu_0}|\boldsymbol{B}|^2\right), \tag{2.1}$$

where ϵ_0 is an electric permittivity of the vacuum, μ_0 is a magnetic permeability of the vacuum, and $\boldsymbol{E}$ and $\boldsymbol{B}$ are electric and magnetic fields, respectively. In this

case, we get conventional Maxwell's equations as

$$\begin{aligned}
\boldsymbol{\nabla}\cdot\boldsymbol{E} =& \frac{\rho}{\epsilon_0},\\
\boldsymbol{\nabla}\cdot\boldsymbol{B} =& 0,\\
\boldsymbol{\nabla}\times\boldsymbol{E} =& -\frac{\partial\boldsymbol{B}}{\partial t},\\
\boldsymbol{\nabla}\times\boldsymbol{B} =& \mu_0\boldsymbol{j}+\epsilon_0\mu_0\frac{\partial\boldsymbol{E}}{\partial t},
\end{aligned} \tag{2.2}$$

where ρ represents charge density and $\boldsymbol{j}$ is the charge-current density.

However, the existence of cross-correlation effects of Rashba conductors indicates that the electric and magnetic fields, $\boldsymbol{E}$ and $\boldsymbol{B}$, are linearly coupled, as was mentioned in Secs 1.3 and 1.4. Therefore, we can expect that there are two possibilities for this form of interaction in the case where spatial-inversion symmetry and time-reversal invariance are broken: The first one is proportional to $\boldsymbol{E}\cdot\boldsymbol{B}$, and the second one is proportional to their vector product $\boldsymbol{E}\times\boldsymbol{B}$, as shown below.

$$\mathcal{H}_\theta = \theta(\boldsymbol{E}\cdot\boldsymbol{B}), \tag{2.3}$$

$$\mathcal{H}_u = \boldsymbol{u}\cdot(\boldsymbol{E}\times\boldsymbol{B}), \tag{2.4}$$

where θ is a constant and $\boldsymbol{u}$ is a constant vector. The first scalar interaction (2.3) does not modify the equation of motion but has a topological effect, and the emergence of such an interaction is restricted to surfaces or interfaces with nontrivial topological properties. For instance, such a scalar coupling leads to a mixing of $\boldsymbol{E}$ and $\boldsymbol{B}$ when the topological number $\theta/2\pi$ has a jump at the interfaces [76,77]. (In Sec. 2.4, the cross-correlation effect induced by the θ-term in Weyl semimetal is briefly discussed.) In contrast, the coupling of the vector product shown in Eq. (2.4) may occur in ordinary materials if a vector $\boldsymbol{u}$ exists because of the breaking of both spatial-inversion symmetry and time-reversal invariance. This term, Eq. (2.4), has not been discussed in the context of high-energy physics because it is not invariant under the Lorentz transformation.

It is known that the vector $\frac{1}{\mu}\boldsymbol{E}\times\boldsymbol{B}$ (where μ is the magnetic permeability of solids) is the Poynting vector representing the momentum of the electromagnetic wave [1]. The vector interaction of Eq. (2.4) can thus be considered to be of the form representing the Doppler shift $\boldsymbol{u}\cdot\boldsymbol{k}$, where $\boldsymbol{k}$ is the wave vector of the electromagnetic wave. In fact, in terms of the photon operators $a_{\boldsymbol{k}}$ and $a^\dagger_{\boldsymbol{k}}$, the coupling of Eq. (2.4) modifies the photon Hamiltonian as

$$H_{\text{photon}} = \sum_{\boldsymbol{k}}(ck-\boldsymbol{u}\cdot\boldsymbol{k})a^\dagger_{\boldsymbol{k}}a_{\boldsymbol{k}}, \tag{2.5}$$

where c is the light velocity. The vector coupling of Eq. (2.4) is thus expected to occur when the medium has an intrinsic flow with a velocity proportional to $\boldsymbol{u}$.

The Doppler shift picture can also be justified at the level of the equation of motion. The following description shows how electromagnetism is modified by the

vector interaction of Eq. (2.4). Two of Maxwell's equations become

$$\begin{aligned}\boldsymbol{\nabla}\cdot\boldsymbol{E} =&\frac{\rho}{\epsilon_0}-\frac{1}{\epsilon_0}\boldsymbol{\nabla}\cdot(\boldsymbol{u}\times\boldsymbol{B}),\\ \boldsymbol{\nabla}\times\boldsymbol{B} =&\mu_0\boldsymbol{j}+\epsilon_0\mu_0\frac{\partial\boldsymbol{E}}{\partial t}+\mu_0\frac{\partial}{\partial t}(\boldsymbol{u}\times\boldsymbol{B})-\mu_0\boldsymbol{\nabla}\times(\boldsymbol{u}\times\boldsymbol{E}),\end{aligned}\tag{2.6}$$

whereas the other two remain unchanged ($\boldsymbol{\nabla}\cdot\boldsymbol{B}=0$ and $\boldsymbol{\nabla}\times\boldsymbol{E}=-\frac{\partial\boldsymbol{B}}{\partial t}$). The total electric and magnetic fields can be represented as follows.

$$\begin{aligned}\boldsymbol{E}_{\rm tot} =&\boldsymbol{E}+\frac{1}{\epsilon_0}(\boldsymbol{u}\times\boldsymbol{B}),\\ \boldsymbol{B}_{\rm tot} =&\boldsymbol{B}+\mu_0(\boldsymbol{u}\times\boldsymbol{E}).\end{aligned}\tag{2.7}$$

These relations representing a cross-correlation effect can be considered as a result of the Doppler shift as we demonstrate here. Taking a derivative of $\boldsymbol{E}_{\rm tot}$ with respect to time, we have, using $\frac{\partial\boldsymbol{B}}{\partial t}=-\boldsymbol{\nabla}\times\boldsymbol{E}$,

$$\frac{\partial\boldsymbol{E}_{\rm tot}}{\partial t}=\frac{\partial\boldsymbol{E}}{\partial t}+\frac{1}{\epsilon_0}[(\boldsymbol{u}\cdot\boldsymbol{\nabla})\boldsymbol{E}-\boldsymbol{\nabla}(\boldsymbol{u}\cdot\boldsymbol{E})].\tag{2.8}$$

For plane waves with the wave vector $\boldsymbol{k}\perp\boldsymbol{E}$, the last term in the above equation is orthogonal to the field $\boldsymbol{E}$; hence, it is neglected as was done for the linear effects in $\boldsymbol{u}$. The time derivative is thus replaced by a "covariant" one,

$$D_t\equiv\frac{\partial}{\partial t}+\frac{1}{\epsilon_0}(\boldsymbol{u}\cdot\boldsymbol{\nabla}),\tag{2.9}$$

which is expected for a flowing medium [78]. Therefore, the electromagnetic cross-correlation effect shown in Eq. (3.4) represents the Doppler shift because of a medium flow with velocity $\boldsymbol{u}$.

It needs to be understood which type of intrinsic flow causes the Doppler shift of the electromagnetic field in solids. One example is an equilibrium flow of spin (spin current) can occur even at macroscopic scales, as known in magnets with noncollinear magnetization structures [2, 79]. Spin current can be spontaneously generated by the spin-orbit interaction because the spin current breaks the spatial-inversion symmetry but not the time-reversal symmetry. In fact, a recent study showed that such an intrinsic spin current generates the Dzyaloshinskii–Moriya interaction (Refs. [80,81]) in magnetic materials as a result of the Doppler shift [82]. (see Appendix D for details of derivation of an effective Hamiltonian induced by the spin current.) Anisotropic spin wave propagation experimentally measured in chiral magnets such as Cu_2OSeO_3 (Ref. [83]) is interpreted as a consequence of the Doppler shift induced by the Dzyaloshinskii–Moriya interaction. Another one is an equilibrium flow of charge which do not induced Joule heat as well spin current. We see that intrinsic flow in medium induced by the vector $\boldsymbol{u}$ is the equilibrium charge current but not the equilibrium spin current because symmetry of the velocity of the electron corresponds to that of $\boldsymbol{u}$ describing medium flow.

Our aim is to demonstrate that the magnetic Rashba conductor induces the vector-coupling term of Eq. (2.4), and the vector $\boldsymbol{u}$ is given by a toroidal moment

$\boldsymbol{\mathcal{A}}_{\rm R}$ which induces the intrinsic charge current in medium. This result indicates that wave propagation is affected by the Doppler shift induced by intrinsic electric current generated by the toroidal moment. This is an interesting result as it indicates that an effective vector potential for an electron spin acts as an effective vector potential for an electromagnetic wave (light) as suggested by Refs. [30, 78]. The directional dichroism predicted in the magnetic Rashba conductor in Ref. [21] can thus be explained based on this result. We should keep in mind, however, that this sceanario is justified up to the linear order of $\boldsymbol{u}$ representing the intrinsic flow in medium.

2.2 Cross-correlation effects on electric permittivity

The section till now describes the effects originating from the vector coupling of Eq. (2.4); however, there may be other effects induced by the quadrupole moment of the system. These effects are described in the section below. The cross-correlation effect because of the quadrupole moment is expressed as [73]

$$\mathcal{H}_Q = \sum_{ij} Q_{ij} E_i B_j, \tag{2.10}$$

where $Q_{ij}(=Q_{ji})$ is the traceless quadrupole moment. The electric and magnetic fields representing the cross-correlation effects due to the total Hamiltonian $\mathcal{H}_u + \mathcal{H}_Q$ after considering the vector $\boldsymbol{u}$ and the quadrupole moment Q_{ij} are

$$\begin{aligned} \boldsymbol{E}_{\rm tot} =& \boldsymbol{E} + \frac{1}{\epsilon_0}\boldsymbol{P}, \\ \boldsymbol{B}_{\rm tot} =& \boldsymbol{B} + \mu_0 \boldsymbol{M}, \end{aligned} \tag{2.11}$$

with

$$\begin{aligned} P_\mu \equiv& (\boldsymbol{u}\times\boldsymbol{B})_\mu - \sum_\nu Q_{\mu\nu} B_\nu, \\ M_\mu \equiv& (\boldsymbol{u}\times\boldsymbol{E})_\mu + \sum_\nu Q_{\mu\nu} E_\nu, \end{aligned} \tag{2.12}$$

where $\boldsymbol{P}$ and $\boldsymbol{M}$ indicate effective electric polarization and effective magnetization, respectively. The wave equation read from Eq. (2.11) is $\sum_\nu [c^2(\boldsymbol{k}^2\delta_{\mu\nu} - k_\mu k_\nu) - \omega^2\epsilon_{\mu\nu}]E_\nu = 0$, where the electric permittivity tensor is

$$\epsilon_{ij} \equiv \epsilon_{ij}^{(0)} + \epsilon_{ij}^{(u)} + \epsilon_{ij}^{(Q)}, \tag{2.13}$$

with

$$\epsilon_{ij}^{(u)} \equiv -\frac{1}{\epsilon_0\omega}\sum_l (u_i\delta_{lj} + \delta_{il}u_j)k_l + \frac{2}{\epsilon_0\omega}\delta_{ij}(\boldsymbol{u}\cdot\boldsymbol{k}), \tag{2.14}$$

$$\epsilon_{ij}^{(Q)} \equiv -\frac{1}{\epsilon_0\omega}\sum_{l\nu} (Q_{i\nu}\epsilon_{\nu jl} + \epsilon_{\nu il}Q_{j\nu})k_l, \tag{2.15}$$

where ϵ_{ijk} is a totally antisymmetric tensor, $\boldsymbol{k}$ and ω are the wave vector and frequency of the electromagnetic field, respectively, and $\epsilon_{ij}^{(0)}$ is the contribution even in k. It can be seen that the cross-correlation effects by $\boldsymbol{u}$ and Q_{ij} lead to generation of linear components in the wave vector $\boldsymbol{k}$ that change signs by time-reversal [84]. Such terms may induce dichroism phenomena of light such as directional dichroism. Compering the result of Eq. (1.24) with that of Eq. (2.13), we can expect that $\boldsymbol{u}$ and Q_{ij} in magnetic Rashba conductor are described as

$$\begin{aligned} \boldsymbol{u} =& d_1(\hat{\boldsymbol{\alpha}}_{\mathrm{R}} \times \hat{\boldsymbol{M}}), \\ Q_{ij} =& d_2(\hat{M}_i \hat{\alpha}_{\mathrm{R},j} + \hat{\alpha}_{\mathrm{R},i} \hat{M}_j), \end{aligned} \tag{2.16}$$

where $\hat{\boldsymbol{\alpha}}_{\mathrm{R}}$ is a unit vector of the Rashba vector, $\hat{\boldsymbol{M}}$ is a unit vector of the magnetization vector, and d_1 and d_2 are coefficients. Note that we neglect the angular frequency dependence of coefficients and the anisotropic terms described by $\hat{\alpha}_{\mathrm{R},\mu}\hat{\alpha}_{\mathrm{R},\nu}$ for simplicity.

First, we take into account only the contribution of Eq (2.14) to directional dichroism. The terms on the right-hand side of Eq. (2.14) indicates that the vector $\boldsymbol{u}$ contributes to the symmetric components of the electric permittivity tensor. The symmetric component on the right-hand side of Eq. (2.14) means that the Doppler shift, $\boldsymbol{u} \cdot \boldsymbol{k}$, leads to the generation of the diagonal component. Setting $\hat{\boldsymbol{\alpha}}_{\mathrm{R}} = (0, 0, 1)$, $\hat{\boldsymbol{M}} = (0, -1, 0)$, and $\epsilon_{ij}^{(0)} = \delta_{ij}$ in order to realize the configuration where $\boldsymbol{u}$ and $\boldsymbol{k}$ take parallel or antiparallel, we obtain the dispersion relation for unpolarized waves traveling in x-axis as $\boldsymbol{k}^2 = \frac{\omega^2}{c^2}[1 + \frac{2d_1}{\epsilon_0 \omega}(\hat{\boldsymbol{\alpha}}_{\mathrm{R}} \times \hat{\boldsymbol{M}}) \cdot \boldsymbol{k}]$. The expression of the dispersion relation indicates that the Doppler shift term induces directional dichroism irrespective of light polarization. In the configuration, contribution of symmetric off-diagonal component vanishes. This Doppler shift term, $\boldsymbol{u} \cdot \boldsymbol{k}$ is known as magneto-chiral dichroism, where magnetization $\boldsymbol{M}$ in chiral materials acts as the vector $\boldsymbol{u}$ [85]. In the case of Rashba spin-orbit system, the Rashba field $\boldsymbol{\alpha}_{\mathrm{R}}$, which is invariant under time reversal, cannot induce $\boldsymbol{u}$ on its own. Our result indicates that the combination $\boldsymbol{\alpha}_{\mathrm{R}} \times \boldsymbol{M}$ plays the role of vector $\boldsymbol{u}$, suggesting possible applications of natural magnetic spin-orbit systems to novel optical materials.

Next, we discuss the contribution of Eq. (2.15) in addition to that of Eq. (2.14). The term on the right-hand side of Eq. (2.15) indicates that the quadrupole moment contributes to the symmetric components of the electric permittivity tensor as with the toroidal moment. The diagonal component arising from Eqs. (2.14) and (2.15) results in directional dichroism for linearly-polarized waves. In fact, a contribution of $\epsilon_{yy}^{(Q)}$ in addition to that of $\epsilon_{yy}^{(u)}$ appears in the dispersion relation for E_y having linear polarization in the same configuration as above. On the other hand, the off-diagonal components of Eqs. (2.14) and (2.15) do not contribute to directional dichroism.

From the above discussion, we thus see that the vector $\boldsymbol{u}$ and the quadrupole moment $Q_{\mu\nu}$ play a same role in the context of the dichroism phenomena. Note that $\boldsymbol{u}$ and $Q_{\mu\nu}$ can not affect circularly-polarized waves since these quantities do not induce the antisymmetric components of the electric permittivity tensor.

2.3 Derivation of effective Hamiltonian

In this section, we derive an effective Hamiltonian based on an imaginary-time path-integral formalism [86] and confirm that the $\boldsymbol{E}$-$\boldsymbol{B}$ coupling in the magnetic Rashba conductor is described by $\mathcal{H}_u$ shown in Eq. (2.4) and $\mathcal{H}_Q$ shown in Eq. (2.10). Here, $\hbar = 1$ is used for simplicity, where $\hbar$ is the Planck constant divided by 2π. The system we consider consists of electrons with Rashba interaction and also interaction with magnetization and electromagnetic fields. The electrons are represented using annihilation and creation fields having two spin components, defined on an imaginary time τ, $c(\boldsymbol{r}, \tau)$ and $\bar{c}(\boldsymbol{r}, \tau)$. The Hamiltonian is $H = H_0 + H_{sd} + H_{\rm R} + H_{\rm em}$, where

$$H_0 = \int \mathrm{d}^3 r \left(\frac{1}{2m} |\boldsymbol{\nabla} c|^2 - \mu \bar{c} c \right) \tag{2.17}$$

describes the kinetic energy of conduction electrons measured from the Fermi energy. m is the electron mass and μ is the chemical potential of the system. The second term,

$$H_{sd} = -J_{sd} \int \mathrm{d}^3 r \boldsymbol{M} \cdot (\bar{c} \boldsymbol{\sigma} c) \,, \tag{2.18}$$

is the exchange interaction between the magnetization and conduction-electron spin. J_{sd} is its strength, $\boldsymbol{M}$ is the magnetization vector, and $\boldsymbol{\sigma}$ is the vector of Pauli matrices. The magnetization is treated as spatially uniform and static. We consider a weak *sd*-exchange interaction up to the linear order. $H_{\rm R}$ is the Rashba spin-orbit interaction,

$$H_{\rm R} = \frac{i}{2} \int \mathrm{d}^3 r \boldsymbol{\alpha}_{\rm R} \cdot \bar{c} (\overleftrightarrow{\nabla} \times \boldsymbol{\sigma}) c, \tag{2.19}$$

where $\bar{c} \overleftrightarrow{\nabla} c \equiv \bar{c} \left(\boldsymbol{\nabla} c \right) - \left(\boldsymbol{\nabla} \bar{c} \right) c$. The term $H_{\rm em}$ describes the interaction between the conduction electron and the electromagnetic field, described by a gauge field $\boldsymbol{A}$. Taking into account the term arising from the Rashba spin-orbit interaction, the interaction reads as,

$$H_{\rm em} = - \int \mathrm{d}^3 r \boldsymbol{A} \cdot \left(\frac{ie}{2m} \bar{c} \overleftrightarrow{\nabla} c - \frac{e^2}{2m} \boldsymbol{A} \bar{c} c - e \bar{c} (\boldsymbol{\alpha}_{\rm R} \times \boldsymbol{\sigma}) c \right), \tag{2.20}$$

where $-e$ is the electron charge ($e > 0$). The current density derived from Eq. (2.20) is

$$\begin{aligned} j_i^{\rm tot} &\equiv - \frac{\delta H_{\rm em}}{\delta A_i} \\ &= - j_i - \frac{e^2}{m} A_i \bar{c} c - 2e \sum_{jk} \epsilon_{ijk} \alpha_{{\rm R},j} s_k, \end{aligned} \tag{2.21}$$

where

$$j_i(\boldsymbol{r},\tau) \equiv -\frac{ie}{2m}\bar{c}(\boldsymbol{r},\tau)\overleftrightarrow{\nabla}_i c(\boldsymbol{r},\tau),$$
$$s_\alpha(\boldsymbol{r},\tau) \equiv \frac{1}{2}\bar{c}(\boldsymbol{r},\tau)\sigma_\alpha c(\boldsymbol{r},\tau), \tag{2.22}$$

are the bare electric current density and spin density, respectively.

The effective Hamiltonian for the electromagnetic field, $H_{\rm eff}$, is calculated by integrating the electrons in the partition function [1]

$$\mathcal{Z}[\boldsymbol{A}] = \int \mathcal{D}\bar{c}\mathcal{D}c e^{-\int_0^\beta d\tau L[\bar{c},c,\boldsymbol{A}]} \tag{2.23}$$

as

$$\int_0^\beta \mathrm{d}\tau H_{\rm eff}[\boldsymbol{A}] \equiv -\mathrm{Tr}\ln\mathcal{Z}, \tag{2.24}$$

where $\mathcal{D}$ denotes the path integral, $L = \int \mathrm{d}^3 r \bar{c}\partial_\tau c + H$ is the imaginary-time Lagrangian, and β is the inverse temperature. The partition function is perturbatively calculated to the second order in the gauge field. The result, diagramatically shown in Fig. 2.1, is

$$\begin{aligned}\ln\mathcal{Z} = &-\int_0^\beta \mathrm{d}\tau \int \mathrm{d}^3 r \sum_{\mu\nu} A_\mu A_\nu \frac{e^2}{2m} n_{\rm e}(\boldsymbol{r},\tau)\delta_{\mu\nu} \\ &+ \frac{1}{2}\int_0^\beta \mathrm{d}\tau \int_0^\beta \mathrm{d}\tau' \int \mathrm{d}^3 r \int \mathrm{d}^3 r' \sum_{\mu\nu} A_\mu A_\nu \\ &\times \left[\chi^{\mu\nu}_{jj}(\boldsymbol{r},\boldsymbol{r}',\tau,\tau') + \chi^{\mu\nu}_{sj}(\boldsymbol{r},\boldsymbol{r}',\tau,\tau') + \chi^{\mu\nu}_{js}(\boldsymbol{r},\boldsymbol{r}',\tau,\tau') + \chi^{\mu\nu}_{ss}(\boldsymbol{r},\boldsymbol{r}',\tau,\tau')\right].\end{aligned} \tag{2.25}$$

Here, $n_{\rm e}(\boldsymbol{r},\tau) \equiv \langle \bar{c}(\boldsymbol{r},\tau)c(\boldsymbol{r},\tau)\rangle$ is the electron density, the thermal average $\langle\ \rangle$ is calculated in the equilibrium state determined by $\int_0^\beta d\tau L_0 \equiv \int_0^\beta d\tau[\int \mathrm{d}^3 r \bar{c}\partial_\tau c + H_0 + H_{sd} + H_{\rm R}]$ and

$$\begin{aligned}\chi^{\mu\nu}_{jj}(\boldsymbol{r},\boldsymbol{r}',\tau,\tau') &\equiv \langle j_\mu(\boldsymbol{r},\tau) j_\nu(\boldsymbol{r}',\tau')\rangle, \\ \chi^{\mu\nu}_{sj}(\boldsymbol{r},\boldsymbol{r}',\tau,\tau') &\equiv 2e\sum_{m\alpha}\epsilon_{\mu m\alpha}\alpha_{{\rm R},m}\langle s_\alpha(\boldsymbol{r},\tau) j_\nu(\boldsymbol{r}',\tau')\rangle, \\ \chi^{\mu\nu}_{js}(\boldsymbol{r},\boldsymbol{r}',\tau,\tau') &\equiv 2e\sum_{m\alpha}\epsilon_{\nu m\alpha}\alpha_{{\rm R},m}\langle j_\mu(\boldsymbol{r},\tau) s_\alpha(\boldsymbol{r}',\tau')\rangle, \\ \chi^{\mu\nu}_{ss}(\boldsymbol{r},\boldsymbol{r}',\tau,\tau') &\equiv 4e^2\sum_{mo\alpha\beta}\epsilon_{\mu o\alpha}\epsilon_{\nu m\beta}\alpha_{{\rm R},o}\alpha_{{\rm R},m}\langle s_\alpha(\boldsymbol{r},\tau) s_\beta(\boldsymbol{r}',\tau')\rangle\end{aligned} \tag{2.26}$$

represent the correlation functions of the current and the spin density. The electron

[1] See Appendix E for details of derivation of the partition function in the imaginary-time path-integral formalism.

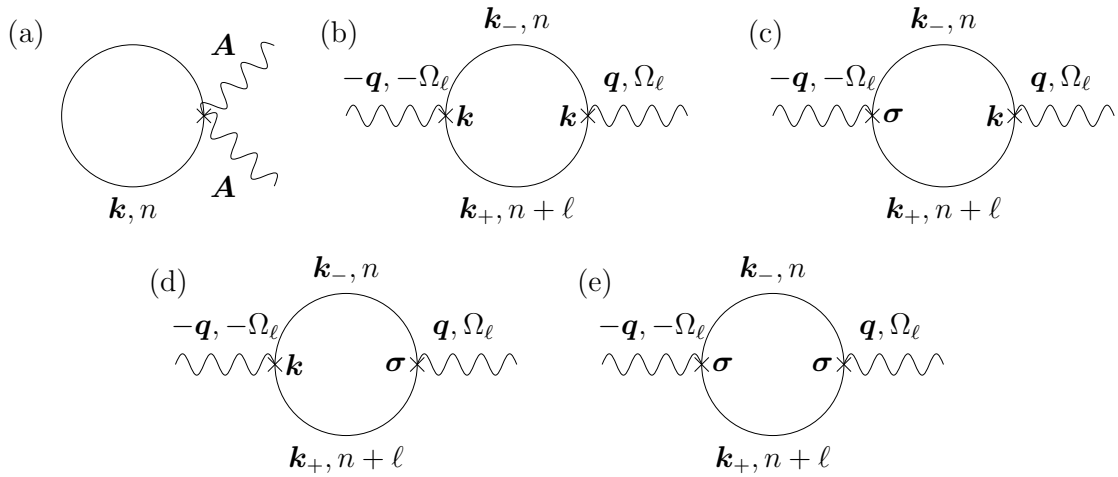

Figure 2.1: The Feynman diagrams for the effective Hamiltonian. Solid lines represent the conducting electrons' Green's function and the wavy lines denote the gauge field, respectively. Diagrams, (a), (b), (c), (d), and (e), correspond to the contributions of $n_{\rm e}$, $\chi^{\mu\nu}_{jj}$, $\chi^{\mu\nu}_{sj}$, $\chi^{\mu\nu}_{js}$, and $\chi^{\mu\nu}_{ss}$ in Eq. (2.25), respectively.

density $n_{\rm e}$ is expressed as

$$n_{\rm e} = -\frac{1}{\beta V}\sum_{n,\boldsymbol{k}} {\rm tr}[\mathscr{G}_{\boldsymbol{k},n,\boldsymbol{M}}], \tag{2.27}$$

where tr is the trace over spin space, V is the volume of the system, and

$$\mathscr{G}_{\boldsymbol{k},n,\boldsymbol{M}} \equiv \frac{1}{i\omega_n - \epsilon_{\boldsymbol{k}} - \boldsymbol{\gamma}_{\boldsymbol{k},\boldsymbol{M}}\cdot\boldsymbol{\sigma} + i\eta{\rm sgn}(\omega_n)} \tag{2.28}$$

is the thermal Green's function for electrons that includes the Rashba and *sd*-exchange interactions. Here, $\boldsymbol{k}$ and $\omega_n \equiv \frac{(2n+1)\pi}{\beta}$ (n is an integer) indicate the wave vector and fermionic thermal frequency, respectively, $\epsilon_{\boldsymbol{k}} = \frac{k^2}{2m} - \mu$ is the electron energy measured from the Fermi energy, and $\boldsymbol{\gamma}_{\boldsymbol{k},\boldsymbol{M}} \equiv \boldsymbol{\gamma}_{\boldsymbol{k}} - J_{sd}\boldsymbol{M}$ with $\boldsymbol{\gamma}_{\boldsymbol{k}} \equiv \boldsymbol{k}\times\boldsymbol{\alpha}_{\rm R}$. We have included a finite electron-elastic-scattering lifetime $\tau_{\rm e}$ as an imaginary part, $\eta \equiv \frac{1}{2\tau_{\rm e}}$, and ${\rm sgn}(\omega_n) \equiv 1$ and -1 for $\omega_n > 0$ and $\omega_n < 0$, respectively. In terms of the Green's function, correlation functions read as

$$\begin{aligned}
\chi^{\mu\nu}_{jj}(\boldsymbol{q}, i\Omega_\ell, \boldsymbol{M}) &= -\frac{e^2}{m^2\beta V}\sum_{n,\boldsymbol{k}} k_\mu k_\nu {\rm tr}[\mathscr{G}_{\boldsymbol{k}_+,n+\ell,\boldsymbol{M}}\mathscr{G}_{\boldsymbol{k}_-,n,\boldsymbol{M}}],\\
\chi^{\mu\nu}_{sj}(\boldsymbol{q}, i\Omega_\ell, \boldsymbol{M}) &= -\frac{e^2}{m\beta V}\sum_{n,\boldsymbol{k}}\sum_{m\alpha} \epsilon_{\mu m\alpha}\alpha_{{\rm R},m}k_\nu {\rm tr}[\sigma_\alpha\mathscr{G}_{\boldsymbol{k}_+,n+\ell,\boldsymbol{M}}\mathscr{G}_{\boldsymbol{k}_-,n,\boldsymbol{M}}],\\
\chi^{\mu\nu}_{js}(\boldsymbol{q}, i\Omega_\ell, \boldsymbol{M}) &= -\frac{e^2}{m\beta V}\sum_{n,\boldsymbol{k}}\sum_{m\alpha} \epsilon_{\nu m\alpha}\alpha_{{\rm R},m}k_\mu {\rm tr}[\mathscr{G}_{\boldsymbol{k}_+,n+\ell,\boldsymbol{M}}\sigma_\alpha\mathscr{G}_{\boldsymbol{k}_-,n,\boldsymbol{M}}],\\
\chi^{\mu\nu}_{ss}(\boldsymbol{q}, i\Omega_\ell, \boldsymbol{M}) &= -\frac{e^2}{\beta V}\sum_{n,\boldsymbol{k}}\sum_{mo\alpha\beta} \epsilon_{\mu o\alpha}\epsilon_{\nu m\beta}\alpha_{{\rm R},o}\alpha_{{\rm R},m} {\rm tr}[\sigma_\alpha\mathscr{G}_{\boldsymbol{k}_+,n+\ell,\boldsymbol{M}}\sigma_\beta\mathscr{G}_{\boldsymbol{k}_-,n,\boldsymbol{M}}],
\end{aligned} \tag{2.29}$$

where $\boldsymbol{k}_\pm \equiv \boldsymbol{k} \pm \frac{\boldsymbol{q}}{2}$. The wave vector and thermal frequency carried by the gauge field are denoted by $\boldsymbol{q}$ and Ω_ℓ, respectively. ($\Omega_\ell \equiv \frac{2\pi\ell}{\beta}$ is a bosonic thermal frequency).

We are interested in a low-energy long-wavelength effective Hamiltonian; hence, we expand the correlation functions given in Eq. (3.17) with respect to $\boldsymbol{q}$. The result up to the linear order of $\boldsymbol{q}$ and $\boldsymbol{M}$ is (see Appendix F)

$$\begin{aligned}\chi^{(1)}_{\mu\nu}(\boldsymbol{q}, i\Omega_\ell, \boldsymbol{M}) &\equiv \chi^{\mu\nu}_{jj} + \chi^{\mu\nu}_{sj} + \chi^{\mu\nu}_{js} + \chi^{\mu\nu}_{ss} \\ &= g_1(i\Omega_\ell)(\boldsymbol{\mathcal{A}}_{\mathrm{R}} \cdot \boldsymbol{q})\delta^\perp_{\mu\nu} + g_2(i\Omega_\ell)(\mathcal{A}_{\mathrm{R},\mu} q_\nu + q_\mu \mathcal{A}_{\mathrm{R},\nu}) \\ &\quad + g_3(i\Omega_\ell)[M^\perp_\mu(\boldsymbol{\alpha}_{\mathrm{R}} \times \boldsymbol{q})_\nu + (\boldsymbol{\alpha}_{\mathrm{R}} \times \boldsymbol{q})_\mu M^\perp_\nu], \end{aligned} \tag{2.30}$$

where $\delta^\perp_{\mu\nu} \equiv \delta_{\mu\nu} - \hat{\alpha}_{\mathrm{R},\mu}\hat{\alpha}_{\mathrm{R},\nu}$, $\hat{\boldsymbol{\alpha}}_{\mathrm{R}} \equiv \boldsymbol{\alpha}_{\mathrm{R}}/|\boldsymbol{\alpha}_{\mathrm{R}}|$ is a unit vector representing the direction of the Rashba field, and $\boldsymbol{M}^\perp \equiv \boldsymbol{M} - (\hat{\boldsymbol{\alpha}}_{\mathrm{R}} \cdot \boldsymbol{M})\hat{\boldsymbol{\alpha}}_{\mathrm{R}}$. We have considered the case where $\boldsymbol{\alpha}_{\mathrm{R}} \cdot \boldsymbol{q} = 0$ depicted in Fig. 1.2 to simplify the angular integration calculation with respect to $\boldsymbol{k}$. This expression otherwise consists of more number of terms. The vector $\boldsymbol{\mathcal{A}}_{\mathrm{R}} \equiv \boldsymbol{\alpha}_{\mathrm{R}} \times \boldsymbol{M}$ represents an effective spin gauge field and a toroidal moment. The coefficients g_1, g_2, and g_3 are defined in Appendix. G.

Eq. (2.30) contributes to directional dichroism as it is linear in $\boldsymbol{q}$. The first and second terms of this equation proportional to g_1 and g_2 indicate that the existence of the toroidal moment governs the anomalous light propagation, whereas the terms proportional to $M^\perp_\mu(\boldsymbol{\alpha}_{\mathrm{R}} \times \boldsymbol{q})_\nu$ and $(\boldsymbol{\alpha}_{\mathrm{R}} \times \boldsymbol{q})_\mu M^\perp_\nu$ represent the contributions arising from the effective quadrupole moment, as shown in the effective theory [21]. The result can be simplified using the gauge invariance of the effective Hamiltonian (see Appendix H). It was observed that $g_1 = -2g_2$ is restricted by the gauge invariance, whereas g_3 is not restricted by this invariance.

Carrying out the analytic continuation, the coefficient, g_1 is calculated. g_1 is written by rewriting the summation over the thermal frequency using the contour integral ($z \equiv i\omega_n$) as

$$\begin{aligned} g_1(i\Omega_\ell) = -2\frac{J_{sd}}{2^4}\left(\frac{e}{m}\right)^2 &\sum_{\boldsymbol{k}} \sum_{\sigma_1\sigma_2\sigma_3\sigma_4} \left(\frac{\gamma_{\boldsymbol{k}}}{\alpha_{\mathrm{R}}}\right)^2 \\ &\times \left[\sigma_1\sigma_2 + \frac{m\alpha^2_{\mathrm{R}}}{\gamma_{\boldsymbol{k}}}(\sigma_2\sigma_3\sigma_4 + 2\sigma_2)\right] \int_C \frac{\mathrm{d}z}{2\pi i} f(z) \mathrm{g}_{\boldsymbol{k},\sigma_1}(z) \mathrm{g}_{\boldsymbol{k},\sigma_2}(z) \\ &\times [\mathrm{g}_{\boldsymbol{k},\sigma_3}(z + i\Omega_\ell)\mathrm{g}_{\boldsymbol{k},\sigma_4}(z + i\Omega_\ell) - \mathrm{g}_{\boldsymbol{k},\sigma_3}(z - i\Omega_\ell)\mathrm{g}_{\boldsymbol{k},\sigma_4}(z - i\Omega_\ell)], \end{aligned} \tag{2.31}$$

where C is a counterclockwise contour surrounding the imaginary axis [87, 88], $\gamma_{\boldsymbol{k}} \equiv |\boldsymbol{\gamma}_{\boldsymbol{k}}|$, $\mathrm{g}_{\boldsymbol{k},\sigma}(z) \equiv [z - \epsilon^\sigma_{\boldsymbol{k}} + i\eta\mathrm{sgn}(\mathrm{Im}[z])]^{-1}$ with $\epsilon^\sigma_{\boldsymbol{k}} = \epsilon_{\boldsymbol{k}} + \sigma\gamma_{\boldsymbol{k}}$ is the Green's function diagonalized in spin space, $\sigma_i = \pm$ ($i = 1 \sim 4$) are the diagonalized spin indices, Im denotes the imaginary part, and $f(z) \equiv (e^{\beta z} + 1)^{-1}$ is the Fermi–Dirac distribution function. We expand the coefficient g_1 with respect to external frequency Ω after the analytic continuation to $\Omega + i0 \equiv i\Omega_\ell$ [87, 88], where $i0$ denotes a small imaginary part. The result up to the linear order in Ω is

$$g_1(\Omega) = 2\Omega g, \tag{2.32}$$

with

$$g \equiv i\frac{J_{sd}}{2^4}\left(\frac{e}{m}\right)^2 \sum_{\boldsymbol{k},\omega}\sum_{\sigma_1\sigma_2\sigma_3\sigma_4}\left(\frac{\gamma_{\boldsymbol{k}}}{\alpha_{\rm R}}\right)^2\left[\sigma_1\sigma_2+\frac{m\alpha_{\rm R}^2}{\gamma_{\boldsymbol{k}}}(\sigma_2\sigma_3\sigma_4+2\sigma_2)\right] \times\left\{\begin{array}{c} f(\omega)[(\mathrm{g}^{\rm r}_{\boldsymbol{k},\omega,\sigma_1}\mathrm{g}^{\rm r}_{\boldsymbol{k},\omega,\sigma_2})\overleftrightarrow{\partial_\omega}(\mathrm{g}^{\rm r}_{\boldsymbol{k},\omega,\sigma_3}\mathrm{g}^{\rm r}_{\boldsymbol{k},\omega,\sigma_4})-c.c.] \\ +f'(\omega)[\mathrm{g}^{\rm a}_{\boldsymbol{k},\omega,\sigma_1}\mathrm{g}^{\rm a}_{\boldsymbol{k},\omega,\sigma_2}\mathrm{g}^{\rm r}_{\boldsymbol{k},\omega,\sigma_3}\mathrm{g}^{\rm r}_{\boldsymbol{k},\omega,\sigma_4}-c.c.] \end{array}\right\}, \tag{2.33}$$

where $\mathrm{g}^{\rm r}_{\boldsymbol{k},\omega,\sigma} \equiv (\omega-\epsilon^\sigma_{\boldsymbol{k}}+i\eta)^{-1}$ and $\mathrm{g}^{\rm a}_{\boldsymbol{k},\omega,\sigma}=(\mathrm{g}^{\rm r}_{\boldsymbol{k},\omega,\sigma})^*$ are the retarded and advanced Green's functions of the conduction electron with wave vector $\boldsymbol{k}$ and angular frequency ω, respectively. $\sum_\omega \equiv \int_{-\infty}^{\infty}\frac{\mathrm{d}\omega}{2\pi}$, $\partial_\omega \equiv \frac{\partial}{\partial\omega}$, $f(\omega)=(e^{\beta\omega}+1)^{-1}$, and $f'(\omega)\equiv\partial_\omega f(\omega)$. g_3 is also given by

$$g_3(\Omega)=\Omega\lambda, \tag{2.34}$$

with

$$\lambda \equiv \frac{i}{2}\frac{J_{sd}}{2^4}\left(\frac{e}{m}\right)^2 \sum_{\boldsymbol{k},\omega}\sum_{\sigma_1\sigma_2\sigma_3\sigma_4}\sigma_1\sigma_2\left(\frac{\gamma_{\boldsymbol{k}}}{\alpha_{\rm R}}\right)^2 \times\left\{\begin{array}{c} f(\omega)[(\mathrm{g}^{\rm r}_{\boldsymbol{k},\omega,\sigma_1}\mathrm{g}^{\rm r}_{\boldsymbol{k},\omega,\sigma_2})\overleftrightarrow{\partial_\omega}(\mathrm{g}^{\rm r}_{\boldsymbol{k},\omega,\sigma_3}\mathrm{g}^{\rm r}_{\boldsymbol{k},\omega,\sigma_4})-c.c.] \\ +f'(\omega)[\mathrm{g}^{\rm a}_{\boldsymbol{k},\omega,\sigma_1}\mathrm{g}^{\rm a}_{\boldsymbol{k},\omega,\sigma_2}\mathrm{g}^{\rm r}_{\boldsymbol{k},\omega,\sigma_3}\mathrm{g}^{\rm r}_{\boldsymbol{k},\omega,\sigma_4}-c.c.] \end{array}\right\}. \tag{2.35}$$

The effective Hamiltonian describing the directional dichroism is finally obtained as

$$H_{\rm eff}=H_{\mathcal{A}_{\rm R}}+H_Q, \tag{2.36}$$

with

$$H_{\mathcal{A}_{\rm R}}=g\int \mathrm{d}^3r\boldsymbol{\mathcal{A}}_{\rm R}\cdot(\boldsymbol{E}\times\boldsymbol{B}), \tag{2.37}$$

$$H_Q=\lambda\int \mathrm{d}^3r\sum_{\mu\nu}Q_{\mu\nu}E_\mu B_\nu, \tag{2.38}$$

where $Q_{\mu\nu}\equiv M^\perp_\mu\alpha_{{\rm R},\nu}$ is the effective quadrupole moment and $\boldsymbol{E}\equiv-\dot{\boldsymbol{A}}$ and $\boldsymbol{B}\equiv\boldsymbol{\nabla}\times\boldsymbol{A}$ are the electric and magnetic fields, respectively.

The effective Hamiltonian of Secs. 2.1 and 2.2, $\mathcal{H}_u+\mathcal{H}_Q$ with $\boldsymbol{u}=\boldsymbol{\mathcal{A}}_{\rm R}$ is thus justified by microscopic derivation based on the imaginary-time path-integral formalism. The toroidal moment thus leads to the Doppler shift and this is the origin of the magnetic Rashba conductor that exhibits directional dichroism discussed in Sec. 2.1.

The coupling constant g consists of terms proportional to $f(\omega)$ and $f'(\omega)$ but it cannot be expressed only in terms of $f'(\omega)$ (Fermi surface term) using integration by parts. The $f'(\omega)$ term represents the contribution arising from the state of electrons in the vicinity of a Fermi surface. The contribution of this term is finite in a metallic system, whereas it does not exist for insulators such as multiferroics. In contrast, the $f(\omega)$ term (Fermi sea term) arises from the equilibrium property of the electrons forming the Fermi sea. The contribution of this term is finite in insulator systems; therefore, directional dichroism can be induced even in broad materials.

2.4 Topological cross-correlation effects and optical responses in Wely semimetal

So far, we have considered the electromagnetic cross-correlation effects in a non-relativistic Rashba spin-orbit system. The cross-correlation effects also occurs in a relativistic spin-orbit system such as 3+1-dimensional Weyl semimetal. It is known that the Weyl semimetal realized in multilayer of topological insulator and magnetic insulator (Ref. [89]) induces topological electromagnetic cross-correlation effects such as anomalous Hall effect and chiral magnetic effect [72]. Recently, Ref. [90] proposed generation mechanism of an electric current by use of an effective magnetic field occurred from a nonlinear effect with respect to an incident electric field.

A Hamiltonian representing Weyl spin-orbit system is made up of two terms, one describing the diagonal components and the other denoting the off-diagonal components (mass term) as [70, 71]

$$\mathcal{H}_{\rm Weyl} = \tau^z(\boldsymbol{\sigma}\cdot\boldsymbol{k}) + \tau^z b_0 + \boldsymbol{\sigma}\cdot\boldsymbol{b}, \tag{2.39}$$

where the first term is the Dirac Hamiltonian being linear in the wave vector $\boldsymbol{k}$ of the Dirac electrons, $\boldsymbol{\tau}$ is the Weyl node degree of freedom, $\boldsymbol{\sigma}$ is the conduction-valence band degree of freedom, b_0 is a constant reflecting the breaking of spatial-inversion symmetry, and $\boldsymbol{b}$ is a constant vector reflecting the breaking of time-reversal invariance. $\mathcal{H}_{\rm Weyl}$ is 4×4 Hamiltonian because of having the Weyl nodes of opposite chirality and conduction-valence band degrees of freedom. By the Fujikawa's method [91], the effective Hamiltonian describing the electromagnetic response of the Weyl system is shown to be [70, 71]

$$H_\theta = \frac{\alpha}{8\pi}\sum_{\mu\nu\alpha\beta}\int \mathrm{d}^3 r\theta(\boldsymbol{r},t)\epsilon^{\mu\nu\alpha\beta}F_{\mu\nu}F_{\alpha\beta}, \tag{2.40}$$

where we set $\hbar = c = \epsilon_0 = 1$, $\alpha \equiv \frac{e^2}{4\pi}$ is the fine structure constant, $\epsilon^{\mu\nu\alpha\beta}$ is a totally antisymmetric tensor, and $F_{\mu\nu} \equiv \partial_\mu A_\nu - \partial_\nu A_\mu$ is the field strength of the electromagnetic field. $\theta(\boldsymbol{r},t) \equiv 2(\boldsymbol{b}\cdot\boldsymbol{r} - b_0 t)$ is the field depending linearly on space $\boldsymbol{r}$ and time t.

Using the fact that $\boldsymbol{E}\cdot\boldsymbol{B} = \frac{1}{4}\sum_{\mu\nu\alpha\beta}\epsilon^{\mu\nu\alpha\beta}F_{\mu\nu}F_{\alpha\beta}$, the effective Hamiltonian, Eq. (2.40), reduces to

$$H_\theta = \frac{\alpha}{2\pi}\int \mathrm{d}^3 r\theta(\boldsymbol{r},t)\boldsymbol{E}\cdot\boldsymbol{B}. \tag{2.41}$$

Maxwell's equations including the above Hamiltonian are given by [76, 77]

$$\begin{aligned}
\boldsymbol{\nabla}\cdot\boldsymbol{E} &= \rho + \frac{\alpha}{\pi}\boldsymbol{\nabla}\cdot(\theta\boldsymbol{B}),\\
\boldsymbol{\nabla}\cdot\boldsymbol{B} &= 0,\\
\boldsymbol{\nabla}\times\boldsymbol{E} &= -\frac{\partial\boldsymbol{B}}{\partial t},\\
\boldsymbol{\nabla}\times\boldsymbol{B} &= \boldsymbol{j} + \frac{\partial\boldsymbol{E}}{\partial t} - \frac{\alpha}{\pi}\frac{\partial}{\partial t}(\theta\boldsymbol{B}) - \frac{\alpha}{\pi}\boldsymbol{\nabla}\times(\theta\boldsymbol{E}),
\end{aligned} \tag{2.42}$$

where ρ represents charge density and $\boldsymbol{j}$ is the charge-current density. Therefore, we see that the total electric and magnetic fields representing the cross-correlation effects become

$$\begin{aligned}\boldsymbol{E}_{\rm tot} \equiv& \boldsymbol{E} + \boldsymbol{P},\\ \boldsymbol{B}_{\rm tot} \equiv& \boldsymbol{B} + \boldsymbol{M},\end{aligned} \tag{2.43}$$

with

$$\begin{aligned}\boldsymbol{P} \equiv& -\frac{\alpha}{\pi}\theta\boldsymbol{B},\\ \boldsymbol{M} \equiv& \frac{\alpha}{\pi}\theta\boldsymbol{E},\end{aligned} \tag{2.44}$$

where $\boldsymbol{P}$ and $\boldsymbol{M}$ are effective electric polarization and effective magnetization, respectively. The electric polarization $\boldsymbol{P}$ leads to a polarization current $\boldsymbol{j}_P \equiv \partial_t \boldsymbol{P}$ while the magnetization $\boldsymbol{M}$ gives rise to a magnetization current as $\boldsymbol{j}_M \equiv -\boldsymbol{\nabla}\times\boldsymbol{M}$. We thus see that a total electric current defined as $\boldsymbol{j}_{\rm tot} \equiv \boldsymbol{j}_P + \boldsymbol{j}_M$ is induced as shown below [72].

$$\boldsymbol{j}_{\rm tot} = \frac{\alpha}{\pi}(-b_0\boldsymbol{B} + \boldsymbol{b}\times\boldsymbol{E}). \tag{2.45}$$

In the case of the system with broken spatial-inversion symmetry by b_0, the current parallel to an applied magnetic field arises (chiral magnetic effect). On the other hand, in the case of the system with broken time-reversal symmetry by $\boldsymbol{b}$, the current perpendicular to an applied electric field is induced (anomalous Hall effect). In terms of an electric permittivity tensor, these effects are represented by antisymmetric off-diagonal components which only affect circular waves as [31, 92]

$$\epsilon_{\mu\nu} = \delta_{\mu\nu} + i\frac{2\alpha}{\pi\omega^2}\sum_l \epsilon_{\mu l\nu}(b_0 k_l + b_l\omega). \tag{2.46}$$

Here, we used the relationship between the electric permittivity tensor and an electric conductivity tensor, $\epsilon_{\mu\nu} = \delta_{\mu\nu} + \frac{i}{\omega}\sigma_{\mu\nu}$, where ω is angular frequency of electromagnetic fields and $\sigma_{\mu\nu}$ is the electric conductivity tensor. In fact, from Eqs. (2.42) and (2.46), the characteristic equation for plane waves traveling along in z-axis is given by

$$\begin{vmatrix} \boldsymbol{k}^2 - \omega^2 & -\omega^2\epsilon_{xy} & 0\\ \omega^2\epsilon_{xy} & \boldsymbol{k}^2 - \omega^2 & 0\\ 0 & 0 & -\omega^2 \end{vmatrix} = 0. \tag{2.47}$$

The dispersion relation for E_x and E_y thus read as

$$\boldsymbol{k}^2 = \omega^2\left[1 \pm \frac{2\alpha}{\pi\omega^2}(b_0|\boldsymbol{k}| + b\omega)\right], \tag{2.48}$$

where $\pm$ stands for a circular polarization of light and we choose $\boldsymbol{b} = (0, 0, b)$. Therefore, the term with b_0 results in the natural optical activity where the electric

field $\boldsymbol{E}$ rotates around the direction of $\boldsymbol{k}$ (Ref. [67]) while the term with $\boldsymbol{b}$ results in the Faraday effect where $\boldsymbol{E}$ rotates around the direction of $\boldsymbol{b}$ [92, 93] when circularly-polarized waves are applied.

Comparing Eq. (2.13) with Eq. (2.46), the field θ which dose not induce the symmetric component turns out to play a different role from the toroidal moment and the quadrupole moment in the context of the anomalous optical responses. Especially, the Doppler shift term does not appear in the Weyl system, as the system is Lorentz invariant.

Chapter 3

Theory of optical activity in Weyl spin-orbit system

Chirality or handedness in condensed matter induces anomalous optical responses such as natural optical activity, rotation of the plane of light polarization, as a result of breaking of spatial-inversion symmetry. In this Chapter, optical properties of a Weyl spin-orbit system with quadratic dispersion, a typical chiral system invariant under time-reversal, are investigated theoretically by deriving an effective Hamiltonian based on an imaginary-time path-integral formalism. We show that the effective Hamiltonian can be indeed written in terms of an optical chirality order parameter suggested by Lipkin [74]. The natural optical activity is discussed based on the Hamiltonian.

3.1 Phenomenological study: Effective Hamiltonian approach

Let us discuss the effective Hamiltonian for electromagnetic fields in the Weyl spin-orbit system from the symmetry point of view.

In vacuum, the effective Hamiltonian of electromagnetic field is [75]

$$H = \int \mathrm{d}^3 r \frac{1}{2} \left(\epsilon_0 |\boldsymbol{E}|^2 + \frac{1}{\mu_0} |\boldsymbol{B}|^2 \right), \tag{3.1}$$

where ϵ_0 and μ_0 are the electric permittivity and magnetic permeability of the vacuum. When coupled to electron system lacking spatial-inversion symmetry, an interaction linear both in $\boldsymbol{E}$ and $\boldsymbol{B}$ is expected to arise in the form

$$H_{EB} = g \int \mathrm{d}^3 r (\boldsymbol{B} \cdot \dot{\boldsymbol{E}} - \boldsymbol{E} \cdot \dot{\boldsymbol{B}}) \equiv \frac{2g}{\epsilon_0} C_\chi, \tag{3.2}$$

where g is a constant reflecting the breaking of spatial-inversion symmetry and C_χ is an optical chirality order parameter defined in Refs. [94, 95].

Here, we show that the interaction of Eq. (3.2) leads to optical activity.

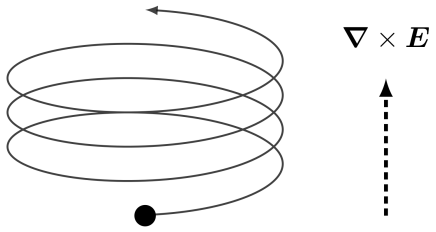

Figure 3.1: Schematic illustration of charged particle's helical motion under the effect of $g\boldsymbol{\nabla}\times\boldsymbol{E}$. Filled circle and solid arrow stand for the particle and its orbital motion, respectively.

Maxwell's equations (equation of motion) including H_{EB} are given by

$$\begin{aligned}\boldsymbol{\nabla}\cdot\boldsymbol{E} =&\frac{\rho}{\epsilon_0}+\frac{g}{\epsilon_0}\boldsymbol{\nabla}\cdot\dot{\boldsymbol{B}},\\ \boldsymbol{\nabla}\times\boldsymbol{B} =&\mu_0\boldsymbol{j}+\epsilon_0\mu_0\frac{\partial\boldsymbol{E}}{\partial t}-\mu_0 g\frac{\partial^2\boldsymbol{B}}{\partial t^2}+\mu_0 g\boldsymbol{\nabla}\times\dot{\boldsymbol{E}},\end{aligned}\tag{3.3}$$

where ρ represents the charge density and $\boldsymbol{j}$ is the charge-current density. The condition of the absence of monopole and the Faraday's induction law are not changed because of U(1) gauge symmetry. From Eq. (3.3), we obtain the electric and magnetic fields including the cross-correlation effect due to Eq. (3.2) as

$$\begin{aligned}\boldsymbol{E}_{\rm tot} \equiv&\boldsymbol{E}-\frac{g}{\epsilon_0}\dot{\boldsymbol{B}},\\ \boldsymbol{B}_{\rm tot} \equiv&\boldsymbol{B}-\mu_0 g\dot{\boldsymbol{E}}.\end{aligned}\tag{3.4}$$

The above expressions are indeed identical to Eq. (1.37) suggested by Ref [62] in the context of the optical activity for circularly-polarized waves. Using $\dot{\boldsymbol{B}} = -\boldsymbol{\nabla}\times\boldsymbol{E}$, $\boldsymbol{E}_{\rm tot}$ in Eq. (3.4) is rewritten as

$$\boldsymbol{E}_{\rm tot} =\boldsymbol{E}+\frac{g}{\epsilon_0}\boldsymbol{\nabla}\times\boldsymbol{E}.\tag{3.5}$$

The equation (3.5) clearly describes a chiral nature of the system. In fact, it indicates that the electric field acquires an additional component proportional to its rotation, $\boldsymbol{\nabla}\times\boldsymbol{E}$. When a charge undergoes a circular motion by $\boldsymbol{E}(\boldsymbol{r})$, therefore, the motion is drifted in the perpendicular direction due to the term $g\boldsymbol{\nabla}\times\boldsymbol{E}$, resulting in a helical motion shown in Fig. 3.1. This helical motion gives rise to optical activities.

In fact, we see directly that Eq. (3.4) results in the optical activity for circularly-polarized waves by deriving the dispersion relation of light. From Eq. (3.3), the wave equation in the medium reads

$$\sum_\nu[c^2(\boldsymbol{k}^2\delta_{\mu\nu}-k_\mu k_\nu)-\omega^2\epsilon_{\mu\nu}]E_\nu =0,\tag{3.6}$$

where c is the light velocity in vacuum, $\boldsymbol{k}$ and ω are the wave vector and angular frequency of electromagnetic waves, respectively, and

$$\epsilon_{\mu\nu} \equiv \delta_{\mu\nu} + i\frac{g}{\epsilon_0}\sum_l \epsilon_{\mu l\nu} k_l, \tag{3.7}$$

is an electric permittivity tensor having the antisymmetric off-diagonal component linear in $\boldsymbol{k}$ due to the violation of spatial-inversion symmetry [84, 85]. Here $\epsilon_{\mu l\nu}$ is a totally antisymmetric tensor. Since Eqs. (3.6) and (3.7) give the characteristic equation for plane waves traveling along in z-axis of the form

$$\begin{vmatrix} c^2\boldsymbol{k}^2 - \omega^2 & -\omega^2\epsilon_{xy} & 0 \\ \omega^2\epsilon_{xy} & c^2\boldsymbol{k}^2 - \omega^2 & 0 \\ 0 & 0 & -\omega^2 \end{vmatrix} = 0, \tag{3.8}$$

we obtain a dispersion relation,

$$\boldsymbol{k}^2 = \frac{\omega^2}{c^2}\left[1 \pm \frac{g}{\epsilon_0}|\boldsymbol{k}|\right], \tag{3.9}$$

where $\pm$ stands for the sense of circular polarization. Therefore, the existence of the optical chirality order parameter leads to a rotation of the electric field in a plane perpendicular to the incident direction, namely, circular dichroism, as pointed out in Ref. [96].

Originally, the optical chirality order parameter was mathematically introduced to describe the solution of Maxwell's equations in order to explore conserved physical quantities reflecting the symmetry of electromagnetic fields [94]. Lipkin called it zilch, meaning that it has no physical effects. The quantity is revisited recently as it determines the polarization of circularly-polarized light [97, 98]. The cross-correlation effects was phenomenologically discussed in terms of the optical chirality in Ref. [95]. Until now, however, the optical chirality has not been discussed based on a microscopic ground. The aim of the present study is to show that the optical chirality indeed appears in the effective Hamiltonian by an imaginary-time path-integral formalism, and present a microscopic scenario on how the optical chirality leads to circular dichroism.

3.2 Derivation of effective Hamiltonian

In this section, we derive the effective Hamiltonian based on the imaginary-time path-integral formalism [86]. We set $\hbar = 1$ for simplicity, where $\hbar$ is the Planck constant divided by 2π. We consider an electron system having the Weyl spin-orbit interaction under the effect of electromagnetic fields described by the gauge field $\boldsymbol{A}$. In the field-representation, the conduction electrons are characterized by two-component annihilation and creation fields, $c(\boldsymbol{r}, \tau)$ and $\bar{c}(\boldsymbol{r}, \tau)$, with spin up and down along the z-axis, where c and $\bar{c}$ are defined on an imaginary time τ. The

imaginary-time Lagrangian of the system thus reads $L[\bar{c}, c, \boldsymbol{A}] = L_0 + L_A$, where

$$L_0(\tau) \equiv \int \mathrm{d}^3 r \bar{c} \left[\frac{\partial}{\partial \tau} - \left(\frac{\boldsymbol{\nabla}^2}{2m} + \mu \right) + \frac{i\lambda}{2} (\overleftrightarrow{\nabla} \cdot \boldsymbol{\sigma}) \right] c, \tag{3.10}$$

$$L_A(\tau) \equiv - \int \mathrm{d}^3 r \boldsymbol{A} \cdot \left(\frac{ie}{2m} \bar{c} \overleftrightarrow{\nabla} c - \frac{e^2}{2m} \boldsymbol{A} \bar{c} c + e\lambda \bar{c} \boldsymbol{\sigma} c \right). \tag{3.11}$$

Here m is the electron mass, μ is the chemical potential of the system, λ stands for the coupling constant of the Weyl spin-orbit interaction, $\boldsymbol{\sigma}$ is the vector of Pauli matrices, $\bar{c} \overleftrightarrow{\nabla} c \equiv \bar{c} (\boldsymbol{\nabla} c) - (\boldsymbol{\nabla} \bar{c})\, c$, and $-e$ is the electron charge ($e > 0$). The effective Hamiltonian for the electromagnetic field $H_{\mathrm{eff}}[\boldsymbol{A}]$ is defined as

$$\int_0^\beta \mathrm{d}\tau H_{\mathrm{eff}}[\boldsymbol{A}] \equiv -\mathrm{Tr} \ln \mathcal{Z}[\boldsymbol{A}], \tag{3.12}$$

where $\mathcal{Z}$ is the partition function in path-integral representation and β denotes the inverse temperature. Equation (3.12) is calculated by integrating out the conduction electrons in the partition function as

$$\mathcal{Z}[\boldsymbol{A}] = \int \mathcal{D}\bar{c}\mathcal{D}c e^{-\int_0^\beta d\tau L[\bar{c}, c, \boldsymbol{A}]}, \tag{3.13}$$

where $\mathcal{D}$ stands for the path-integral. By carrying out the path integral over the electrons, the contribution to the second order in the gauge field reads (diagrammatically shown in Fig. 3.2)

$$\begin{aligned} \ln \mathcal{Z} = &- \int_0^\beta \mathrm{d}\tau \int \mathrm{d}^3 r \sum_{\mu\nu} A_\mu A_\nu \frac{e^2}{2m} n_{\mathrm{e}}(\boldsymbol{r}, \tau) \delta_{\mu\nu} \\ &+ \frac{1}{2} \int_0^\beta \mathrm{d}\tau \int_0^\beta \mathrm{d}\tau' \int \mathrm{d}^3 r \int \mathrm{d}^3 r' \sum_{\mu\nu} A_\mu A_\nu \chi_{jj}^{\mu\nu}(\boldsymbol{r}, \boldsymbol{r}', \tau, \tau'). \end{aligned} \tag{3.14}$$

Here $n_{\mathrm{e}}(\boldsymbol{r}, \tau) \equiv \langle \bar{c}(\boldsymbol{r}, \tau) c(\boldsymbol{r}, \tau) \rangle$ is the electron density and

$$\chi_{jj}^{\mu\nu}(\boldsymbol{r}, \boldsymbol{r}', \tau, \tau') \equiv \langle \tilde{j}_\mu(\boldsymbol{r}, \tau) \tilde{j}_\nu(\boldsymbol{r}', \tau') \rangle \tag{3.15}$$

represents the current-current correlation function. The total electric current is denoted by

$$\tilde{j}_\mu = - j_\mu + 2e\lambda s_\mu, \tag{3.16}$$

where $\boldsymbol{j} \equiv -\frac{ie}{2m} \bar{c} \overleftrightarrow{\nabla} c$ and $\boldsymbol{s} \equiv \frac{1}{2} \bar{c} \boldsymbol{\sigma} c$ are the bare electric current density and electron spin density, respectively. The thermal average $\langle\ \rangle$ in Eq. (F.9) is calculated in the equilibrium state determined by the Lagrangian $L_0(\tau)$. Using Wick's theorem, the electron density and the correlation function are expressed as $n_{\mathrm{e}} = -\frac{1}{\beta V} \sum_{n,\boldsymbol{k}} \mathrm{tr}[\mathscr{G}_{\boldsymbol{k},n}]$ and

$$\chi_{jj}^{\mu\nu}(\boldsymbol{q}, i\Omega_\ell) = -\frac{e^2}{\beta V} \sum_{n,\boldsymbol{k}} \mathrm{tr}[\tilde{v}_{\boldsymbol{k},\mu} \mathscr{G}_{\boldsymbol{k}_+, n+\ell} \tilde{v}_{\boldsymbol{k},\nu} \mathscr{G}_{\boldsymbol{k}_-, n}], \tag{3.17}$$

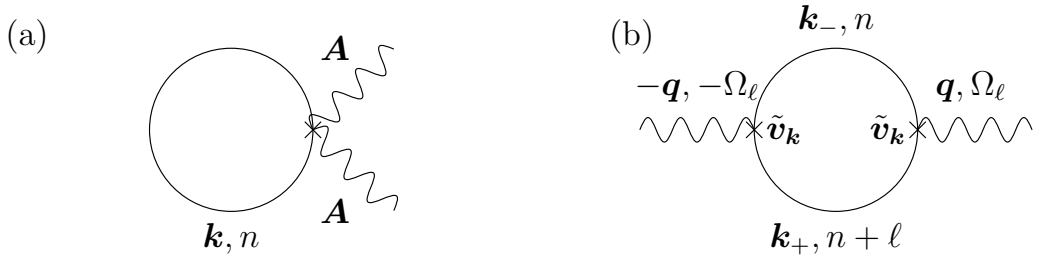

Figure 3.2: Diagrammatic representation of the contribution to the effective Hamiltonian. Solid lines represent the thermal Green's function for electron and the wavy lines denote the gauge field, respectively. Diagrams, (a) and (b), correspond to the contributions of $n_{\rm e}$ and $\chi^{\mu\nu}_{jj}$ in Eq. (3.14), respectively.

respectively, where $\tilde{\boldsymbol{v}}_{\boldsymbol{k}} \equiv \boldsymbol{v} - \lambda\boldsymbol{\sigma}$ with $\boldsymbol{v} \equiv \frac{\boldsymbol{k}}{m}$, tr is the trace over spin space, V is the volume of the system, and

$$\mathscr{G}_{\boldsymbol{k},n} \equiv \frac{1}{i\omega_n - \epsilon_{\boldsymbol{k}} - \boldsymbol{\gamma}_{\boldsymbol{k}}\cdot\boldsymbol{\sigma} + i\eta\mathrm{sgn}(\omega_n)} \tag{3.18}$$

is the 2×2 thermal Green's function for electrons. It includes the Weyl spin-orbit interaction and a finite electron-elastic-scattering lifetime $\tau_{\rm e}$ as $\eta \equiv \frac{1}{2\tau_{\rm e}}$, and $\mathrm{sgn}(\omega_n) \equiv 1$ and -1 for $\omega_n > 0$ and $\omega_n < 0$, respectively. Here $\boldsymbol{k}_\pm \equiv \boldsymbol{k} \pm \frac{\boldsymbol{q}}{2}$, $\epsilon_{\boldsymbol{k}} = \frac{k^2}{2m} - \mu$ is the electron energy measured from the Fermi energy, $\boldsymbol{\gamma}_{\boldsymbol{k}} \equiv -\lambda\boldsymbol{k}$, and $\boldsymbol{k}$ and $\omega_n \equiv \frac{(2n+1)\pi}{\beta}$ with n being an integer are the wave vector and fermionic thermal frequency of the conduction electron, respectively. The wave vector and thermal frequency carried by the gauge field are denoted by $\boldsymbol{q}$ and $\Omega_\ell \equiv \frac{2\pi\ell}{\beta}$ with ℓ being an integer, respectively.

Since we are interested in the effective Hamiltonian in the long-wavelength and low-energy region, we expand the correlation functions Eq. (3.17) with respect to $\boldsymbol{q}$. Up to the first order of $\boldsymbol{q}$, Eq. (3.17) reduces to (see Appendix I)

$$\chi^{\mu\nu}_{jj}(\boldsymbol{q}, i\Omega_\ell) \simeq \chi^{\mu\nu}_{jj}(\boldsymbol{q}=0, i\Omega_\ell) - ig(i\Omega_\ell)\sum_\rho \epsilon_{\mu\rho\nu}q_\rho, \tag{3.19}$$

with

$$\begin{aligned} g(i\Omega_\ell) \equiv{}& \frac{e^2\lambda^3}{24}\sum_{\boldsymbol{k}}\sum_{\sigma_1\sigma_2\sigma_3}\xi_{\boldsymbol{k},\sigma_1\sigma_2\sigma_3} \\ &\times\left(-\frac{1}{\beta}\right)\sum_n \mathrm{g}_{\boldsymbol{k},n,\sigma_1}\mathrm{g}_{\boldsymbol{k},n,\sigma_2}(\mathrm{g}_{\boldsymbol{k},n+\ell,\sigma_3} + \mathrm{g}_{\boldsymbol{k},n-\ell,\sigma_3}), \end{aligned} \tag{3.20}$$

where

$$\xi_{\boldsymbol{k},\sigma_1\sigma_2\sigma_3} \equiv \frac{k}{\lambda m}(\sigma_3 - 3\sigma_1\sigma_2\sigma_3) + 3 - (\sigma_1\sigma_2 + 2\sigma_2\sigma_3). \tag{3.21}$$

Here $\mathrm{g}_{\boldsymbol{k},n,\sigma} \equiv \left[i\omega_n - \epsilon^\sigma_{\boldsymbol{k}} + i\eta\mathrm{sgn}(\omega_n)\right]^{-1}$ with $\epsilon^\sigma_{\boldsymbol{k}} = \epsilon_{\boldsymbol{k}} + \sigma\lambda|\boldsymbol{k}|$ is the Green's function diagonalized in the spin space and $\sigma_i = \pm 1$ (i=1$\sim$3) is the diagonalized spin index.

$\chi^{\mu\nu}_{jj}(\boldsymbol{q}=0)$ and the coefficient g on the right-hand side of Eq. (3.19) are calculated by the analytic continuation. We first show that the first term with $\boldsymbol{q}=0$ is irrelevant. Expanding $\chi^{\mu\nu}_{jj}(\boldsymbol{q}=0)$ with respect to the external frequency Ω defined by the analytic continuation to $\Omega+i\delta\equiv i\Omega_\ell$ [87,88], where δ is a small positive imaginary part, the result up to the second order in Ω reduces to

$$\chi^{\mu\nu}_{jj}(\boldsymbol{q}=0,\Omega+i\delta)\simeq\chi^{\mu\nu,\Omega^0}_{jj}+\chi^{\mu\nu,\Omega^1}_{jj}+\chi^{\mu\nu,\Omega^2}_{jj}. \tag{3.22}$$

The first term in the above equation is $\chi^{\mu\nu,\Omega^0}_{jj}=-\frac{e^2}{m}n_{\rm e}\delta_{\mu\nu}$; hence, the contribution of $\chi^{\mu\nu,\Omega^0}_{jj}$ and that of $n_{\rm e}$ shown in Eq. (2.25) cancel each other, as is required by the gauge invariance. The second term on the right-hand side of Eq. (3.22), $\chi^{\mu\nu,\Omega^1}_{jj}$, is a term with $i\Omega\delta_{\mu\nu}$, but we drop the term proportional to $i\Omega A_\mu(-\Omega)A_\mu(\Omega)$ by noting the fact that $\int {\rm d}t A_\mu\dot{A}_\mu=0$. In Eq. (3.22), there appear the odd orders with respect to Ω, but these terms also become total differential with respect to time. The third term on the right-hand side of Eq. (3.22), $\chi^{\mu\nu,\Omega^2}_{jj}$, gives rise to a term with $\Omega^2\delta_{\mu\nu}$, which represents renormalization of the electric permittivity ϵ_0 and we do not consider it further. The correlation function, Eq. (3.19), is therefore dominated by the $\boldsymbol{q}$-linear contribution with a coefficient $g(i\Omega_\ell)$,

$$\chi^{\mu\nu}_{jj}(\boldsymbol{q},i\Omega_\ell)\simeq -ig(i\Omega_\ell)\sum_\rho\epsilon_{\mu\rho\nu}q_\rho. \tag{3.23}$$

By rewriting the summation over the thermal frequency using the contour integral ($z\equiv i\omega_n$), Eq. (3.20) becomes

$$\begin{aligned} g(i\Omega_\ell)=&\frac{e^2\lambda^3}{24}\sum_{\boldsymbol{k}}\sum_{\sigma_1\sigma_2\sigma_3}\xi_{\boldsymbol{k},\sigma_1\sigma_2\sigma_3}\\ &\int_C\frac{{\rm d}z}{2\pi i}f(z){\rm g}_{\boldsymbol{k},\sigma_1}(z){\rm g}_{\boldsymbol{k},\sigma_2}(z)[{\rm g}_{\boldsymbol{k},\sigma_3}(z+i\Omega_\ell)+{\rm g}_{\boldsymbol{k},\sigma_3}(z-i\Omega_\ell)], \end{aligned} \tag{3.24}$$

where C is a counterclockwise contour surrounding the imaginary axis [87,88], and ${\rm g}_{\boldsymbol{k},\sigma}(z)\equiv[z-\epsilon^\sigma_{\boldsymbol{k}}+i\eta{\rm sgn}({\rm Im}[z])]^{-1}$, $f(z)\equiv(e^{\beta z}+1)^{-1}$ is the Fermi–Dirac distribution function, and Im is the imaginary part. The retarded and advanced Green's function are defined as ${\rm g}^{\rm r}_{\boldsymbol{k},\omega,\sigma}\equiv{\rm g}_{\boldsymbol{k},\sigma}(\omega+i\delta)$ and ${\rm g}^{\rm a}_{\boldsymbol{k},\omega,\sigma}\equiv{\rm g}_{\boldsymbol{k},\sigma}(\omega-i\delta)$, respectively, where ω is an angular frequency of conduction electrons. Expanding g with respect to Ω after the analytic continuation, the result up to the order of Ω^2 reduces to

$$g(\Omega+i\delta)\simeq g^{(0)}+i\Omega g^{(1)}+\Omega^2 g^{(2)}, \tag{3.25}$$

with

$$
\begin{aligned}
g^{(0)} &\equiv \frac{e^2\lambda^3}{6}\sum_{\boldsymbol{k},\omega}\sum_{\sigma_1\sigma_2\sigma_3}\xi_{\boldsymbol{k},\sigma_1\sigma_2\sigma_3}f(\omega)\mathrm{Im}[\mathrm{g}^{\mathrm{r}}_{\boldsymbol{k},\omega,\sigma_1}\mathrm{g}^{\mathrm{r}}_{\boldsymbol{k},\omega,\sigma_2}\mathrm{g}^{\mathrm{r}}_{\boldsymbol{k},\omega,\sigma_3}],\\
g^{(1)} &\equiv \frac{e^2\lambda^3}{12}\sum_{\boldsymbol{k},\omega}\sum_{\sigma_1\sigma_2\sigma_3}\xi_{\boldsymbol{k},\sigma_1\sigma_2\sigma_3}f'(\omega)\mathrm{Re}[\mathrm{g}^{\mathrm{r}}_{\boldsymbol{k},\omega,\sigma_1}\mathrm{g}^{\mathrm{r}}_{\boldsymbol{k},\omega,\sigma_2}(\mathrm{g}^{\mathrm{r}}_{\boldsymbol{k},\omega,\sigma_3}-\mathrm{g}^{\mathrm{a}}_{\boldsymbol{k},\omega,\sigma_3})],\\
g^{(2)} &\equiv -i\frac{e^2\lambda^3}{12}\sum_{\boldsymbol{k},\omega}\sum_{\sigma_1\sigma_2\sigma_3}\xi_{\boldsymbol{k},\sigma_1\sigma_2\sigma_3}\\
&\quad\times\left\{\begin{array}{c}
2if(\omega)\mathrm{Im}\left[\begin{array}{c}\mathrm{g}^{\mathrm{r}}_{\boldsymbol{k},\omega,\sigma_1}\mathrm{g}^{\mathrm{r}}_{\boldsymbol{k},\omega,\sigma_2}\mathrm{g}^{\mathrm{r}}_{\boldsymbol{k},\omega,\sigma_3}\\ \times[(\mathrm{g}^{\mathrm{r}}_{\boldsymbol{k},\omega,\sigma_1})^2+(\mathrm{g}^{\mathrm{r}}_{\boldsymbol{k},\omega,\sigma_2})^2\\ +(\mathrm{g}^{\mathrm{r}}_{\boldsymbol{k},\omega,\sigma_3})^2+\mathrm{g}^{\mathrm{r}}_{\boldsymbol{k},\omega,\sigma_1}\mathrm{g}^{\mathrm{r}}_{\boldsymbol{k},\omega,\sigma_2}]\end{array}\right]\\
-f'(\omega)\left[\begin{array}{l}\mathrm{g}^{\mathrm{a}}_{\boldsymbol{k},\omega,\sigma_1}\mathrm{g}^{\mathrm{a}}_{\boldsymbol{k},\omega,\sigma_2}(\mathrm{g}^{\mathrm{r}}_{\boldsymbol{k},\omega,\sigma_3})^2\\ +(\mathrm{g}^{\mathrm{r}}_{\boldsymbol{k},\omega,\sigma_1})^2\mathrm{g}^{\mathrm{r}}_{\boldsymbol{k},\omega,\sigma_2}\mathrm{g}^{\mathrm{a}}_{\boldsymbol{k},\omega,\sigma_3}\\ +\mathrm{g}^{\mathrm{r}}_{\boldsymbol{k},\omega,\sigma_1}(\mathrm{g}^{\mathrm{r}}_{\boldsymbol{k},\omega,\sigma_2})^2\mathrm{g}^{\mathrm{a}}_{\boldsymbol{k},\omega,\sigma_3}\end{array}\right]
\end{array}\right\},
\end{aligned}
\tag{3.26}
$$

where $\mathrm{g}^{\mathrm{r}}_{\boldsymbol{k},\omega,\sigma}\equiv(\omega-\epsilon^{\sigma}_{\boldsymbol{k}}+i\eta)^{-1}$, $\mathrm{g}^{\mathrm{a}}_{\boldsymbol{k},\omega,\sigma}=(\mathrm{g}^{\mathrm{r}}_{\boldsymbol{k},\omega,\sigma})^*$, Re is the real part, $f(\omega)$=$(e^{\beta\omega}+1)^{-1}$, and $f'(\omega)\equiv\frac{\partial}{\partial\omega}f(\omega)$. The result can be simplified using the gauge invariance which impose $g^{(0)}=0$. The second term on the right-hand side of Eq. (3.25), the Ω-linear term, generally arises from integrating out fermions coupled to bosons [99], and gives rise to a term with $\boldsymbol{E}\cdot\boldsymbol{B}$, where $\boldsymbol{E}\equiv-\dot{\boldsymbol{A}}$ and $\boldsymbol{B}\equiv\boldsymbol{\nabla}\times\boldsymbol{A}$ are the electric and magnetic fields, respectively. However, we drop the term because $\boldsymbol{E}\cdot\boldsymbol{B}=\frac{1}{4}\sum_{\mu\nu\alpha\beta}\epsilon^{\mu\nu\alpha\beta}F_{\mu\nu}F_{\alpha\beta}$ reduces to a surface term by the divergence theorem, where $\epsilon^{\mu\nu\alpha\beta}$ is a totally antisymmetric tensor, $F_{\mu\nu}\equiv\partial_\mu A_\nu-\partial_\nu A_\mu$ is the field strength of the electromagnetic field. We thus have $g\sim\Omega^2 g^{(2)}$ and the effective Hamiltonian finally turns out to be Eq. (3.2) with $g=\frac{g^{(2)}}{4}$.

Chapter 4

Conclusions

In Chapter 2, we have derived an effective Hamiltonian describing directional dichroism in a magnetic Rashba conductor, and showed that it is made up of a toroidal-moment term and a quadrupole-moment term, as in insulator multiferroics. The toroidal-moment term is given by the vector coupling between the toroidal moment and the Poynting vector, such that this term leads to directional dichroism irrespective of light polarization as a result of the Doppler shift. Furthermore, the quadrupole-moment term induces directional dichroism when linearly-polarized waves are applied. The microscopic analysis done in this study indicates that the toroidal moment plays the role of an effective vector potential for light, causing dichroism as a result of the Doppler shift. The effective Hamiltonian approach clearly shows that electromagnetic cross-correlation effects in the magnetic Rashba system is qualitatively distinct from those in relativistic Weyl systems (3+1dimensional Weyl semimetals) described by topological θ-term.

Using an imaginary-time path-integral formalism, we derived an effective Hamiltonian of the electromagnetic fields in terms of an optical chirality order parameter in a Weyl spin-orbit system having quadratic dispersion in Chapter 3. The effective Hamiltonian approach clearly revealed that natural optical activity in the system is due to the emergence of the optical chirality order parameter.

Appendix A

Edelstein Effect and inverse Edelstein Effect

A.1 Microscopic calculation of Edelstein effect

By calculating a magnetization induced by Edelstein effect by use of Keldysh Green's function method [100], we derive Eq. (1.13). For simplicity, we set $\hbar = 1$. In the second quantized representation, the Lagrangian we consider is given by

$$\begin{aligned} L &= L_0 + L_A^{(1)} \\ L_0 &\equiv \int \mathrm{d}^3 r c^\dagger \left[i\frac{\partial}{\partial t} + \left(\frac{\boldsymbol{\nabla}^2}{2m} + \epsilon_\mathrm{F} \right) - \frac{i}{2}\boldsymbol{\alpha}_\mathrm{R} \cdot (\overleftrightarrow{\nabla} \times \boldsymbol{\sigma}) \right] c, \\ L_A^{(1)} &\equiv \int \mathrm{d}^3 r \boldsymbol{A} \cdot \left[\frac{ie}{2m} c^\dagger \overleftrightarrow{\nabla} c - \frac{e^2}{2m} \boldsymbol{A} c^\dagger c - e c^\dagger (\boldsymbol{\alpha}_\mathrm{R} \times \boldsymbol{\sigma}) c \right], \end{aligned} \tag{A.1}$$

where $c^\dagger$ and c are the conduction electron's creation and annihilation operators having two spin components, respectively, m is the electron mass, ϵ_F is the Fermi energy of the system, $\boldsymbol{\sigma}$ is the vector of Pauli matrices, $\boldsymbol{\alpha}_\mathrm{R}$ is the Rashba field representing the strength and direction of the Rashba spin-orbit interaction, $-e$ is the electron charge ($e > 0$), and $c^\dagger \overleftrightarrow{\nabla} c \equiv c^\dagger (\boldsymbol{\nabla} c) - \left(\boldsymbol{\nabla} c^\dagger\right) c$. The term $L_A^{(1)}$ is the interaction between the conduction electron and the applied electric field described by $\boldsymbol{E} \equiv -\dot{\boldsymbol{A}}$, where $\boldsymbol{A}$ is a gauge field. Note that $L_A^{(1)}$ includes the term arising from the Rashba spin-orbit interaction.

The magnetization is defined as

$$\boldsymbol{M} \equiv -\gamma \boldsymbol{s}_\mathrm{e}, \tag{A.2}$$

where $\gamma \equiv \frac{e}{2m}$ is gyromagnetic ratio, $\boldsymbol{s}_\mathrm{e} \equiv \frac{1}{2}\langle c^\dagger \boldsymbol{\sigma} c \rangle$ is the expectation value of a electron spin density, $\langle\ \rangle$ is the expectation value for L. In the Green's function representation, the spin density reads

$$\boldsymbol{s}_\mathrm{e}(\boldsymbol{r}, t) = -\lim_{\substack{\boldsymbol{r}' \to \boldsymbol{r} \\ t' \to t}} \frac{i}{2} \mathrm{tr}[\boldsymbol{\sigma} G^<(\boldsymbol{r}, \boldsymbol{r}', t, t')], \tag{A.3}$$

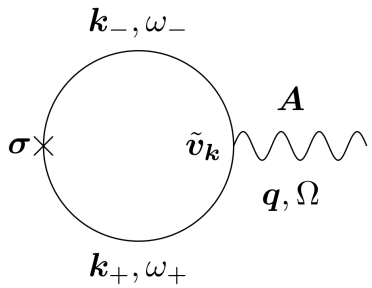

Figure A.1: The Feynman diagrams for the spin density induced by Edelstein effect. Solid lines represent the conducting electrons' Green's function including the Rashba interaction and the wavy lines denote the gauge field, respectively.

where $\boldsymbol{r}$ and t are space and time, respectively, tr is the trace over the spin space, and $G^<(\boldsymbol{r}, \boldsymbol{r}', t, t') \equiv i\langle c^\dagger(\boldsymbol{r}', t')c(\boldsymbol{r}, t)\rangle$ is a lesser component of contour ordered Green's function. We calculate Eq. (A.3) up to the first order of the gauge field based on linear response theory [101]. Using the Dyson equation,

$$G(\boldsymbol{r}, \boldsymbol{r}', t, t') = \frac{1}{V}\sum_{\boldsymbol{k},\omega}\left\{\begin{array}{c} e^{i\boldsymbol{k}\cdot(\boldsymbol{r}-\boldsymbol{r}')-i\omega(t'-t)}g_{\boldsymbol{k},\omega} \\ +e\sum_\nu\sum_{\boldsymbol{q},\Omega} e^{i(\boldsymbol{k}_+\cdot\boldsymbol{r}-\boldsymbol{k}_-\cdot\boldsymbol{r}')-i(\omega_+ t-\omega_- t')}A_\nu(\boldsymbol{q},\Omega)g_{\boldsymbol{k}_+,\omega_+}\tilde{v}_{\boldsymbol{k},\nu}g_{\boldsymbol{k}_-,\omega_-} \end{array}\right\}, \tag{A.4}$$

the spin density, Eq. (A.3), is given by (diagrammatically shown in Fig. A.1)

$$s_{\mathrm{e},\mu} = \sum_{\boldsymbol{q},\Omega}\sum_\nu e^{i\boldsymbol{q}\cdot\boldsymbol{r}-i\Omega t}\frac{e}{2\Omega}\chi^{sj}_{\mu\nu}(\boldsymbol{q},\Omega)E_\nu(\boldsymbol{q},\Omega), \tag{A.5}$$

where

$$\chi^{sj}_{\mu\nu}(\boldsymbol{q},\Omega) \equiv -\frac{1}{V}\sum_{\boldsymbol{k}}\int_{-\infty}^{\infty}\frac{\mathrm{d}\omega}{2\pi i}\mathrm{tr}[\sigma_\mu g_{\boldsymbol{k}_+,\omega_+}\tilde{v}_{\boldsymbol{k},\nu}g_{\boldsymbol{k}_-,\omega_-}]^< \tag{A.6}$$

is spin-current correlation function, $g_{\boldsymbol{k},\omega}$ is 2×2 free Green's function including the Rashba interaction with wave vector $\boldsymbol{k}$ and angular frequency ω, whose lesser component is given by

$$g^<_{\boldsymbol{k},\omega} = f(\omega)(g^{\mathrm{a}}_{\boldsymbol{k},\omega} - g^{\mathrm{r}}_{\boldsymbol{k},\omega}). \tag{A.7}$$

Here, $g^{\mathrm{r}}_{\boldsymbol{k},\omega} \equiv (\omega - \epsilon_{\boldsymbol{k}} - \boldsymbol{\gamma}_{\boldsymbol{k}}\cdot\boldsymbol{\sigma} + i0)^{-1}$ and $g^{\mathrm{a}}_{\boldsymbol{k},\omega} = (g^{\mathrm{r}}_{\boldsymbol{k},\omega})^\dagger$ are the retarded and advanced Green's functions, respectively, $\epsilon_{\boldsymbol{k}} = \frac{k^2}{2m} - \epsilon_{\mathrm{F}}$ is the electron energy measured from the Fermi energy ϵ_{F}, $\boldsymbol{\gamma}_{\boldsymbol{k}} \equiv \boldsymbol{k}\times\boldsymbol{\alpha}_{\mathrm{R}}$, 0 is a positive infinitesimal, $f(\omega) \equiv (e^{\beta\omega}+1)^{-1}$ is the Fermi–Dirac distribution function, and β is the inverse temperature. $\boldsymbol{k}_\pm \equiv \boldsymbol{k} \pm \frac{\boldsymbol{q}}{2}$, $\omega_\pm \equiv \omega \pm \frac{\Omega}{2}$, and $\tilde{\boldsymbol{v}}_{\boldsymbol{k}} \equiv \boldsymbol{v} + \boldsymbol{\alpha}_{\mathrm{R}}\times\boldsymbol{\sigma}$ with $\boldsymbol{v} \equiv \frac{\boldsymbol{k}}{m}$. The wave vector and angular frequency carried by the gauge field are denoted by $\boldsymbol{q}$ and Ω, respectively. The lesser component of the correlation function, Eq. (A.6), is calculated by use of the Langreth's methods [100, 102],

$$[g_{\boldsymbol{k}_+,\omega_+}g_{\boldsymbol{k}_-,\omega_-}]^< = g^{\mathrm{r}}_{\boldsymbol{k}_+,\omega_+}g^<_{\boldsymbol{k}_-,\omega_-} + g^<_{\boldsymbol{k}_+,\omega_+}g^{\mathrm{a}}_{\boldsymbol{k}_-,\omega_-}. \tag{A.8}$$

Since we are interested in the long wavelength region, we estimate $\chi^{sj}_{\mu\nu}$ at $\boldsymbol{q}=0$. The spin trace is performed by use of

$$\begin{aligned}
\mathrm{tr}[\sigma_\mu g_{\boldsymbol{k},\omega_+} g_{\boldsymbol{k},\omega_-}] &= \hat{\gamma}^\mu_{\boldsymbol{k}} \sum_\sigma \sigma g_{\boldsymbol{k},\omega_+,\sigma} g_{\boldsymbol{k},\omega_-,\sigma}, \\
\mathrm{tr}[\sigma_\mu g_{\boldsymbol{k},\omega_+} \sigma_\nu g_{\boldsymbol{k},\omega_-}] &= \sum_\sigma [\delta_{\mu\nu} g_{\boldsymbol{k},\omega_+,\sigma} g_{\boldsymbol{k},\omega_-,-\sigma} + \hat{\gamma}^\mu_{\boldsymbol{k}} \hat{\gamma}^\nu_{\boldsymbol{k}} (g_{\boldsymbol{k},\omega_+,\sigma} g_{\boldsymbol{k},\omega_-,\sigma} - g_{\boldsymbol{k},\omega_+,\sigma} g_{\boldsymbol{k},\omega_-,-\sigma})],
\end{aligned} \tag{A.9}$$

where $\sigma = \pm$ is the diagonalized spin index, $g_{\boldsymbol{k},\omega,\sigma}$ is the Green's function diagonalized in spin space, and $\hat{\boldsymbol{\gamma}}_{\boldsymbol{k}} \equiv \boldsymbol{\gamma}_{\boldsymbol{k}}/|\boldsymbol{\gamma}_{\boldsymbol{k}}|$. Using Eqs. (A.7), (A.8), and (A.9), the result becomes

$$\chi^{sj}_{\mu\nu}(\boldsymbol{q}=0,\Omega) = -\frac{8i}{V} \sum_{\boldsymbol{k}} \sum_\sigma \sum_{ij} \epsilon_{\nu ij} \alpha_{\mathrm{R},i} (\delta_{\nu j} - \hat{\gamma}^\mu_{\boldsymbol{k}} \hat{\gamma}^j_{\boldsymbol{k}}) \frac{\gamma_{\boldsymbol{k}} \sigma f(\epsilon^\sigma_{\boldsymbol{k}})}{(\Omega+i0)^2 - 4\gamma^2_{\boldsymbol{k}}}, \tag{A.10}$$

where $\gamma_{\boldsymbol{k}} \equiv |\boldsymbol{\gamma}_{\boldsymbol{k}}|$ and $\epsilon^\sigma_{\boldsymbol{k}} \equiv \epsilon_{\boldsymbol{k}} + \sigma\gamma_{\boldsymbol{k}}$. For the $\boldsymbol{k}$-integral, we choose the z axis along the Rashba field, i.e., $\boldsymbol{\alpha}_{\mathrm{R}} = \alpha_{\mathrm{R}} \hat{\boldsymbol{z}}$ ($\hat{\boldsymbol{z}} \equiv (0,0,1)$) and $\boldsymbol{k}$ is represented using the polar and azimuthal angles θ and φ, respectively. Using the following relation,

$$\int_0^{2\pi} \frac{\mathrm{d}\varphi}{2\pi} \hat{\gamma}^\mu_{\boldsymbol{k}} \hat{\gamma}^\nu_{\boldsymbol{k}} = \frac{1}{2} (\delta_{\mu\nu} - \hat{\alpha}_{\mathrm{R},\mu} \hat{\alpha}_{\mathrm{R},\nu}), \tag{A.11}$$

where $\hat{\boldsymbol{\alpha}}_{\mathrm{R}} \equiv \boldsymbol{\alpha}_{\mathrm{R}}/|\boldsymbol{\alpha}_{\mathrm{R}}|$, we thus get the correlation function as

$$\chi^{sj}_{\mu\nu} = -\frac{i n_{\mathrm{e}}}{\tilde{\beta}^2 \epsilon_{\mathrm{F}}} \sum_i \epsilon_{\nu i\mu} \alpha_{\mathrm{R},i} C(\Omega), \tag{A.12}$$

with

$$C(\Omega) \equiv -\frac{4\tilde{\beta}^2 \epsilon_{\mathrm{F}}}{n_{\mathrm{e}}} \sum_{\boldsymbol{k}} \frac{\gamma_{\boldsymbol{k}} s}{H_{\boldsymbol{k}}(\Omega)}, \tag{A.13}$$

where $s \equiv \sigma f(\epsilon^\sigma_{\boldsymbol{k}})$, $H_{\boldsymbol{k}}(\Omega) \equiv (\Omega+i0)^2 - 4\gamma_{\boldsymbol{k}}$, $n_{\mathrm{e}} \equiv n^{(0)}_{\mathrm{e}}(1+2\Delta_{\tilde{\beta}})$, $n^{(0)}_{\mathrm{e}} \equiv \frac{k^3_{\mathrm{F}}}{6\pi^2}$, k_{F} is Fermi wave number, $\Delta_{\tilde{\beta}} \equiv \frac{3}{4\tilde{\beta}^2}\left(1 + \frac{1+\tilde{\beta}^2}{\tilde{\beta}} \tan^{-1}\tilde{\beta}\right)$, $\tilde{\beta} \equiv \frac{m\alpha_{\mathrm{R}}}{k_{\mathrm{F}}}$.

The results of Eqs. (A.2), (A.5) and Eq. (A.12) are summarized in Eq. (1.13) with $\gamma_{ME} = \frac{\gamma e n_{\mathrm{e}}}{m\alpha_{\mathrm{R}}} \frac{\mathrm{Im}[C]}{\Omega}$. The electron density n_{e} is defined as (A.28) by use of Green's function. n_{e} and $C(\Omega)$ are calculated in Appendix B.

A.2 Microscopic calculation of inverse Edelstein effect

Here, we derive Eq. (1.14) as the same manner in Sec. A.1. We calculate the electric current density induced by Zeeman term describing the interaction

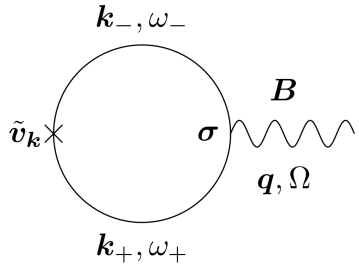

Figure A.2: The Feynman diagrams for the electric current density induced by inverse Edelstein effect. Solid lines represent the conducting electrons' Green's function including the Rashba interaction. The dotted and wavy lines denote the Rashba field and magnetic field, respectively. Note that the contribution arising from the third term on the right-hand side of Eq. (A.16) vanishes at $\boldsymbol{q} = 0$.

between electron spin and the applied magnetic field. The Lagrangian we consider is given by

$$\begin{aligned} L &= L_0 + L_A^{(2)}, \\ L_0 &\equiv \int \mathrm{d}^3 r c^\dagger \left[i\frac{\partial}{\partial t} + \left(\frac{\boldsymbol{\nabla}^2}{2m} + \epsilon_\mathrm{F} \right) - \frac{i}{2}\boldsymbol{\alpha}_\mathrm{R} \cdot (\overleftrightarrow{\nabla} \times \boldsymbol{\sigma}) \right] c, \\ L_A^{(2)} &\equiv \gamma \int \mathrm{d}^3 r \boldsymbol{A} \cdot \boldsymbol{\nabla} \times (c^\dagger \boldsymbol{\sigma} c). \end{aligned} \tag{A.14}$$

The term $L_A^{(2)}$ represents the interaction between electron spin and the applied magnetic field defined by $\boldsymbol{B} \equiv \boldsymbol{\nabla} \times \boldsymbol{A}$, called Zeeman interaction, where $\gamma \equiv \frac{e}{2m}$ is gyromagnetic ratio.

The expectation value of electric current density in this Rashba system is

$$j_\mu(\boldsymbol{r}, t) = \frac{ie}{2m}\langle c^\dagger \overleftrightarrow{\nabla}_\mu c \rangle - e\sum_{ij} \epsilon_{\mu ij}\alpha_{\mathrm{R},i}\langle c^\dagger \sigma_j c \rangle - \gamma \sum_{ij} \epsilon_{\mu ij} \nabla_i \langle c^\dagger \sigma_j c \rangle, \tag{A.15}$$

where $\langle\ \rangle$ means the expectation value for L. In the Green's function representation, the electric current density reads

$$j_\mu = \lim_{\substack{\boldsymbol{r}' \to \boldsymbol{r} \\ t' \to t}} \mathrm{tr} \left\{ \begin{array}{c} \frac{e}{2m}[(\nabla_{\boldsymbol{r}',\mu} - \nabla_{\boldsymbol{r},\mu}) G^<(\boldsymbol{r}, \boldsymbol{r}', t, t')] + ie\sum_{ij} \epsilon_{\mu ij}\alpha_{\mathrm{R},i}[\sigma_k G^<(\boldsymbol{r}, \boldsymbol{r}', t, t')] \\ + i\gamma \sum_{ij} \epsilon_{\mu ij}[(\nabla_{\boldsymbol{r}',j} + \nabla_{\boldsymbol{r},j})\sigma_k G^<(\boldsymbol{r}, \boldsymbol{r}', t, t')] \end{array} \right\}, \tag{A.16}$$

where $G^<(\boldsymbol{r}, \boldsymbol{r}', t, t') \equiv i\langle c^\dagger(\boldsymbol{r}', t') c(\boldsymbol{r}, t) \rangle$ is a lesser component of contour ordered Green's function. We calculate Eq. (A.16) up to the first order of the magnetic field. Using the Dyson equation,

$$G(\boldsymbol{r}, \boldsymbol{r}', t, t') = \frac{1}{V}\sum_{\boldsymbol{k},\omega} \left\{ \begin{array}{c} e^{i\boldsymbol{k}\cdot(\boldsymbol{r}-\boldsymbol{r}') - i\omega(t-t')} g_{\boldsymbol{k},\omega} \\ + \sum_\nu \sum_{\boldsymbol{q},\Omega} e^{i(\boldsymbol{k}_+ \cdot \boldsymbol{r} - \boldsymbol{k}_- \cdot \boldsymbol{r}') - i(\omega_+ t - \omega_- t')} \gamma B_\nu(\boldsymbol{q}, \Omega) g_{\boldsymbol{k}_+,\omega_+} \sigma_\nu g_{\boldsymbol{k}_-,\omega_-} \end{array} \right\}, \tag{A.17}$$

the electric current density, Eq. (A.16), is given by (diagrammatically shown in Fig. A.2)

$$j_\mu = ie\gamma \sum_{\boldsymbol{q},\Omega} \sum_{\nu} e^{i\boldsymbol{q}\cdot\boldsymbol{r}-i\Omega t} \chi^{js}_{\mu\nu}(\boldsymbol{q},\Omega) B_\nu(\boldsymbol{q},\Omega), \tag{A.18}$$

where

$$\chi^{js}_{\mu\nu}(\boldsymbol{q},\Omega) \equiv -\frac{1}{V}\sum_{\boldsymbol{k}} \int_{-\infty}^{\infty} \frac{\mathrm{d}\omega}{2\pi i} \mathrm{tr}[\tilde{v}_{\boldsymbol{k},\mu} g_{\boldsymbol{k}_+,\omega_+} \sigma_\nu g_{\boldsymbol{k}_-,\omega_-}]^< \tag{A.19}$$

is current-spin correlation function and and $\tilde{\boldsymbol{v}}_{\boldsymbol{k}} \equiv \boldsymbol{v} + \boldsymbol{\alpha}_{\mathrm{R}} \times \boldsymbol{\sigma}$ with $\boldsymbol{v} \equiv \frac{\boldsymbol{k}}{m}$. As is the case in the Edelstein effect, we calculate $\chi^{js}_{\mu\nu}$ in the long wavelength region ($\boldsymbol{q}$=0). Using Eqs. (A.7), (A.8), (A.9) and (A.11), the correlation function reduces to

$$\chi^{js}_{\mu\nu} = -\frac{n_{\mathrm{e}}}{\tilde{\beta}^2 \epsilon_{\mathrm{F}}} \sum_i \epsilon_{\mu i\nu} \alpha_{\mathrm{R},i} C(\Omega), \tag{A.20}$$

The results of Eqs. (A.18) and Eq. (A.20) are summarized in Eq. (1.14) with $\gamma_{jB} = i\Omega\gamma_{ME}$.

A.3 Microscopic calculation of Rashba-induced direct coupling effect

In this section, we derive Eq. (1.21). We calculate the electric current density induced by a direct coupling between Edelstein and inverse Edelstein effects by use of linear response theory. The Lagrangian we consider is given by

$$\begin{aligned} L &= L_0 + L_A^{(1)} \\ L_0 &\equiv \int \mathrm{d}^3 r c^\dagger \left[i\frac{\partial}{\partial t} + \left(\frac{\boldsymbol{\nabla}^2}{2m} + \epsilon_{\mathrm{F}} \right) - \frac{i}{2}\boldsymbol{\alpha}_{\mathrm{R}} \cdot (\overleftrightarrow{\nabla} \times \boldsymbol{\sigma}) \right] c, \\ L_A^{(1)} &\equiv \int \mathrm{d}^3 r \boldsymbol{A} \cdot \left[\frac{ie}{2m} c^\dagger \overleftrightarrow{\nabla} c - \frac{e^2}{2m} \boldsymbol{A} c^\dagger c - e c^\dagger (\boldsymbol{\alpha}_{\mathrm{R}} \times \boldsymbol{\sigma}) c \right]. \end{aligned} \tag{A.21}$$

The expectation value of the electric current density in this system is given by

$$j_\mu(\boldsymbol{r},t) = \frac{ie}{2m}\langle c^\dagger \overleftrightarrow{\nabla}_\mu c\rangle - \frac{e^2}{m} A_\mu \langle c^\dagger c\rangle - e\sum_{ij} \epsilon_{\mu ij}\alpha_{\mathrm{R},i}\langle c^\dagger \sigma_j c\rangle, \tag{A.22}$$

where $\langle\ \rangle$ stands for the expectation value for L. In the Green's function representation, the electric current density reads

$$j_\mu = \lim_{\substack{\boldsymbol{r}'\to\boldsymbol{r} \\ t'\to t}} \mathrm{tr} \left\{ \begin{array}{c} \frac{e}{2m}[(\nabla_{\boldsymbol{r}',\mu} - \nabla_{\boldsymbol{r},\mu}) G^<(\boldsymbol{r},\boldsymbol{r}',t,t')] + \frac{ie^2}{m} A_\mu G^<(\boldsymbol{r},\boldsymbol{r}',t,t') \\ + ie\sum_{ij} \epsilon_{\mu ij}\alpha_{\mathrm{R},i} \mathrm{tr}[\sigma_k G^<(\boldsymbol{r},\boldsymbol{r}',t,t')] \end{array} \right\}, \tag{A.23}$$

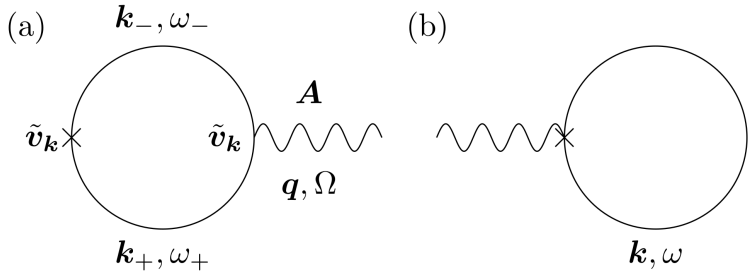

Figure A.3: The Feynman diagrams for the electric current density arising from Edelstein and inverse Edelstein effects. Solid lines represent the conducting electrons' Green's function including the Rashba interaction and the wavy lines denote the gauge field, respectively. Diagrams, (a) and (b) correspond to the contributions of $\chi^{jj}_{\mu\nu}$ and $n_{\rm e}$ on the right-hand side of Eq. (A.26), respectively.

where $G^<(\boldsymbol{r}, \boldsymbol{r}', t, t') \equiv i\langle c^\dagger(\boldsymbol{r}', t')c(\boldsymbol{r}, t)\rangle$ is a lesser component of contour ordered Green's function. We calculate Eq. (A.23) up to the first order of the gauge field. Using the Dyson equation,

$$G(\boldsymbol{r}, \boldsymbol{r}', t, t') = \frac{1}{V}\sum_{\boldsymbol{k},\omega}\left\{\begin{array}{c} e^{i\boldsymbol{k}\cdot(\boldsymbol{r}-\boldsymbol{r}')-i\omega(t-t')}g_{\boldsymbol{k},\omega} \\ +e\sum_\nu\sum_{\boldsymbol{q},\Omega} e^{i(\boldsymbol{k}_+\cdot\boldsymbol{r}-\boldsymbol{k}_-\cdot\boldsymbol{r}')-i(\omega_+ t-\omega_- t')}A_\nu(\boldsymbol{q},\Omega)g_{\boldsymbol{k}_+,\omega_+}\tilde{v}_{\boldsymbol{k},\nu}g_{\boldsymbol{k}_-,\omega_-} \end{array}\right\}, \tag{A.24}$$

the electric current density, Eq. (A.23) reduces to (diagrammatically shown in Fig. A.3)

$$j_\mu = \sum_{\boldsymbol{q},\Omega}\sum_\nu e^{i\boldsymbol{q}\cdot\boldsymbol{r}-i\Omega t}\sigma_{\mu\nu}(\boldsymbol{q},\Omega)E_\nu(\boldsymbol{q},\Omega), \tag{A.25}$$

where

$$\sigma_{\mu\nu}(\boldsymbol{q},\Omega) \equiv \frac{ie^2}{\Omega}\left[\chi^{jj}_{\mu\nu}(\boldsymbol{q},\Omega) - \frac{n_{\rm e}}{m}\delta_{\mu\nu}\right] \tag{A.26}$$

is an electric conductivity tensor. Here current-current correlation function $\chi^{jj}_{\mu\nu}$ and electron density $n_{\rm e}$ are defined as

$$\chi^{\mu\nu}_{jj}(\boldsymbol{q},\Omega) \equiv -\frac{1}{V}\sum_{\boldsymbol{k}}\int_{-\infty}^{\infty}\frac{{\rm d}\omega}{2\pi i}{\rm tr}[\tilde{v}_{\boldsymbol{k},\mu}g_{\boldsymbol{k}_+,\omega_+}\tilde{v}_{\boldsymbol{k},\nu}g_{\boldsymbol{k}_-,\omega_-}]^<, \tag{A.27}$$

$$n_{\rm e} \equiv \frac{1}{V}\sum_{\boldsymbol{k}}\int_{-\infty}^{\infty}\frac{{\rm d}\omega}{2\pi i}{\rm tr}[g_{\boldsymbol{k},\omega}]^<. \tag{A.28}$$

We estimate the contributions of $\chi^{jj}_{\mu\nu}$ at $\boldsymbol{q} = 0$. Using Eqs. (A.9), (A.8), and (A.11), the correlation function reduces to

$$\chi^{\mu\nu}_{jj}(\boldsymbol{q}=0,\Omega) = \frac{n_{\rm e}}{m}C(\Omega)(\delta_{\mu\nu} - \hat{\alpha}_{{\rm R},\mu}\hat{\alpha}_{{\rm R},\nu}). \tag{A.29}$$

The results of Eqs. (A.26) and Eq. (A.29) are summarized in Eq. (1.21).

Appendix B

Calculation of Eq. (A.28) and Eq. (A.13)

First, let us calculate Eq. (A.28). By use of Eq. (A.7). the electron density, $n_{\rm e}$, read as

$$n_{\rm e} = \frac{1}{4}\sum_{\sigma}\frac{1}{6\pi^2}\int_0^{\pi} {\rm d}\theta \sin\theta k_{{\rm F},\sigma}^3(\theta), \tag{B.1}$$

where $k_{{\rm F},\sigma}(\theta) \equiv k_{\rm F}[\sqrt{1+(\tilde{\beta}\sin\theta)^2} - \sigma\tilde{\beta}\sin\theta]$, $k_{\rm F}$ is Fermi wave number, $\sigma = \pm$ is the diagonalized spin index, and $\tilde{\beta} \equiv \frac{m\alpha_{\rm R}}{k_{\rm F}}$. Carrying out the integration of θ as

$$\int_0^{\pi} {\rm d}\theta \sin\theta\sqrt{1+(\tilde{\beta}\sin\theta)} = 1 + \frac{1+\tilde{\beta}^2}{\tilde{\beta}}\tan^{-1}\tilde{\beta},$$
$$\int_0^{\pi} {\rm d}\theta \sin^3\theta = \frac{1}{4\tilde{\beta}^2}\left(1+3\tilde{\beta}^2 + (3\tilde{\beta}^2-1)\frac{1+\tilde{\beta}^2}{\tilde{\beta}}\tan^{-1}\tilde{\beta}\right), \tag{B.2}$$

we can get the electron density as

$$n_{\rm e} = n_{\rm e}^{(0)}(1+2\Delta_{\tilde{\beta}}), \tag{B.3}$$

where $n_{\rm e}^{(0)} \equiv \frac{k_{\rm F}^3}{6\pi^2}$ and $\Delta_{\tilde{\beta}} \equiv \frac{3}{4\tilde{\beta}^2}\left(1+\frac{1+\tilde{\beta}^2}{\tilde{\beta}}\tan^{-1}\tilde{\beta}\right)$.

Next, we calculate Eq. (A.13). Using the following relation,

$$\frac{1}{2k\alpha_{\rm R}\sin\theta \pm (\Omega + i0)} = \frac{1}{2k\alpha_{\rm R}\sin\theta\pm\Omega} \mp i\pi\delta(2k\alpha_{\rm R}\sin\theta\pm\Omega), \tag{B.4}$$

we see that Eq. (A.13) is decomposed into Real part and Imaginary part as shown

below.

$$\mathrm{Re}[C(\Omega)] = -\frac{\tilde{\beta}^2\epsilon_{\mathrm{F}}}{n_{\mathrm{e}}}\frac{1}{2\pi^2}\int_0^{\pi}\mathrm{d}\theta\sin\theta\int_{k_{\mathrm{F},-}(\theta)}^{k_{\mathrm{F},+}(\theta)}\mathrm{d}kk^2\left[\frac{1}{2k\alpha_{\mathrm{R}}\sin\theta-\Omega}-\frac{1}{2k\alpha_{\mathrm{R}}\sin\theta+\Omega}\right], \tag{B.5}$$

$$\mathrm{Im}[C(\Omega)] = -\frac{\tilde{\beta}^2\epsilon_{\mathrm{F}}}{n_{\mathrm{e}}}\frac{1}{4\pi}\int_0^{\pi}\mathrm{d}\theta\sin\theta\int_{k_{\mathrm{F},-}(\theta)}^{k_{\mathrm{F},+}(\theta)}\mathrm{d}kk^2 \times\left[\delta(2k\alpha_{\mathrm{R}}\sin\theta-\Omega)-\delta(2k\alpha_{\mathrm{R}}\sin\theta+\Omega)\right]. \tag{B.6}$$

B.1 Calculation of $\mathrm{Re}[C(\Omega)]$

Carrying out the $\boldsymbol{k}$-integral, Eq. (B.5) is expressed as

$$\mathrm{Re}[C] = -\frac{\tilde{\beta}^2\epsilon_{\mathrm{F}}k_{\mathrm{F}}^2}{2\pi^2\alpha_{\mathrm{R}}n_{\mathrm{e}}}[\tilde{\beta}I_1+\nu^2I_2], \tag{B.7}$$

where $\nu \equiv \frac{\Omega}{2\alpha_{\mathrm{R}}k_{\mathrm{F}}}$,

$$I_1 \equiv \int_0^{\pi}\mathrm{d}\theta\sin\theta\sqrt{1+(\tilde{\beta}\sin\theta)}, \tag{B.8}$$

$$I_2 \equiv \frac{1}{4}\sum_{\sigma}\sigma\int_0^{\pi}\mathrm{d}\theta\frac{1}{\sin^2\theta}\ln[(k_{\mathrm{F},\sigma}(\theta)\sin\theta)^2-\nu^2]. \tag{B.9}$$

Using Eq. (B.2), Eq. (B.8) reads

$$I_1 = \frac{4}{3\tilde{\beta}^2}\Delta_{\tilde{\beta}}. \tag{B.10}$$

Carrying out the integration of θ by use of the partial integration after change of variable as $x \equiv \tilde{\beta}\sin\theta$, Eq. (B.9) reads

$$I_2 = \frac{\tilde{\beta}}{2}\sum_{\sigma}\sigma\int_0^{\tilde{\beta}}\mathrm{d}x\sqrt{\frac{\tilde{\beta}^2-x^2}{1+x^2}}\frac{k_{\mathrm{F},\sigma}^3(x)}{(k_{\mathrm{F},\sigma}(x)x)^2-\tilde{\omega}^2}, \tag{B.11}$$

where $\tilde{\omega} \equiv \tilde{\beta}\nu$. Performing the summation of σ, we can get I_2 as

$$I_2 = \frac{\tilde{\beta}}{2\tilde{\omega}}\sum_{\eta}(\eta-\tilde{\omega})\int_0^{\tilde{\beta}}\mathrm{d}x\sqrt{\frac{\tilde{\beta}^2-x^2}{1+x^2}}\frac{x}{x^2-A_\eta}, \tag{B.12}$$

with $A_\eta \equiv \frac{\tilde{\omega}}{1-2\eta\tilde{\omega}}$, where $\eta = \pm 1$. Here we used the following relation,

$$\sum_{\sigma}\sigma\frac{k_{\mathrm{F},\sigma}^3(x)}{(k_{\mathrm{F},\sigma}(x)x)^2-\tilde{\omega}^2} = \frac{x}{\tilde{\omega}}\sum_{\eta}\frac{\eta-\tilde{\omega}}{x^2-A_\eta}. \tag{B.13}$$

Changing a variable to $y = \sqrt{\frac{\tilde{\beta}^2 - x}{1+x}}$ after change of variable as $x^2 = x$, Eq.(B.12) reads

$$I_2 = -\frac{\tilde{\beta}}{2\tilde{\omega}} \sum_{\eta} (\eta - \tilde{\omega}) \int_0^{\tilde{\beta}} \mathrm{d}y \left[\frac{Q_\eta}{y^2 + Q_\eta} - \frac{1}{1+y^2} \right], \tag{B.14}$$

with $Q_\eta \equiv \frac{A_\eta - \tilde{\beta}^2}{1+A_\eta}$. Carrying out the integration of y as

$$\int_0^{\tilde{\beta}} \mathrm{d}y \left[\frac{Q_\eta}{y^2 + Q_\eta} - \frac{1}{1+y^2} \right] = -\tan^{-1}\tilde{\beta} + \sqrt{Q_\eta} \tan^{-1} \frac{\tilde{\beta}}{\sqrt{Q_\eta}}, \tag{B.15}$$

Eq. (B.14) becomes

$$I_2 = -\frac{\tilde{\beta}}{2} \left[\frac{1}{\tilde{\omega}} \sum_{\eta} (\eta - \tilde{\omega}) \sqrt{Q_\eta} \tan^{-1} \frac{\tilde{\beta}}{\sqrt{Q_\eta}} + 2 \tan^{-1} \tilde{\beta}. \right]. \tag{B.16}$$

From the results, Eqs (B.10) and (B.16), we thus obtain $\mathrm{Re}[C]$ as

$$\mathrm{Re}[C] = \frac{3}{4} \frac{1}{1 + 2\Delta_{\tilde{\beta}}} \left[\tilde{\omega} \sum_{\eta} (\eta - \tilde{\omega}) \sqrt{Q_\eta} \tan^{-1} \frac{\tilde{\beta}}{\sqrt{Q_\eta}} + 2\tilde{\omega}^2 \tan^{-1} \tilde{\beta} \right] - 2 \frac{\Delta_{\tilde{\beta}}}{1 + 2\Delta_{\tilde{\beta}}}. \tag{B.17}$$

B.2 Calculation of $\mathrm{Im}[C(\Omega)]$

Carrying out the $\boldsymbol{k}$-integral, Eq. (B.6) is expressed as

$$\mathrm{Im}[C] = \frac{\tilde{\beta}^4 \epsilon_{\mathrm{F}} k_{\mathrm{F}}^2}{8\pi \alpha_{\mathrm{R}} n_{\mathrm{e}}} \int_0^{\tilde{\beta}} \mathrm{d}x \frac{1}{\sqrt{\tilde{\beta}^2 - x^2}} \Theta \left(\sqrt{1+x^2} - x < \frac{x}{|\tilde{\omega}|} < \sqrt{1+x^2} + x \right), \tag{B.18}$$

where $\Theta(x)$ is a step function. Integrating out a variable x in response to case analysis of Θ, we see that $\mathrm{Im}[C]$ reads

$$\mathrm{Im}[C] = -\frac{3\pi}{8} \frac{\tilde{\beta}}{1 + 2\Delta_{\tilde{\beta}}} \tilde{\omega} \begin{Bmatrix} S_+ - S_- & \tilde{\omega} < \tilde{\omega}_- \\ -S_- & \tilde{\omega}_- < \tilde{\omega} < \tilde{\omega}_+ \\ 0 & \tilde{\omega}_+ < \tilde{\omega} \end{Bmatrix}, \tag{B.19}$$

where $\tilde{\omega}_\pm \equiv \tilde{\beta}(\sqrt{1+\tilde{\beta}^2} \pm \tilde{\beta})$, $S_\lambda \equiv \sqrt{\tilde{\beta}^2 - 2\lambda\tilde{\beta}^2|\tilde{\omega}| - |\tilde{\omega}|^2}$, and $\lambda = \pm 1$.

Appendix C

Derivation of Rashba-induced spin gauge field

C.1 Pumped current induced by magnetization texture

Here, we calculate the pumped electric current induced by nonuniform magnetization texture. For simplicity, we set $\hbar = 1$. The system we consider is a ferromagnetic metal with broken spatial-inversion symmetry, where conduction electrons, represented by two-component annihilation and creation operators, $c(\boldsymbol{r}, t)$ and $c^\dagger(\boldsymbol{r}, t)$, interact with magnetization texture, described by the vector field $\boldsymbol{n}(\boldsymbol{r}, t)$, via the *sd* exchange interaction. The Hamiltonian thus reads

$$H = H_0 + H_{sd} + H_{\mathrm{R}}, \tag{C.1}$$

$$H_0 = \int \mathrm{d}^3 r \left(\frac{1}{2m} |\boldsymbol{\nabla} c|^2 - \mu c^\dagger c \right), \tag{C.2}$$

$$H_{sd} = -\Delta_{sd} \int \mathrm{d}^3 r \boldsymbol{n} \cdot \left(c^\dagger \boldsymbol{\sigma} c \right), \tag{C.3}$$

$$H_{\mathrm{R}} = \frac{i}{2} \int \mathrm{d}^3 r \boldsymbol{\alpha}_{\mathrm{R}} \cdot c^\dagger (\overleftrightarrow{\nabla} \times \boldsymbol{\sigma}) c, \tag{C.4}$$

where The term H_{sd} is the exchange interaction between the magnetization and conduction-electron spin and Δ_{sd} is its strength. The term H_{R} is Rashba spin-orbit interaction. $\boldsymbol{\alpha}_{\mathrm{R}}$ is the Rashba field representing the strength and direction of the Rashba spin-orbit interaction. The Lagrangian of the system is

$$L \equiv i \int \mathrm{d}^3 r c^\dagger \partial_t c - H, \tag{C.5}$$

where $\partial_t \equiv \frac{\partial}{\partial t}$. The expectation value of the electric current density in this system is given by

$$j_\mu(\boldsymbol{r}, t) = \frac{ie}{2m} \langle c^\dagger \overleftrightarrow{\nabla}_\mu c \rangle - e \sum_{jk} \epsilon_{\mu jk} \alpha_{\mathrm{R},j} \langle c^\dagger \sigma_k c \rangle, \tag{C.6}$$

where $\langle\ \rangle$ stands for the expectation value for L. We are interested in the case where the *sd* exchange interaction is large and thus the conduction electron spin is aligned parallel to the magnetization direction $\boldsymbol{n}$, i.e., the adiabatic limit. To describe this limit, the use of the spin gauge field, which characterizes the deviation from the adiabatic limit, is convenient [2]. The spin gauge field is introduced by diagonalizing the *sd* interaction using a unitary transformation, $c(\boldsymbol{r},t) = U(\boldsymbol{r},t)a(\boldsymbol{r},t)$, where $U(\boldsymbol{r},t)$ is a 2×2 unitary matrix and a is a new electron field operator. A convenient choice of $U(\boldsymbol{r},t)$ is $U(\boldsymbol{r},t) = \boldsymbol{m}(\boldsymbol{r},t)\cdot\boldsymbol{\sigma}$ with $\boldsymbol{m}(\boldsymbol{r},t) = \left(\sin\frac{\theta}{2}\cos\phi, \sin\frac{\theta}{2}\sin\phi, \cos\frac{\theta}{2}\right)$, where θ and ϕ are the polar angles of $\boldsymbol{n}$. It is easy to confirm that $U^\dagger(\boldsymbol{n}\ \cdot\ \boldsymbol{\sigma})U = \sigma_z$ is satisfied. Because of this local unitary transformation, derivatives of the electron field become covariant derivatives $\partial_\mu c = U(\partial_\mu + ieA_{\mathrm{s},\mu})a$, where $A_{\mathrm{s},\mu} \equiv -\frac{i}{e}U^{-1}\partial_\mu U$ is the gauge field. Since U is a 2×2 matrix, the gauge field $A_{\mathrm{s},\mu}$ is written using Pauli matrices as $A_{\mathrm{s},\mu} = \sum_\alpha A^\alpha_{\mathrm{s},\mu}\sigma_\alpha$ ($\mu = x,y,z,\tau$ is a suffix for space and time and $\alpha = x,y,z$ is for spin). It is thus an SU(2) gauge field, which we call the spin gauge field. The Lagrangian in the rotated space is thus given by

$$L \equiv L_0 + L^{(1)}_{A_\mathrm{s}}, \tag{C.7}$$

$$L_0 \equiv \int \mathrm{d}^3 r a^\dagger \left(i\partial_t + \frac{1}{2m}\boldsymbol{\nabla}^2 + \mu + \Delta_{sd}\sigma_z \right) a, \tag{C.8}$$

$$\begin{aligned} L^{(1)}_{A_\mathrm{s}} \equiv \int \mathrm{d}^3 r \Bigg[& -ea^\dagger A_{\mathrm{s},t} a - \sum_{i,\alpha} A^\alpha_{\mathrm{s},i} j^\alpha_{\mathrm{s},i}. - \frac{e^2}{2m}\sum_{i,\alpha}(A^\alpha_{\mathrm{s},i})^2 a^\dagger a \\ & + \frac{1}{2}\sum_{ijkn}\epsilon_{ijk}\alpha_{\mathrm{R},i}R_{kn}\left(-\frac{2m}{e}j^n_{\mathrm{s},j} - 2eA^n_{\mathrm{s},j}a^\dagger a\right)\Bigg], \end{aligned} \tag{C.9}$$

where $j^\alpha_{\mathrm{s},i} \equiv -ie\frac{1}{2m}a^\dagger \overleftrightarrow{\nabla}_i \sigma^\alpha a$ is the spin current, ϵ_{ijk} is a totally antisymmetric tensor, and $R_{kn} \equiv 2m_k m_n - \delta_{kn}$ is a 3×3 rotation matrix elements. The electron field a is strongly spin-polarized owing to the *sd* exchange interaction (the last term of L_0). In the rotated frame, Eq. (C.6) reads

$$j_\mu(\boldsymbol{r},t) = \frac{ie}{2m}\langle a^\dagger \overleftrightarrow{\nabla}_\mu a\rangle - \frac{e}{m}\sum_\ell A^\ell_{\mathrm{s},\mu}\langle a^\dagger\sigma_\ell a\rangle - e\sum_{jk\ell}\epsilon_{\mu jk\ell}\alpha_{\mathrm{R},j}R_{k\ell}\langle a^\dagger\sigma_\ell a\rangle. \tag{C.10}$$

In the Green's function representation, the electric current density in the rotated frame becomes

$$j_\mu = \lim_{\substack{\boldsymbol{r}'\to\boldsymbol{r}\\ t'\to t}} \mathrm{tr}\left\{ \begin{array}{c} \frac{e}{2m}[(\nabla_{\boldsymbol{r}',\mu} - \nabla_{\boldsymbol{r},\mu})G^<(\boldsymbol{r},\boldsymbol{r}',t,t')] + \frac{ie^2}{m}\sum_\ell A^\ell_{\mathrm{s},\mu}[\sigma_\ell G^<(\boldsymbol{r},\boldsymbol{r}',t,t')] \\ +ie\sum_{jk\ell}\epsilon_{\mu jk}\alpha_{\mathrm{R},j}R_{k\ell}[\sigma_\ell G^<(\boldsymbol{r},\boldsymbol{r}',t,t')] \end{array} \right\}, \tag{C.11}$$

where $G^<(\boldsymbol{r},\boldsymbol{r}',t,t') \equiv i\langle a^\dagger(\boldsymbol{r}',t')a(\boldsymbol{r},t)\rangle$ is a lesser component of contour ordered Green's function. We calculate the above expression up to the first order in the Rashba field $\boldsymbol{\alpha}_\mathrm{R}$ based on linear response theory [101]. In the calculation, we use

the following Dyson equation,

$$
\begin{aligned}
G(\boldsymbol{r},\boldsymbol{r}',t,t') = & \frac{1}{V}\sum_{\boldsymbol{k},\omega} e^{i\boldsymbol{k}\cdot(\boldsymbol{r}-\boldsymbol{r}')-i\omega(t-t')} g_{\boldsymbol{k},\omega} \\
& + \frac{1}{mV}\sum_{\boldsymbol{k},\omega}\sum_{\boldsymbol{q},\Omega}\sum_{j\mu} e^{i\boldsymbol{k}\cdot\boldsymbol{r}-i\omega t-i(\boldsymbol{k}+\boldsymbol{q})\cdot\boldsymbol{r}'+i(\omega+\Omega)t'} \\
& \times A^{j}_{\mathrm{s},\mu}(\boldsymbol{q},\Omega)\left(\boldsymbol{k}+\frac{\boldsymbol{q}}{2}\right)_{\mu} g_{\boldsymbol{k},\omega}\sigma_j g_{\boldsymbol{k}+\boldsymbol{q},\omega+\Omega} \\
& + \frac{1}{V}\sum_{\boldsymbol{k},\omega}\sum_{\boldsymbol{p},\bar{\Omega}}\sum_{\ell mno} e^{i\boldsymbol{k}\cdot\boldsymbol{r}-i\omega t-i(\boldsymbol{k}+\boldsymbol{p})\cdot\boldsymbol{r}'+i(\omega+\bar{\Omega})t'} \\
& \times \epsilon_{\ell mn}\alpha_{\mathrm{R},\ell} R_{no}(\boldsymbol{p},\bar{\Omega})\left(\boldsymbol{k}+\frac{\boldsymbol{p}}{2}\right)_{m} g_{\boldsymbol{k},\omega}\sigma_o g_{\boldsymbol{k}+\boldsymbol{p},\omega+\bar{\Omega}} \\
& + \frac{1}{V}\sum_{\boldsymbol{k},\omega}\sum_{\boldsymbol{p},\boldsymbol{q}}\sum_{\bar{\Omega},\Omega}\sum_{\ell mno} e^{i\boldsymbol{k}\cdot\boldsymbol{r}-i\omega t-i(\boldsymbol{k}+\boldsymbol{p}+\boldsymbol{q})\cdot\boldsymbol{r}'+i(\omega+\bar{\Omega}+\Omega)t'} \\
& \times \epsilon_{\ell mn}\alpha_{\mathrm{R},\ell} R_{no}(\boldsymbol{p},\bar{\Omega}) A^{o}_{\mathrm{s},m}(\boldsymbol{q},\Omega) g_{\boldsymbol{k},\omega} g_{\boldsymbol{k}+\boldsymbol{p}+\boldsymbol{q},\omega+\bar{\Omega}+\Omega} \\
& + \frac{1}{mV}\sum_{\boldsymbol{k},\omega}\sum_{\boldsymbol{p},\boldsymbol{q}}\sum_{\bar{\Omega},\Omega}\sum_{\mu j\ell mno} e^{i\boldsymbol{k}\cdot\boldsymbol{r}-i\omega t-i(\boldsymbol{k}+\boldsymbol{p}+\boldsymbol{q})\cdot\boldsymbol{r}'+i(\omega+\bar{\Omega}+\Omega)t'} \\
& \times \epsilon_{\ell mn}\alpha_{\mathrm{R},\ell} A^{j}_{\mathrm{s},\mu}(\boldsymbol{q},\Omega) R_{no}(\boldsymbol{p},\bar{\Omega}) \\
& \times \begin{bmatrix} \left(\boldsymbol{k}+\frac{\boldsymbol{q}}{2}\right)_{\mu}\left(\boldsymbol{k}+\boldsymbol{q}+\frac{\boldsymbol{p}}{2}\right)_{m} g_{\boldsymbol{k},\omega}\sigma_j g_{\boldsymbol{k}+\boldsymbol{q},\omega+\Omega}\sigma_o g_{\boldsymbol{k}+\boldsymbol{q}+\boldsymbol{p},\omega+\Omega+\bar{\Omega}} \\ +\left(\boldsymbol{k}+\frac{\boldsymbol{p}}{2}\right)_{m}\left(\boldsymbol{k}+\boldsymbol{p}+\frac{\boldsymbol{q}}{2}\right)_{\mu} g_{\boldsymbol{k},\omega}\sigma_o g_{\boldsymbol{k}+\boldsymbol{p},\omega+\bar{\Omega}}\sigma_j g_{\boldsymbol{k}+\boldsymbol{q}+\boldsymbol{p},\omega+\Omega+\bar{\Omega}} \end{bmatrix},
\end{aligned}
\tag{C.12}
$$

where $\boldsymbol{p}$ and $\boldsymbol{q}$ are the wave vector carried by the magnetization texture, Ω and $\bar{\Omega}$ are the angular frequency carried by the magnetization texture, $g_{\boldsymbol{k},\omega}$ is 2×2 free Green's function including the *sd*-exchange interaction with a finite electron-elastic-scattering lifetime, whose lesser component is given by $g^{<}_{\boldsymbol{k},\omega} = f(\omega)(g^{\mathrm{a}}_{\boldsymbol{k},\omega} - g^{\mathrm{r}}_{\boldsymbol{k},\omega})$ with $f(\omega) \equiv (e^{\beta\omega}+1)^{-1}$. Here, $g^{\mathrm{r}}_{\boldsymbol{k},\omega} \equiv (\omega - \epsilon_{\boldsymbol{k}} + \frac{i}{2\tau_{\mathrm{e}}})^{-1}$ and $g^{\mathrm{a}}_{\boldsymbol{k},\omega} = (g^{\mathrm{r}}_{\boldsymbol{k},\omega})^{\dagger}$ are the retarded and advanced Green's functions, respectively, $\epsilon_{\boldsymbol{k}} = \frac{k^2}{2m} - \epsilon_{\mathrm{F}} - \Delta_{sd}\sigma_z$ is the electron energy in the matrix representation, τ_{e} is the electron elastic scattering lifetime.

Using the Dyson equation, the result up to the first order in the Rashba field is given by (diagrammatically shown in Fig. 1.5)

$$
\boldsymbol{j}_{\mathrm{pump}} = \boldsymbol{j}^{(\mathrm{A})} + \boldsymbol{j}^{(\mathrm{B})} + \boldsymbol{j}^{(\mathrm{C})}, \tag{C.13}
$$

with

$$j_\mu^{(\mathrm{A})} = -\frac{ie}{mV}\sum_{\boldsymbol{k},\omega}\sum_{\boldsymbol{p},\bar{\Omega}}\sum_{\ell mno} e^{-i\boldsymbol{p}\cdot\boldsymbol{r}+i\bar{\Omega}t}\epsilon_{\ell mn}\alpha_{\mathrm{R},\ell}R_{no}(\boldsymbol{p},\bar{\Omega}) \times \mathrm{tr}\left[k_\mu k_m g_{\boldsymbol{k}-\frac{\boldsymbol{p}}{2},\omega-\frac{\bar{\Omega}}{2}}\sigma_o g_{\boldsymbol{k}+\frac{\boldsymbol{p}}{2},\omega+\frac{\bar{\Omega}}{2}} + m\delta_{\mu m}\sigma_o g_{\boldsymbol{k},\omega}\right]^<, \tag{C.14}$$

$$\begin{aligned} j_\mu^{(\mathrm{B})} =& -\frac{ie}{mV}\sum_{\boldsymbol{k},\omega}\sum_{\boldsymbol{p},\boldsymbol{q}}\sum_{\bar{\Omega},\Omega}\sum_{\nu j\ell mno} e^{-i(\boldsymbol{p}+\boldsymbol{q})\cdot\boldsymbol{r}+i(\bar{\Omega}+\Omega)t}\epsilon_{\ell mn}\alpha_{\mathrm{R},\ell}R_{no}(\boldsymbol{p},\bar{\Omega})A^j_{\mathrm{s},\nu}(\boldsymbol{q},\Omega) \\ &\times \mathrm{tr}\Bigg[\frac{k_\mu}{m}\left(\boldsymbol{k}+\frac{\boldsymbol{q}}{2}\right)_m\left(\boldsymbol{k}-\frac{\boldsymbol{p}}{2}\right)_\nu \\ &\times g_{\boldsymbol{k}-\frac{\boldsymbol{q}}{2}-\frac{\boldsymbol{p}}{2},\omega-\frac{\Omega}{2}-\frac{\bar{\Omega}}{2}}\sigma_j g_{\boldsymbol{k}+\frac{\boldsymbol{q}}{2}-\frac{\boldsymbol{p}}{2},\omega+\frac{\Omega}{2}-\frac{\bar{\Omega}}{2}}\sigma_o g_{\boldsymbol{k}+\frac{\boldsymbol{q}}{2}+\frac{\boldsymbol{p}}{2},\omega+\frac{\Omega}{2}+\frac{\bar{\Omega}}{2}} \\ &+ \frac{k_\mu}{m}\left(\boldsymbol{k}-\frac{\boldsymbol{q}}{2}\right)_m\left(\boldsymbol{k}+\frac{\boldsymbol{p}}{2}\right)_\nu \\ &\times g_{\boldsymbol{k}-\frac{\boldsymbol{q}}{2}-\frac{\boldsymbol{p}}{2},\omega-\frac{\Omega}{2}-\frac{\bar{\Omega}}{2}}\sigma_o g_{\boldsymbol{k}-\frac{\boldsymbol{q}}{2}+\frac{\boldsymbol{p}}{2},\omega-\frac{\Omega}{2}+\frac{\bar{\Omega}}{2}}\sigma_j g_{\boldsymbol{k}+\frac{\boldsymbol{q}}{2}+\frac{\boldsymbol{p}}{2},\omega+\frac{\Omega}{2}+\frac{\bar{\Omega}}{2}} \\ &+ \delta_{\mu m}k_\nu\sigma_o g_{\boldsymbol{k}-\frac{\boldsymbol{q}}{2},\omega-\frac{\Omega}{2}}\sigma_j g_{\boldsymbol{k}+\frac{\boldsymbol{q}}{2},\omega+\frac{\Omega}{2}} + \delta_{\mu\nu}k_m\sigma_j g_{\boldsymbol{k}-\frac{\boldsymbol{p}}{2},\omega-\frac{\bar{\Omega}}{2}}\sigma_o g_{\boldsymbol{k}+\frac{\boldsymbol{p}}{2},\omega+\frac{\bar{\Omega}}{2}}\Bigg]^<, \end{aligned} \tag{C.15}$$

$$\begin{aligned} j_\mu^{(\mathrm{C})} =& -\frac{ie}{mV}\sum_{\boldsymbol{k},\omega}\sum_{\boldsymbol{p},\boldsymbol{q}}\sum_{\bar{\Omega},\Omega}\sum_{\ell mno} e^{-i(\boldsymbol{p}+\boldsymbol{q})\cdot\boldsymbol{r}+i(\bar{\Omega}+\Omega)t}\epsilon_{\ell mn}\alpha_{\mathrm{R},\ell}R_{no}(\boldsymbol{p},\bar{\Omega})A^o_{\mathrm{s},m}(\boldsymbol{q},\Omega) \\ &\times k_\mu \mathrm{tr}\left[g_{\boldsymbol{k}-\frac{\boldsymbol{q}}{2}-\frac{\boldsymbol{p}}{2},\omega-\frac{\Omega}{2}-\frac{\bar{\Omega}}{2}}g_{\boldsymbol{k}+\frac{\boldsymbol{q}}{2}+\frac{\boldsymbol{p}}{2},\omega+\frac{\Omega}{2}+\frac{\bar{\Omega}}{2}}\right]^<. \end{aligned} \tag{C.16}$$

First, we calculate Eq. (C.14). Performing trace over the spin after use of the Langreth's methods [100, 102], $\boldsymbol{j}^{(\mathrm{A})}$ becomes

$$j_\mu^{(\mathrm{A})} = -\sum_{\boldsymbol{p},\bar{\Omega}}\sum_m e^{-i\boldsymbol{p}\cdot\boldsymbol{r}+i\bar{\Omega}t}a_{\mu m}(\boldsymbol{p},\bar{\Omega})[\boldsymbol{\alpha}_{\mathrm{R}}\times\boldsymbol{n}(\boldsymbol{p},\bar{\Omega})]_m, \tag{C.17}$$

with

$$\begin{aligned} a_{\mu m} =& -\frac{ie}{mV}\sum_{\boldsymbol{k},\omega}\sum_\sigma \sigma\Bigg\{\left[f(\omega+\frac{\bar{\Omega}}{2})-f(\omega-\frac{\bar{\Omega}}{2})\right]k_\mu k_m g^{\mathrm{r}}_{\boldsymbol{k}-\frac{\boldsymbol{p}}{2},\omega-\frac{\bar{\Omega}}{2},\sigma}g^{\mathrm{a}}_{\boldsymbol{k}+\frac{\boldsymbol{p}}{2},\omega+\frac{\bar{\Omega}}{2},\sigma} \\ &+ f(\omega-\frac{\bar{\Omega}}{2})k_\mu k_m g^{\mathrm{a}}_{\boldsymbol{k}-\frac{\boldsymbol{p}}{2},\omega-\frac{\bar{\Omega}}{2},\sigma}g^{\mathrm{a}}_{\boldsymbol{k}+\frac{\boldsymbol{p}}{2},\omega+\frac{\bar{\Omega}}{2},\sigma} + f(\omega+\frac{\bar{\Omega}}{2})k_\mu k_m g^{\mathrm{r}}_{\boldsymbol{k}-\frac{\boldsymbol{p}}{2},\omega-\frac{\bar{\Omega}}{2},\sigma}g^{\mathrm{r}}_{\boldsymbol{k}+\frac{\boldsymbol{p}}{2},\omega+\frac{\bar{\Omega}}{2},\sigma} \\ &+ m\delta_{\mu m}f(\omega)(g^{\mathrm{a}}_{\boldsymbol{k},\omega,\sigma}-g^{\mathrm{r}}_{\boldsymbol{k},\omega,\sigma})\Bigg\}, \end{aligned} \tag{C.18}$$

where we use the fact that $R_{kz} = n_k$, $\sigma = \pm$ is the diagonalized spin index, $g^{\mathrm{r}}_{\boldsymbol{k},\omega,\sigma} \equiv (\omega - \epsilon_{\boldsymbol{k},\sigma} + \frac{i}{2\tau_{\mathrm{e}}})^{-1}$, $g^{\mathrm{a}}_{\boldsymbol{k},\omega,\sigma} = (g^{\mathrm{r}}_{\boldsymbol{k},\omega,\sigma})^*$, and $\epsilon_{\boldsymbol{k},\sigma} = \frac{k^2}{2m} - \epsilon_{\mathrm{F}} - \sigma\Delta_{sd}$. We expand $a_{\mu m}$ with respect to the external wave vector $\boldsymbol{p}$ and frequency $\bar{\Omega}$. Carrying out the integration by parts with respect to $\boldsymbol{k}$ and ω, the result up to the first order in $\bar{\Omega}$ and the second order in $\boldsymbol{p}$ is

$$a_{\mu m} = i\bar{\Omega}\delta_{\mu m}a_1 + (\boldsymbol{p}^2 - p_\mu p_m)a_2, \tag{C.19}$$

where we use the fact that $f'(\omega) \equiv \frac{\partial f(\omega)}{\partial \omega} = -\delta(\omega)$ and a rotational symmetry in k-space, i.e., $k_\mu k_\nu = \frac{\boldsymbol{k}^2}{3}\delta_{\mu\nu}$, and a_1 and a_2 are defined as

$$a_1 \equiv \frac{e}{6m}\sum_{\boldsymbol{k}}\sum_{\sigma}\sigma\boldsymbol{k}^2(g^{\rm a}_{\boldsymbol{k},\sigma} - g^{\rm r}_{\boldsymbol{k},\sigma})^2, \tag{C.20}$$

$$a_2 \equiv -\frac{ie}{12m}\sum_{\boldsymbol{k}}\sum_{\sigma}\sigma(g^{\rm a}_{\boldsymbol{k},\sigma} - g^{\rm r}_{\boldsymbol{k},\sigma}). \tag{C.21}$$

We thus obtain $\boldsymbol{j}^{(\rm A)}$ as

$$\boldsymbol{j}^{(\rm A)} = -a_1\frac{\partial}{\partial t}(\boldsymbol{\alpha}_{\rm R}\times\boldsymbol{n}) + a_2\boldsymbol{\nabla}\times[\boldsymbol{\nabla}\times(\boldsymbol{\alpha}_{\rm R}\times\boldsymbol{n})]. \tag{C.22}$$

Next, we calculate $\boldsymbol{j}^{(\rm B)}$ in the same manner as $\boldsymbol{j}^{(\rm A)}$. Expanding Eq. (C.15) with respect to $\boldsymbol{p}$ and $\boldsymbol{q}$, the result up to the first order in $\boldsymbol{p}$ and $\boldsymbol{q}$ is given by

$$\begin{aligned} j^{(\rm B)}_\mu =& -\frac{ie}{3mV}\sum_{\boldsymbol{k},\omega}\sum_{\boldsymbol{p},\boldsymbol{q}}\sum_{\bar\Omega,\Omega}\sum_{\nu j\ell mno} e^{-i(\boldsymbol{p}+\boldsymbol{q})\cdot\boldsymbol{r}+i(\bar\Omega+\Omega)t}\epsilon_{\ell mn}\alpha_{{\rm R},\ell}R_{no}(\boldsymbol{p},\bar\Omega)A^j_{{\rm s},\nu}(\boldsymbol{q},\Omega) \\ &\times\frac{\boldsymbol{k}^2}{2m}[(\boldsymbol{q}+\boldsymbol{p})_m\delta_{\mu\nu} - (\boldsymbol{q}+\boldsymbol{p})_\nu\delta_{\mu m}]{\rm tr}\Big[\sigma_j g_{\boldsymbol{k},\omega}\sigma_o(g_{\boldsymbol{k},\omega})^2 - \sigma_o g_{\boldsymbol{k},\omega}\sigma_j(g_{\boldsymbol{k},\omega})^2\Big]^<. \end{aligned} \tag{C.23}$$

Using the spin trace formula

$${\rm tr}[\sigma_j g_{\boldsymbol{k},\omega}\sigma_o(g_{\boldsymbol{k},\omega})^2 - \sigma_o g_{\boldsymbol{k},\omega}\sigma_j(g_{\boldsymbol{k},\omega})^2] = 2i\epsilon_{joz}\sum_{\sigma} g_{\boldsymbol{k},\omega,-\sigma}(g_{\boldsymbol{k},\omega,\sigma})^2, \tag{C.24}$$

where $g_{\boldsymbol{k},\omega,\sigma}$ is Green's function diagonalized in spin space, Eq. (C.23) reduces to

$$\begin{aligned} j^{(\rm B)}_\mu =& a_3\sum_{\boldsymbol{k},\omega}\sum_{\boldsymbol{p},\boldsymbol{q}}\sum_{\bar\Omega,\Omega}\sum_{\nu j\ell mno} e^{-i(\boldsymbol{p}+\boldsymbol{q})\cdot\boldsymbol{r}+i(\bar\Omega+\Omega)t}2i\epsilon_{\ell mn}\epsilon_{joz}\alpha_{{\rm R},\ell}R_{no}(\boldsymbol{p},\bar\Omega)A^j_{{\rm s},\nu}(\boldsymbol{q},\Omega) \\ &\times[(\boldsymbol{q}+\boldsymbol{p})_m\delta_{\mu\nu} - (\boldsymbol{q}+\boldsymbol{p})_\nu\delta_{\mu m}], \end{aligned} \tag{C.25}$$

where

$$a_3 \equiv \frac{ie}{6m}\sum_{\boldsymbol{k}}\sum_{\sigma}\sigma\left(\frac{\boldsymbol{k}^2}{2m}\right)^2[g^{\rm a}_{\boldsymbol{k},-\sigma}(g^{\rm a}_{\boldsymbol{k},\omega,\sigma})^2 - g^{\rm r}_{\boldsymbol{k},-\sigma}(g^{\rm r}_{\boldsymbol{k},\omega,\sigma})^2]. \tag{C.26}$$

By use of the following equation,

$$\begin{aligned} [\boldsymbol{\nabla}\times[\boldsymbol{\nabla}\times(\boldsymbol{\alpha}_{\rm R}\times\boldsymbol{n})]]_\mu =& 2i\sum_{\boldsymbol{p},\boldsymbol{q}}\sum_{\bar\Omega,\Omega}\sum_{\nu j\ell mno} e^{-i(\boldsymbol{p}+\boldsymbol{q})\cdot\boldsymbol{r}+i(\bar\Omega+\Omega)t}\epsilon_{\ell mn}\epsilon_{joz}\alpha_{{\rm R},\ell}R_{no}(\boldsymbol{p},\bar\Omega) \\ &\times[(\boldsymbol{q}+\boldsymbol{p})_m\delta_{\mu\nu}A^j_{{\rm s},\nu}(\boldsymbol{q},\Omega) - (\boldsymbol{q}+\boldsymbol{p})_\nu\delta_{\mu m}A^j_{{\rm s},\nu}(\boldsymbol{q},\Omega)], \end{aligned} \tag{C.27}$$

Eq. (C.23) reads

$$\boldsymbol{j}^{(\rm B)} = a_3\boldsymbol{\nabla}\times[\boldsymbol{\nabla}\times(\boldsymbol{\alpha}_{\rm R}\times\boldsymbol{n})]. \tag{C.28}$$

From the results of Eqs. (C.22) and Eq. (C.28), the pumped electric current is thus given by

$$\boldsymbol{j}_{\rm pump} = -a_1\frac{\partial}{\partial t}(\boldsymbol{\alpha}_{\rm R}\times\boldsymbol{n}) + b_1\boldsymbol{\nabla}\times[\boldsymbol{\nabla}\times(\boldsymbol{\alpha}_{\rm R}\times\boldsymbol{n})], \tag{C.29}$$

where $b_1 \equiv a_2 + a_3$.

C.2 Spin Hall current induced by Rashba-induced spin magnetic field

As was pointed out in Refs. [28, 46], the result of the pumped current is not useful in order to estimate magnetic components in solids, the effective magnetic filed and the spin-dependent magnetic permeability, simultaneously. Therefore, we should calculate the spin Hall current induced by the effective magnetic fields under the effect of an applied electric field to achieve the decision of the magnetic components. In this calculation, we introduce the static magnetization texture and the spatially uniformed electric field.

The Lagrangian we consider in the rotated space is given by

$$L \equiv L_0 + L^{(2)}_{A_{\rm s}}, \tag{C.30}$$

$$L_0 \equiv \int {\rm d}^3 r a^\dagger \left(i\partial_t + \frac{1}{2m}\boldsymbol{\nabla}^2 + \mu + \Delta_{sd}\sigma_z \right) a, \tag{C.31}$$

$$\begin{aligned} L^{(2)}_{A_{\rm s}} \equiv \int {\rm d}^3 r \Big[. &- \sum_i A_i j_i - \frac{e^2}{2m}\sum_i (A_i)^2 a^\dagger a - \sum_{i,\alpha} A^\alpha_{{\rm s},i} j^\alpha_{{\rm s},i} - \frac{e^2}{2m}\sum_{i,\alpha}(A^\alpha_{{\rm s},i})^2 a^\dagger a \\ &+ e\sum_{jk\ell n}\epsilon_{jk\ell}\alpha_{{\rm R},j}A_k R_{\ell n} a^\dagger \sigma_n a - \frac{e}{m}\sum_{i\alpha} A_i A^\alpha_{{\rm s},i} a^\dagger \sigma_\alpha a \\ &+ \frac{1}{2}\sum_{ijkn}\epsilon_{ijk}\alpha_{{\rm R},i}R_{kn}\left(-\frac{2m}{e} j^n_{{\rm s},j} - 2eA^n_{{\rm s},j} a^\dagger a \right) \Big], \end{aligned} \tag{C.32}$$

where $j^\alpha_i \equiv -ie\frac{1}{2m} a^\dagger \overleftrightarrow{\nabla}_i a$ is the charge current. In the rotated frame, the electric current reads

$$j_\mu(\boldsymbol{r}, t) = \frac{ie}{2m}\langle a^\dagger \overleftrightarrow{\nabla}_\mu a\rangle - \frac{e^2}{m}\sum_\ell A_\mu \langle a^\dagger a\rangle - e\sum_{jk\ell}\epsilon_{\mu jk\ell}\alpha_{{\rm R},j}R_{k\ell}\langle a^\dagger \sigma_\ell a\rangle, \tag{C.33}$$

where $\langle\ \rangle$ denotes the expectation value for L. In terms of Green's function, Eq. (C.33) becomes

$$j_\mu = \lim_{\substack{\boldsymbol{r}'\to\boldsymbol{r} \\ t'\to t}} {\rm tr} \left\{ \begin{array}{c} \frac{e}{2m}[(\nabla_{\boldsymbol{r}',\mu} - \nabla_{\boldsymbol{r},\mu})G^<(\boldsymbol{r}, \boldsymbol{r}', t, t')] + \frac{ie^2}{m}A_\mu G^<(\boldsymbol{r}, \boldsymbol{r}', t, t') \\ +ie\sum_{jk\ell}\epsilon_{\mu jk}\alpha_{{\rm R},j}R_{k\ell}[\sigma_\ell G^<(\boldsymbol{r}, \boldsymbol{r}', t, t')] \end{array} \right\}, \tag{C.34}$$

where $G^<(\boldsymbol{r}, \boldsymbol{r}', t, t') \equiv i\langle a^\dagger(\boldsymbol{r}', t')a(\boldsymbol{r}, t)\rangle$ is a lesser component of contour ordered Green's function. We calculate the electric current up to the linear order in both the Rashba field and the gauge filed. In the calculation, we use the following Dyson

equation,

$$
\begin{aligned}
G(\boldsymbol{r},\boldsymbol{r}',t,t') =& \frac{1}{V}\sum_{\boldsymbol{k},\omega} e^{i\boldsymbol{k}\cdot(\boldsymbol{r}-\boldsymbol{r}')-i\omega(t-t')} g_{\boldsymbol{k},\omega} \\
&+ \frac{e}{mV}\sum_{\boldsymbol{k},\omega}\sum_{\Omega}\sum_{j} e^{i\boldsymbol{k}\cdot(\boldsymbol{r}-\boldsymbol{r}')-i\omega t+i(\omega+\Omega)t'} A_j(\Omega) k_j g_{\boldsymbol{k},\omega}\sigma_j g_{\boldsymbol{k},\omega+\Omega} \\
&- \frac{1}{V}\sum_{\boldsymbol{k},\omega}\sum_{\boldsymbol{p}}\sum_{jl\ell n} e^{i\boldsymbol{k}\cdot\boldsymbol{r}-i(\boldsymbol{k}+\boldsymbol{p})\cdot\boldsymbol{r}'-i\omega(t-t')} \\
&\times \epsilon_{jk\ell}\alpha_{\mathrm{R},j} R_{\ell n}(\boldsymbol{p}) \left(\boldsymbol{k}+\frac{\boldsymbol{p}}{2}\right)_k g_{\boldsymbol{k},\omega}\sigma_n g_{\boldsymbol{k}+\boldsymbol{p},\omega} \\
&- \frac{e}{V}\sum_{\boldsymbol{k},\omega}\sum_{\boldsymbol{p},\Omega}\sum_{jk\ell n} e^{i\boldsymbol{k}\cdot\boldsymbol{r}-i\omega t-i(\boldsymbol{k}+\boldsymbol{p})\cdot\boldsymbol{r}'+i(\omega+\Omega)t'} \\
&\times \epsilon_{jk\ell}\alpha_{\mathrm{R},j} R_{\ell n}(\boldsymbol{p}) A_k(\Omega) g_{\boldsymbol{k},\omega}\sigma_n g_{\boldsymbol{k}+\boldsymbol{p},\omega+\Omega} \\
&- \frac{e}{mV}\sum_{\boldsymbol{k},\omega}\sum_{\boldsymbol{p},\Omega}\sum_{jk\ell mn} e^{i\boldsymbol{k}\cdot\boldsymbol{r}-i\omega t-i(\boldsymbol{k}+\boldsymbol{p})\cdot\boldsymbol{r}'+i(\omega+\Omega)t'} \epsilon_{jk\ell}\alpha_{\mathrm{R},j} A_m(\Omega) R_{\ell n}(\boldsymbol{p}) \\
&\times \begin{bmatrix} \left(\boldsymbol{k}+\frac{\boldsymbol{p}}{2}\right)_k (\boldsymbol{k}+\boldsymbol{p})_m g_{\boldsymbol{k},\omega}\sigma_n g_{\boldsymbol{k}+\boldsymbol{p},\omega} g_{\boldsymbol{k}+\boldsymbol{p},\omega+\Omega} \\ +k_m \left(\boldsymbol{k}+\frac{\boldsymbol{p}}{2}\right)_k g_{\boldsymbol{k},\omega} g_{\boldsymbol{k},\omega+\Omega}\sigma_n g_{\boldsymbol{k}+\boldsymbol{p},\omega+\Omega} \end{bmatrix},
\end{aligned}
\tag{C.35}
$$

where where $\boldsymbol{p}$ is the wave vector carried by the magnetization texture and Ω is the angular frequency carried by the gauge field.

Using the Dyson equation, the result being bilinear in the Rashba field and the gauge field is given by (diagrammatically shown in Fig. 1.6)

$$
\boldsymbol{j}_{\mathrm{Hall}} = \boldsymbol{j}^{(\mathrm{Hall},1)} + \boldsymbol{j}^{(\mathrm{Hall},2)},
\tag{C.36}
$$

with

$$
\begin{aligned}
j_\mu^{(\mathrm{Hall},1)} =& -\frac{ie^2}{mV}\sum_{\boldsymbol{k},\omega}\sum_{\boldsymbol{p},\Omega}\sum_{jk\ell mn} e^{-i\boldsymbol{p}\cdot\boldsymbol{r}+i\Omega t}\epsilon_{jk\ell}\alpha_{\mathrm{R},j} R_{\ell n}(\boldsymbol{p}) A_m(\Omega) \\
&\times \mathrm{tr}\Bigg[-\delta_{km}k_\mu g_{\boldsymbol{k}-\frac{\boldsymbol{p}}{2},\omega-\frac{\Omega}{2}}\sigma_n g_{\boldsymbol{k}+\frac{\boldsymbol{p}}{2},\omega+\frac{\Omega}{2}} \\
&- \frac{k_\mu k_k}{m}\left(\boldsymbol{k}+\frac{\boldsymbol{p}}{2}\right)_m g_{\boldsymbol{k}-\frac{\boldsymbol{p}}{2},\omega-\frac{\Omega}{2}}\sigma_n g_{\boldsymbol{k}+\frac{\boldsymbol{p}}{2},\omega+\frac{\Omega}{2}} g_{\boldsymbol{k}+\frac{\boldsymbol{p}}{2},\omega+\frac{\Omega}{2}} \\
&- \frac{k_\mu k_k}{m}\left(\boldsymbol{k}-\frac{\boldsymbol{p}}{2}\right)_m g_{\boldsymbol{k}-\frac{\boldsymbol{p}}{2},\omega-\frac{\Omega}{2}} g_{\boldsymbol{k}-\frac{\boldsymbol{p}}{2},\omega+\frac{\Omega}{2}}\sigma_n g_{\boldsymbol{k}+\frac{\boldsymbol{p}}{2},\omega+\frac{\Omega}{2}}\Bigg]^<,
\end{aligned}
\tag{C.37}
$$

$$
\begin{aligned}
j_\mu^{(\mathrm{Hall},2)} =& -\frac{ie^2}{mV}\sum_{\boldsymbol{k},\omega}\sum_{\boldsymbol{p},\Omega}\sum_{jk\ell mn} e^{-i\boldsymbol{p}\cdot\boldsymbol{r}+i\Omega t}\epsilon_{jk\ell}\alpha_{\mathrm{R},j} R_{\ell n}(\boldsymbol{p}) A_m(\Omega) \\
&\times \mathrm{tr}\left[\delta_{\mu k}k_m\sigma_n g_{\boldsymbol{k},\omega-\frac{\Omega}{2}} g_{\boldsymbol{k},\omega+\frac{\Omega}{2}} - \delta_{\mu m}k_k g_{\boldsymbol{k}-\frac{\boldsymbol{p}}{2},\omega}\sigma_n g_{\boldsymbol{k}+\frac{\boldsymbol{p}}{2},\omega}\right]^<,
\end{aligned}
\tag{C.38}
$$

Let us calculate Eq. (C.37). Expanding $\boldsymbol{j}^{(\mathrm{Hall},1)}$ with respect to Ω and $\boldsymbol{p}$, the result up to the linear order in both Ω and $\boldsymbol{p}$ is given by

$$
j_\mu^{(\mathrm{Hall},1)} = -c_1\sum_{\boldsymbol{p},\Omega} e^{-i\boldsymbol{p}\cdot\boldsymbol{r}+i\Omega t}\sum_{jk\ell mn}\epsilon_{jk\ell}\alpha_{\mathrm{R},j} R_{\ell n}(\boldsymbol{p}) A_m(\Omega)\delta_{nz}\Omega(p_\mu\delta_{km}-p_m\delta_{\mu k}),
\tag{C.39}
$$

where

$$c_1 \equiv \frac{ie^2}{3m^2}\sum_{\boldsymbol{k}}\sum_{\sigma}\sigma\boldsymbol{k}^2[(g^{\rm a}_{\boldsymbol{k},\omega,\sigma})^3-(g^{\rm r}_{\boldsymbol{k},\omega,\sigma})^3]. \tag{C.40}$$

Using the following equation,

$$\begin{aligned}[\boldsymbol{E}\times[\boldsymbol{\nabla}\times(\boldsymbol{\alpha}_{\rm R}\times\boldsymbol{n})]]_\mu =& \sum_{\boldsymbol{p},\Omega} e^{-i\boldsymbol{p}\cdot\boldsymbol{r}+i\Omega t}\sum_{jk\ell mn}\epsilon_{jk\ell}\alpha_{{\rm R},j}R_{\ell n}(\boldsymbol{p})A_m(\Omega)\\ &\times\delta_{nz}\Omega(p_\mu\delta_{km}-p_m\delta_{\mu k}),\end{aligned} \tag{C.41}$$

we thus obtain the Hall current as

$$\boldsymbol{j}_{\rm Hall} = -\,c_1\boldsymbol{E}\times[\boldsymbol{\nabla}\times(\boldsymbol{\alpha}_{\rm R}\times\boldsymbol{n})]. \tag{C.42}$$

Appendix D

Microscopic derivation of Dzyaloshinskii-Moriya interaction

In this section, we show that the equilibrium spin current induces the Dzyaloshinskii-Moriya interaction by deriving an effective Hamiltonian for the magnetization based on the imaginary-time path-integral formalism. In this calculation, we introduce the static magnetization texture.

The imaginary-time Lagrangian we consider in the laboratory frame is

$$L = \int \mathrm{d}^3 r \bar{c} \left[\partial_\tau - \frac{1}{2m} \boldsymbol{\nabla}^2 - \mu - \Delta_{sd} \boldsymbol{n} \cdot \boldsymbol{\sigma} + \frac{i}{2} \sum_i \boldsymbol{\lambda}_i \cdot \boldsymbol{\sigma} \overleftrightarrow{\nabla}_i \right] c, \tag{D.1}$$

where $\boldsymbol{\lambda}$ is the spin-orbit field representing the breaking of spatial-inversion symmetry and conduction electrons are represented by two component annihilation and creation fields, c and $\bar{c}$ defined on imaginary-time, τ. By introducing the spin gauge field by use of the local unitary transformation in order to diagonalize the sd interaction, the Lagrangian in the rotated space is thus decomposed L_0 into L_{A_s} as shown below.

$$L_0 \equiv \int \mathrm{d}^3 r \bar{a} \left(\partial_\tau - \frac{1}{2m} \boldsymbol{\nabla}^2 - \mu - \Delta_{sd} \sigma_z + \frac{i}{2} \sum_{i,\alpha\beta} R_{\alpha\beta} \lambda_i^\beta \overleftrightarrow{\nabla}_i \sigma_\alpha \right) a, \tag{D.2}$$

$$L_{A_\mathrm{s}} \equiv \int \mathrm{d}^3 r \left[\sum_{i,\alpha} A^\alpha_{\mathrm{s},i} j^\alpha_{\mathrm{s},i} + \frac{e^2}{2m} \sum_{i,\alpha} (A^\alpha_{\mathrm{s},i})^2 \bar{a} a - e \sum_{i,\alpha\beta} R_{\alpha\beta} \lambda_i^\beta A^\alpha_{\mathrm{s},j} \bar{a} a \right], \tag{D.3}$$

where a and $\bar{a}$ are annihilation and creation fields describing the spin-polarized conduction electrons in the rotated frame. The effective Hamiltonian for the magnetization, $H_\mathrm{eff} \equiv -\ln \mathcal{Z}$, is calculated by integrating out of the variables of the electrons in the partition function, $\mathcal{Z}(\boldsymbol{A}_\mathrm{s}) = \int \mathcal{D}\bar{c}\mathcal{D}c e^{-\int_0^\beta d\tau L(\bar{c},c,\boldsymbol{A}_\mathrm{s})}$, where $\mathcal{D}$ denotes the path integral. The contribution of the first order in the spin gauge field, diagramatically shown in Fig. D.1, reads,

$$\ln \mathcal{Z} = -\int_0^\beta \mathrm{d}\tau \int \mathrm{d}^3 r \sum_{\mu\alpha} A^\alpha_{\mathrm{s},\mu} \tilde{j}^\alpha_{\mathrm{s},\mu}, \tag{D.4}$$

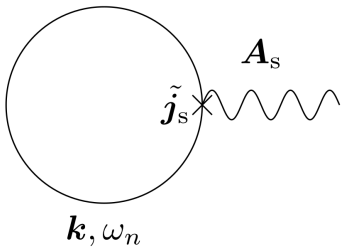

Figure D.1: Diagrammatic representation of the contribution to the effective Hamiltonian. Solid lines represent the thermal Green's function including the spin-orbit and *sd* exchange interactions and the wavy lines denote the spin gauge field, respectively.

where

$$\tilde{j}^{\alpha}_{{\rm s},\mu} = -\frac{1}{\beta V}\sum_{\boldsymbol{k},n}{\rm tr}\left[-\frac{k_\mu}{m}\sigma_\alpha \mathscr{G}_{\boldsymbol{k},n,sd} - \sum_\beta R_{\alpha\beta}\lambda^\beta_\mu \mathscr{G}_{\boldsymbol{k},n,sd}\right] \tag{D.5}$$

is the spin current density in rotated frame and

$$\mathscr{G}_{\boldsymbol{k},n,sd} \equiv \frac{1}{i\omega_n - \epsilon_{\boldsymbol{k}} + \boldsymbol{\gamma}_{\boldsymbol{k},sd}\cdot\boldsymbol{\sigma} + i\eta{\rm sgn}(\omega_n)} \tag{D.6}$$

is the thermal Green's function for electrons that includes the spin-orbit and *sd*-exchange interactions. Here, $\boldsymbol{k}$ and $\omega_n \equiv \frac{(2n+1)\pi}{\beta}$ (n is an integer) indicate the wave vector and fermionic thermal frequency, respectively, $\epsilon_{\boldsymbol{k}} = \frac{k^2}{2m} - \mu$ is the electron energy measured from the Fermi energy, and $\gamma^\alpha_{\boldsymbol{k},sd} \equiv \sum_{i\beta} R_{\alpha\beta}\lambda^\beta_i k_i + \Delta_{sd}\hat{z}^\alpha$ with $\hat{z} \equiv (0,0,1)$. We have included a finite electron-elastic-scattering lifetime $\tau_{\rm e}$ as an imaginary part, $\eta \equiv \frac{1}{2\tau_{\rm e}}$, and ${\rm sgn}(\omega_n) \equiv 1$ and -1 for $\omega_n > 0$ and $\omega_n < 0$, respectively.

Expanding Eq. (D.5) with respect to $\boldsymbol{\lambda}$ by use of the resolvent expansion, the result up to the linear order in $\boldsymbol{\lambda}$ and the zero-order in Δ_{sd} is reduced to

$$\tilde{j}^{\alpha}_{{\rm s},\mu} \simeq \sum_\beta R_{\alpha\beta} j^\beta_{{\rm s},\mu}, \tag{D.7}$$

where

$$\boldsymbol{j}_{\rm s} \equiv 2n_{\rm e}\boldsymbol{\lambda} \tag{D.8}$$

is the spin current density in the laboratory frame and $n_{\rm e} \equiv \frac{1}{V}\sum_{\boldsymbol{k}}\sum_\sigma f(\epsilon_{\boldsymbol{k}})$ is the electron density. Using the following relation,

$$\sum_\alpha R_{\alpha\beta}A^\alpha_{{\rm s},\mu} = \frac{1}{2}(\nabla_\mu \boldsymbol{n}\times\boldsymbol{n})^\beta + n^\beta A_{{\rm s},\mu}, \tag{D.9}$$

we thus get the effective Hamiltonian as [82]

$$H_{\rm eff} = \int {\rm d}^3 r\left[\sum_{i,\alpha} D^\alpha_i(\boldsymbol{n}\times\nabla_i\boldsymbol{n})^\alpha + \boldsymbol{j}^{\parallel}_{\rm s}\cdot\boldsymbol{A}^z_{\rm s}\right], \tag{D.10}$$

with

$$\boldsymbol{D} \equiv \boldsymbol{j}_{\mathrm{s}}^{\perp}, \tag{D.11}$$

where $j_{\mathrm{s},\mu}^{\perp,\alpha} \equiv j_{\mathrm{s},\mu}^{\alpha} - n^{\alpha} j_{\mathrm{s},\mu}^{\parallel}$ and $j_{\mathrm{s},\mu}^{\parallel} \equiv \boldsymbol{n} \cdot \boldsymbol{j}_{\mathrm{s},\mu}$. The first term on the right-hand side of Eq. (D.10) describes the Dzyaloshinskii-Moriya interaction induced by the spin current density with the spin component perpendicular to the magnetization vector. The second term on the right-hand side of Eq. (D.10) means the spin-transfer term originated from the spin current density with the spin component parallel to the magnetization vector.

Appendix E

Partition function in path integral formalism

Under the effect of a finite temperature, the equilibrium properties is determined by the partition function as shown below.

$$\mathcal{Z}(\beta) = \mathrm{Tr}\ e^{-\beta \hat{H}_{\mathrm{T}}}, \tag{E.1}$$

where $\hat{H}_{\mathrm{T}} \equiv \hat{H} - \mu \hat{N}$, $\hat{H}$ is the Hamiltonian of the system, $\hat{N}$ is the particle number operator, μ is the chemical potential of the system, β is the inverse temperature, Tr is over the entire Hilbert space. In fermion system, Eq. (E.1) reduces to

$$\mathcal{Z} = \sum_{n=0}^{1} \langle n | e^{-\beta \hat{H}_{\mathrm{T}}} | n \rangle, \tag{E.2}$$

where $|n\rangle$ is the Fock space state.

In order to construct the path integral representation of the partition function in fermion system, we introduce the fermionic coherent states, $|\psi\rangle$ and $\langle\psi|$, as

$$\begin{aligned} |\psi\rangle &= |0\rangle + |1\rangle\psi, \\ \langle\psi| &= \langle 0| + \bar{\psi}\langle\psi|. \end{aligned} \tag{E.3}$$

Here, ψ and $\bar{\psi}$ are the Grassmann numbers satisfying $\{\psi, \psi\} = 0$, $\{\bar{\psi}, \bar{\psi}\} = 0$, $\{\psi, \bar{\psi}\} = 0$, $\hat{\psi}|\psi\rangle = \psi|\psi\rangle$, and $\langle\psi|\hat{\psi}^{\dagger} = \langle\psi|\bar{\psi}$, where $\{A, B\} \equiv AB + BA$ and $\hat{\psi}$ and $\hat{\psi}^{\dagger}$ represent annihilation and creation operators, respectively. Since integration over Grassmann variable ψ is defined by $\int \mathrm{d}\psi = 0$ and $\int \mathrm{d}\psi\psi = 1$, the resolution of identity for the coherent states is given by

$$\int \mathrm{d}\bar{\psi}\mathrm{d}\psi e^{-\bar{\psi}\psi} |\psi\rangle\langle\psi| = 1. \tag{E.4}$$

Using the above equation, the partition function, Eq, (E.2), reads

$$\mathcal{Z} = \int \mathrm{d}\bar{\psi}\mathrm{d}\psi e^{-\bar{\psi}\psi} \langle -\psi | e^{-\beta \hat{H}_{\mathrm{T}}} | \psi \rangle. \tag{E.5}$$

Dividing β into N segments of infinitesimal length $\Delta\tau \equiv \frac{\beta}{N}$ and inserting coherent states resolution of identity, Eq. (E.5) becomes

$$\mathcal{Z} = \int_{\substack{\bar{\psi}_N=-\bar{\psi}_0 \\ \psi_N=-\psi_0}} \prod_{i=1}^{N} \mathrm{d}\bar{\psi}_i \mathrm{d}\psi_i \exp\left[-\Delta\tau \sum_{j=1} N\left(\bar{\psi}_j \frac{\psi_j - \psi_{j-1}}{\Delta\tau} + H_{\mathrm{T}}(\bar{\psi}_j, \psi_{j-1})\right)\right], \tag{E.6}$$

where $H_{\mathrm{T}}(\bar{\psi}_j, \psi_{j-1}) \equiv \langle\psi_j|\hat{H}_{\mathrm{T}}(\hat{\psi}^\dagger, \hat{\psi})|\psi_{j-1}\rangle$ and $\bar{\psi}_N = -\bar{\psi}_0$ ($\psi_N = -\psi_0$) means the anti-periodic boundary condition for $\bar{\psi}$ (ψ). Here we used the fact that $\hat{H}_{\mathrm{T}}$ is described by the annihilation and creation operators in second quantized representation. In the limit $N \to \infty$ and $\Delta\tau \to 0$, the path integral representation of partition function is thus obtained as [86]

$$\mathcal{Z} = \int \mathcal{D}\bar{\psi}\mathcal{D}\psi e^{-\int_0^\beta \mathrm{d}\tau L(\tau)}, \tag{E.7}$$

with

$$\mathcal{D}\bar{\psi}\mathcal{D}\psi \equiv \lim_{\substack{N\to\infty \\ \Delta\tau\to 0}} \prod_{i=1}^{N} \mathrm{d}\bar{\psi}_i \mathrm{d}\psi_i, \tag{E.8}$$

where $L(\tau) \equiv \bar{\psi}\frac{\partial}{\partial\tau}\psi + H_{\mathrm{T}}$ is corresponding to an imaginary-time Lagrangian and $\bar{\psi}(\tau)$ and $\psi(\tau)$ are creation and annihilation fields defined on an imaginary-time τ. We should keep in mind that $\bar{\psi}(\tau)$ ($\psi(\tau)$) satisfies the the anti-periodic boundary condition for fermion field $\bar{\psi}(\beta) = -\bar{\psi}(0)$ ($\psi(\beta) = -\psi(0)$).

Appendix F

Derivation of Eq. (2.30)

This section shows the detailed derivation of Eq. (2.30) from Eq. (2.29). Let us first calculate $\chi_{jj}^{\mu\nu}$ shown in Eq. (2.29). Expanding $\mathscr{G}_{\boldsymbol{k},n,\boldsymbol{M}}$ with respect to $\boldsymbol{M}$ by use of the resolvent expansion, the term proportional to the linear order of $\boldsymbol{M}$ is given by

$$\begin{aligned}\chi_{jj}^{\mu\nu,(\boldsymbol{M}^1)} \simeq & -\frac{e^2 J_{sd}}{m^2\beta V}\sum_{n,\boldsymbol{k}}\sum_{\alpha}(-M_\alpha) \\ & \times \mathrm{tr}\Bigg[\frac{1}{2}\Bigg[\left(\boldsymbol{k}+\frac{\boldsymbol{q}}{2}\right)_\mu\left(\boldsymbol{k}+\frac{\boldsymbol{q}}{2}\right)_\nu \mathscr{G}_{\boldsymbol{k}+\boldsymbol{q},n+\ell} + \left(\boldsymbol{k}-\frac{\boldsymbol{q}}{2}\right)_\mu\left(\boldsymbol{k}-\frac{\boldsymbol{q}}{2}\right)_\nu \mathscr{G}_{\boldsymbol{k}-\boldsymbol{q},n-\ell}\Bigg] \\ & \times \{\mathscr{G}_{\boldsymbol{k},n},\sigma_\alpha\} \\ & + 2j_{\boldsymbol{k},n}^2 \sum_{mn'op}\epsilon_{\alpha mn'}\epsilon_{n'op}\hat{\gamma}_{\boldsymbol{k}}^m\hat{\gamma}_{\boldsymbol{k}}^o \\ & \times \Bigg[\left(\boldsymbol{k}+\frac{\boldsymbol{q}}{2}\right)_\mu\left(\boldsymbol{k}+\frac{\boldsymbol{q}}{2}\right)_\nu \mathscr{G}_{\boldsymbol{k}+\boldsymbol{q},n+\ell} + \left(\boldsymbol{k}-\frac{\boldsymbol{q}}{2}\right)_\mu\left(\boldsymbol{k}-\frac{\boldsymbol{q}}{2}\right)_\nu \mathscr{G}_{\boldsymbol{k}-\boldsymbol{q},n-\ell}\Bigg]\sigma_p\Bigg],\end{aligned} \tag{F.1}$$

with

$$j_{\boldsymbol{k},n} \equiv \frac{1}{2}\sum_{\sigma=\pm}\sigma \mathrm{g}_{\boldsymbol{k},n,\sigma}, \tag{F.2}$$

where $\hat{\boldsymbol{\gamma}}_{\boldsymbol{k}} \equiv \boldsymbol{\gamma}_{\boldsymbol{k}}/|\boldsymbol{\gamma}_{\boldsymbol{k}}|$, $\mathscr{G}_{\boldsymbol{k},n} \equiv [i\omega_n - \epsilon_{\boldsymbol{k}} - \boldsymbol{\gamma}_{\boldsymbol{k}}\cdot\boldsymbol{\sigma} + i\eta\mathrm{sgn}(n)]^{-1}$, $\boldsymbol{\gamma}_{\boldsymbol{k}} \equiv \boldsymbol{k}\times\boldsymbol{\alpha}_{\mathrm{R}}$, $\mathrm{g}_{\boldsymbol{k},n,\sigma} \equiv [i\omega_n - \epsilon_{\boldsymbol{k}}^\sigma + i\eta\mathrm{sgn}(n)]^{-1}$ with $\epsilon_{\boldsymbol{k}}^\sigma = \epsilon_{\boldsymbol{k}} + \sigma\gamma_{\boldsymbol{k}}$ ($\gamma_{\boldsymbol{k}} \equiv |\boldsymbol{\gamma}_{\boldsymbol{k}}|$) is the Green's function diagonalized in the spin space, $\sigma = \pm$ is the diagonalized spin index, and $\{A,B\} \equiv AB + BA$. Expanding Eq. (F.1) with respect to $\boldsymbol{q}$, the term being

bilinear in $\boldsymbol{M}$ and $\boldsymbol{q}$ is given by

$$\chi_{jj}^{\mu\nu,(\boldsymbol{M}^1,\boldsymbol{q}^1)} \simeq -\frac{e^2 J_{sd}}{2m^2\beta V}\sum_{n,\boldsymbol{k}}\sum_{\alpha}(-M_\alpha) \times \mathrm{tr}\left\{ \begin{array}{c} k_\mu k_\nu \left[\begin{array}{c} \frac{\boldsymbol{k}\cdot\boldsymbol{q}}{m}(\mathscr{G}^2_{\boldsymbol{k},n+\ell}-\mathscr{G}^2_{\boldsymbol{k},n-\ell})\{\mathscr{G}^2_{\boldsymbol{k},n},\sigma_\alpha\} \\ +\sum_\rho \gamma^\rho_{\boldsymbol{q}} \left[\begin{array}{c} \frac{1}{2}(\{\mathscr{G}^2_{\boldsymbol{k},n+\ell},\sigma_\rho\}-\{\mathscr{G}^2_{\boldsymbol{k},n-\ell},\sigma_\rho\}) \\ \times\{\mathscr{G}^2_{\boldsymbol{k},n},\sigma_\alpha\} \\ +2(j^2_{\boldsymbol{k},n+\ell}-j^2_{\boldsymbol{k},n-\ell}) \\ \times \sum_{\rho mn'op}\epsilon_{\rho mn'}\epsilon_{n'op}\hat{\gamma}^m_{\boldsymbol{k}}\hat{\gamma}^o_{\boldsymbol{k}}\sigma_p\{\mathscr{G}^2_{\boldsymbol{k},n},\sigma_\alpha\} \end{array} \right] \end{array} \right] \\ +\frac{1}{2}(k_\mu q_\nu + k_\nu q_\mu)(\mathscr{G}_{\boldsymbol{k},n+\ell}-\mathscr{G}_{\boldsymbol{k},n-\ell})\{\mathscr{G}^2_{\boldsymbol{k},n},\sigma_\alpha\} \\ +4j^2_{\boldsymbol{k},n}\sum_{mn'op}\epsilon_{\alpha mn'}\epsilon_{n'op}\hat{\gamma}^m_{\boldsymbol{k}}\hat{\gamma}^o_{\boldsymbol{k}} \\ \times\left[k_\mu k_\nu \left[\begin{array}{c} \frac{\boldsymbol{k}\cdot\boldsymbol{q}}{m}(\mathscr{G}^2_{\boldsymbol{k},n+\ell}-\mathscr{G}^2_{\boldsymbol{k},n-\ell})\sigma_p \\ +\sum_\rho \gamma^\rho_{\boldsymbol{q}} \left[\begin{array}{c} \frac{1}{2}(\{\mathscr{G}^2_{\boldsymbol{k},n+\ell},\sigma_\rho\}-\{\mathscr{G}^2_{\boldsymbol{k},n-\ell},\sigma_\rho\})\sigma_p \\ +2(j^2_{\boldsymbol{k},n+\ell}-j^2_{\boldsymbol{k},n-\ell}) \\ \times \sum_{\rho m'o'm''o''}\epsilon_{\rho m'o'}\epsilon_{o'm''o''}\hat{\gamma}^{m'}_{\boldsymbol{k}}\hat{\gamma}^{m''}_{\boldsymbol{k}}\sigma_{o''}\sigma_p \end{array} \right] \end{array} \right] \right. \\ \left. +\frac{1}{2}(k_\mu q_\nu + k_\nu q_\mu)(\mathscr{G}_{\boldsymbol{k},n+\ell}-\mathscr{G}_{\boldsymbol{k},n-\ell})\sigma_p \right] \end{array} \right\}. \tag{F.3}$$

Performing the trace over the spin using

$$\mathrm{tr}[\sigma_\alpha\sigma_\beta\sigma_\gamma\sigma_\delta] = 2(\delta_{\alpha\beta}\delta_{\gamma\delta}+\delta_{\beta\gamma}\delta_{\alpha\delta}-\delta_{\alpha\gamma}\delta_{\beta\delta}), \tag{F.4}$$

the result up to the linear order in $\boldsymbol{q}$ and $\boldsymbol{M}$ is obtained as

$$\chi_{jj}^{\mu\nu}(\boldsymbol{q},i\Omega_\ell,\boldsymbol{M}) \simeq -\frac{e^2 J_{sd}}{m^2\beta V}\sum_{n,\boldsymbol{k}}\sum_{\alpha}(-M_\alpha)(k_\mu q_\nu + q_\mu k_\nu)\hat{\gamma}^\alpha_{\boldsymbol{k}} \times\left[2h_{\boldsymbol{k},n}j_{\boldsymbol{k},n}(h_{\boldsymbol{k},n+\ell}-h_{\boldsymbol{k},n-\ell})+(h^2_{\boldsymbol{k},n}+j^2_{\boldsymbol{k},n})(j_{\boldsymbol{k},n+\ell}-j_{\boldsymbol{k},n-\ell})\right], \tag{F.5}$$

with

$$h_{\boldsymbol{k},n} \equiv \frac{1}{2}\sum_{\sigma=\pm}\mathrm{g}_{\boldsymbol{k},n,\sigma}. \tag{F.6}$$

Other correlation functions are calculated similarly as

$$\chi^{\mu\nu}_{sj}(\boldsymbol{q}, i\Omega_\ell, \boldsymbol{M}) \simeq -\frac{e^2 J_{sd}}{m\beta V}\sum_{n,\boldsymbol{k}}\sum_{m\alpha\beta\rho}\epsilon_{\mu m\alpha}\alpha_{\mathrm{R},m}(-M_\beta)$$
$$\times\left\{\begin{array}{c} -\frac{4}{m}q_\rho(k_\nu k_\rho\delta_{\alpha\beta} - k_\nu k_\rho\hat{\gamma}^\alpha_{\boldsymbol{k}}\hat{\gamma}^\beta_{\boldsymbol{k}})j^2_{\boldsymbol{k},n}(h^2_{\boldsymbol{k},n+\ell} - h^2_{\boldsymbol{k},n-\ell}) \\ +4\gamma^\rho_{\boldsymbol{q}}(\delta_{\rho\alpha}k_\nu\hat{\gamma}^\beta_{\boldsymbol{k}} - \delta_{\alpha\beta}k_\nu\hat{\gamma}^\rho_{\boldsymbol{k}})h_{\boldsymbol{k},n}j_{\boldsymbol{k},n} \\ \times[(h^2_{\boldsymbol{k},n+\ell} - h^2_{\boldsymbol{k},n-\ell}) - (j^2_{\boldsymbol{k},n+\ell} - j^2_{\boldsymbol{k},n-\ell})] \\ +q_\rho\delta_{\rho j}\begin{bmatrix}\delta_{\alpha\beta}(h^2_{\boldsymbol{k},n} - j^2_{\boldsymbol{k},n})(h_{\boldsymbol{k},n+\ell} - h_{\boldsymbol{k},n-\ell}) \\ +2\hat{\gamma}^\alpha_{\boldsymbol{k}}\hat{\gamma}^\beta_{\boldsymbol{k}}[h_{\boldsymbol{k},n}j_{\boldsymbol{k},n}(j_{\boldsymbol{k},n+\ell} - j_{\boldsymbol{k},n-\ell}) \\ +j^2_{\boldsymbol{k},n}(h_{\boldsymbol{k},n+\ell} - h_{\boldsymbol{k},n-\ell})]\end{bmatrix}\end{array}\right\},$$
$$\chi^{\mu\nu}_{ss}(\boldsymbol{q}, i\Omega_\ell, \boldsymbol{M}) \simeq -\frac{e^2 J_{sd}}{\beta V}\sum_{n,\boldsymbol{k}}\sum_{mo\alpha\beta\gamma}\sum_{\mu'\nu'\rho}\epsilon_{\mu o\alpha}\epsilon_{\nu m\beta}\alpha_{\mathrm{R},o}\alpha_{\mathrm{R},m}(-M_\gamma)$$
$$\times\left\{\begin{array}{c} -\frac{4}{m}q_{\nu'}\begin{bmatrix} k_{\nu'}\hat{\gamma}^{\mu'}_{\boldsymbol{k}}(\epsilon_{\alpha\mu'\rho}\epsilon_{\rho\gamma\beta} + \epsilon_{\alpha\gamma\rho}\epsilon_{\rho\mu'\beta}) \\ \times h_{\boldsymbol{k},n}j_{\boldsymbol{k},n}[(h^2_{\boldsymbol{k},n+\ell} - h^2_{\boldsymbol{k},n-\ell}) + (j^2_{\boldsymbol{k},n+\ell} - j^2_{\boldsymbol{k},n-\ell})] \\ +2\sum_{ijkp}\epsilon_{\gamma ij}\epsilon_{jkp}k_{\nu'}\hat{\gamma}^i_{\boldsymbol{k}}\hat{\gamma}^k_{\boldsymbol{k}}\hat{\gamma}^{\mu'}_{\boldsymbol{k}}(\epsilon_{\alpha p\rho}\epsilon_{\rho\mu'\beta} + \delta_{\mu'\beta}\delta_{\alpha p}) \\ \times h_{\boldsymbol{k},n}j_{\boldsymbol{k},n}(j^2_{\boldsymbol{k},n+\ell} - j^2_{\boldsymbol{k},n-\ell})\end{bmatrix} \\ +4\sum_{ijk}\gamma^{\mu'}_{\boldsymbol{q}}\hat{\gamma}^i_{\boldsymbol{k}}\hat{\gamma}^k_{\boldsymbol{k}}\epsilon_{jk\nu'}\begin{bmatrix}\epsilon_{\mu' ij}(\epsilon_{\alpha\gamma\rho}\epsilon_{\rho\nu'\beta} + \delta_{\nu'\beta}\delta_{\alpha\gamma}) \\ -\epsilon_{\gamma ij}(\epsilon_{\alpha\nu'\rho}\epsilon_{\rho\mu'\beta} + \delta_{\mu'\beta}\delta_{\alpha\nu'})\end{bmatrix} \\ \times h^2_{\boldsymbol{k},n}(j^2_{\boldsymbol{k},n+\ell} - j^2_{\boldsymbol{k},n-\ell})\end{array}\right\}, \tag{F.7}$$

where we should keep in mind that $\chi^{\mu\nu}_{js}(\boldsymbol{q}, i\Omega_\ell, \boldsymbol{M}) = \chi^{\nu\mu}_{sj}(-\boldsymbol{q}, -i\Omega_\ell, \boldsymbol{M})$ holds.

To carry out the $\boldsymbol{k}$-integral, we choose the z axis along the Rashba field, i.e., $\boldsymbol{\alpha}_{\mathrm{R}} = \alpha_{\mathrm{R}}\hat{\boldsymbol{z}}$ ($\hat{\boldsymbol{z}} \equiv (0,0,1)$) and $\boldsymbol{k}$ is represented using the polar and azimuthal angles θ and φ, respectively. We consider an electromagnetic wave with $q_z = 0$, i.e., propagation perpendicular to the Rashba field. Let us calculate Eq. (F.5). Calculating the integral over φ by use of

$$\int_0^{2\pi}\frac{\mathrm{d}\varphi}{2\pi}k_\mu\hat{\gamma}^\nu_{\boldsymbol{k}} = -\frac{\gamma_{\boldsymbol{k}}}{2\alpha_{\mathrm{R}}}\epsilon_{\mu\nu l}\hat{\alpha}_{\mathrm{R},l}, \tag{F.8}$$

where $\hat{\boldsymbol{\alpha}}_{\mathrm{R}} \equiv \boldsymbol{\alpha}_{\mathrm{R}}/|\boldsymbol{\alpha}_{\mathrm{R}}|$, we obtain

$$\chi^{\mu\nu}_{jj}(\boldsymbol{q}, i\Omega_\ell, \boldsymbol{M}) = -\frac{J_{sd}}{\beta}\left(\frac{e}{m}\right)^2\sum_{n,\boldsymbol{k}}\left(-\frac{\gamma_{\boldsymbol{k}}}{2\alpha^2_{\mathrm{R}}}\right)\phi^{(0)}_{\boldsymbol{k},n}(i\Omega_\ell)(\mathcal{A}_{\mathrm{R},\mu}q_\nu + q_\mu\mathcal{A}_{\mathrm{R},\nu}), \tag{F.9}$$

with

$$\phi^{(0)}_{\boldsymbol{k},n}(i\Omega_\ell) \equiv 2h_{\boldsymbol{k},n}j_{\boldsymbol{k},n}(h_{\boldsymbol{k},n+\ell} - h_{\boldsymbol{k},n-\ell}) + (h^2_{\boldsymbol{k},n} + j^2_{\boldsymbol{k},n})(j_{\boldsymbol{k},n+\ell} - j_{\boldsymbol{k},n-\ell}). \tag{F.10}$$

Here, $\boldsymbol{\mathcal{A}}_{\rm R} \equiv \boldsymbol{\alpha}_{\rm R} \times \boldsymbol{M}$. Other correlation functions are calculated similarly as

$$\begin{aligned}
\chi_{sj}^{\mu\nu}(\boldsymbol{q}, i\Omega_\ell, \boldsymbol{M}) &= -\frac{J_{sd}}{\beta}\left(\frac{e}{m}\right)^2 \sum_{n,\boldsymbol{k}} \\
&\quad \times \begin{Bmatrix} -\frac{\gamma_{\boldsymbol{k}}^2}{2\alpha_{\rm R}^2}\phi_{\boldsymbol{k},n}^{(1)}(i\Omega_\ell)[2(\boldsymbol{\mathcal{A}}_{\rm R}\cdot\boldsymbol{q})\delta_{\mu\nu}^{\perp} - 3\mathcal{A}_{{\rm R},\mu}q_\nu + M_\mu^{\perp}(\boldsymbol{\alpha}_{\rm R}\times\boldsymbol{q})_\nu] \\ +2m\alpha_{\rm R}\gamma_{\boldsymbol{k}}\phi_{\boldsymbol{k},n}^{(2)}(i\Omega_\ell)(\mathcal{A}_{{\rm R},\mu}q_\nu - q_\mu\mathcal{A}_{{\rm R},\nu}) - m\phi_{\boldsymbol{k},n}^{(3)}(i\Omega_\ell)\mathcal{A}_{{\rm R},\mu}q_\nu \end{Bmatrix}, \\
\chi_{ss}^{\mu\nu}(\boldsymbol{q}, i\Omega_\ell, \boldsymbol{M}) &= -\frac{J_{sd}}{\beta}\left(\frac{e}{m}\right)^2 \sum_{n,\boldsymbol{k}} (-2m\gamma_{\boldsymbol{k}}) \\
&\quad \times \begin{Bmatrix} \phi_{\boldsymbol{k},n}^{(4)}(i\Omega_\ell)(\boldsymbol{\mathcal{A}}_{\rm R}\cdot\boldsymbol{q})\delta_{\mu\nu}^{\perp} \\ +\phi_{\boldsymbol{k},n}^{(5)}(i\Omega_\ell)[2(\boldsymbol{\mathcal{A}}_{\rm R}\cdot\boldsymbol{q})\delta_{\mu\nu}^{\perp} - (\mathcal{A}_{{\rm R},\mu}q_\nu + q_\mu\mathcal{A}_{{\rm R},\nu})] \end{Bmatrix},
\end{aligned} \tag{F.11}$$

with

$$\begin{aligned}
\phi_{\boldsymbol{k},n}^{(1)}(i\Omega_\ell) &\equiv j_{\boldsymbol{k},n}^2(h_{\boldsymbol{k},n+\ell}^2 - h_{\boldsymbol{k},n-\ell}^2), \\
\phi_{\boldsymbol{k},n}^{(2)}(i\Omega_\ell) &\equiv h_{\boldsymbol{k},n}j_{\boldsymbol{k},n}[(h_{\boldsymbol{k},n+\ell}^2 - h_{\boldsymbol{k},n-\ell}^2) - (j_{\boldsymbol{k},n+\ell}^2 - j_{\boldsymbol{k},n-\ell}^2)], \\
\phi_{\boldsymbol{k},n}^{(3)}(i\Omega_\ell) &\equiv h_{\boldsymbol{k},n}^2(h_{\boldsymbol{k},n+\ell} - h_{\boldsymbol{k},n-\ell}) + h_{\boldsymbol{k},n}j_{\boldsymbol{k},n}(j_{\boldsymbol{k},n+\ell} - j_{\boldsymbol{k},n-\ell}), \\
\phi_{\boldsymbol{k},n}^{(4)}(i\Omega_\ell) &\equiv h_{\boldsymbol{k},n}j_{\boldsymbol{k},n}(j_{\boldsymbol{k},n+\ell}^2 - j_{\boldsymbol{k},n-\ell}^2), \\
\phi_{\boldsymbol{k},n}^{(5)}(i\Omega_\ell) &\equiv h_{\boldsymbol{k},n}j_{\boldsymbol{k},n}(h_{\boldsymbol{k},n+\ell}^2 - h_{\boldsymbol{k},n-\ell}^2),
\end{aligned} \tag{F.12}$$

where $\delta_{\mu\nu}^{\perp} \equiv \delta_{\mu\nu} - \hat{\alpha}_{{\rm R},\mu}\hat{\alpha}_{{\rm R},\nu}$ and $\boldsymbol{M}^{\perp} \equiv \boldsymbol{M} - (\hat{\boldsymbol{\alpha}}_{\rm R}\cdot\boldsymbol{M})\hat{\boldsymbol{\alpha}}_{\rm R}$.

The results of Eq. (F.9) and Eq. (F.11) are summarized in Eq. (2.30). The coefficients g_1, g_2, and g_3 are defined in Appendix G.

Appendix G

Definition of coefficients g_1, g_2, and g_3

From (F.9) and (F.11), coefficients g_1, g_2, and g_3 of Eq. (2.30) are obtained as

$$
\begin{aligned}
g_1(i\Omega_\ell) &\equiv -\frac{J_{sd}}{\beta}\left(\frac{e}{m}\right)^2 \sum_{n,\boldsymbol{k}} \left(-\frac{2\gamma_{\boldsymbol{k}}^2}{\alpha_{\mathrm{R}}^2}\right)\left[\phi_{\boldsymbol{k},n}^{(1)}(i\Omega_\ell) + \frac{m\alpha_{\mathrm{R}}^2}{\gamma_{\boldsymbol{k}}}(\phi_{\boldsymbol{k},n}^{(4)}(i\Omega_\ell) + 2\phi_{\boldsymbol{k},n}^{(5)}(i\Omega_\ell))\right], \\
g_2(i\Omega_\ell) &\equiv -\frac{J_{sd}}{\beta}\left(\frac{e}{m}\right)^2 \sum_{n,\boldsymbol{k}} \frac{\gamma_{\boldsymbol{k}}^2}{2\alpha_{\mathrm{R}}^2}\left[-\frac{1}{\gamma_{\boldsymbol{k}}}\phi_{\boldsymbol{k},n}^{(0)}(i\Omega_\ell) + 3\phi_{\boldsymbol{k},n}^{(1)}(i\Omega_\ell) - \frac{2m\alpha_{\mathrm{R}}^2}{\gamma_{\boldsymbol{k}}^2}\phi_{\boldsymbol{k},n}^{(3)}(i\Omega_\ell)\right. \\
&\quad \left. + \frac{4m\alpha_{\mathrm{R}}^2}{\gamma_{\boldsymbol{k}}}\phi_{\boldsymbol{k},n}^{(5)}(i\Omega_\ell)\right], \\
g_3(i\Omega_\ell) &\equiv -\frac{J_{sd}}{\beta}\left(\frac{e}{m}\right)^2 \sum_{n,\boldsymbol{k}} \left(-\frac{\gamma_{\boldsymbol{k}}^2}{2\alpha_{\mathrm{R}}^2}\right)\phi_{\boldsymbol{k},n}^{(1)}(i\Omega_\ell).
\end{aligned} \tag{G.1}
$$

Using Eqs. (F.2), (F.6) and Eq. (F.12), the coefficients g_1 and g_3 can be written as

$$
\begin{aligned}
g_1(i\Omega_\ell) &= -2\frac{J_{sd}}{2^4}\left(\frac{e}{m}\right)^2 \sum_{\boldsymbol{k}} \sum_{\sigma_1\sigma_2\sigma_3\sigma_4} \left(\frac{\gamma_{\boldsymbol{k}}}{\alpha_{\mathrm{R}}}\right)^2 \left[\sigma_1\sigma_2 + \frac{m\alpha_{\mathrm{R}}^2}{\gamma_{\boldsymbol{k}}}(\sigma_2\sigma_3\sigma_4 + 2\sigma_2)\right] \\
&\quad \times \left(-\frac{1}{\beta}\right) \sum_n \mathrm{g}_{\boldsymbol{k},n,\sigma_1}\mathrm{g}_{\boldsymbol{k},n,\sigma_2}(\mathrm{g}_{\boldsymbol{k},n+\ell,\sigma_3}\mathrm{g}_{\boldsymbol{k},n+\ell,\sigma_4} - \mathrm{g}_{\boldsymbol{k},n-\ell,\sigma_3}\mathrm{g}_{\boldsymbol{k},n-\ell,\sigma_4}), \\
g_3(i\Omega_\ell) &= -\frac{1}{2}\frac{J_{sd}}{2^4}\left(\frac{e}{m}\right)^2 \sum_{\boldsymbol{k}} \sum_{\sigma_1\sigma_2\sigma_3\sigma_4} \sigma_1\sigma_2 \left(\frac{\gamma_{\boldsymbol{k}}}{\alpha_{\mathrm{R}}}\right)^2 \\
&\quad \times \left(-\frac{1}{\beta}\right) \sum_n \mathrm{g}_{\boldsymbol{k},n,\sigma_1}\mathrm{g}_{\boldsymbol{k},n,\sigma_2}(\mathrm{g}_{\boldsymbol{k},n+\ell,\sigma_3}\mathrm{g}_{\boldsymbol{k},n+\ell,\sigma_4} - \mathrm{g}_{\boldsymbol{k},n-\ell,\sigma_3}\mathrm{g}_{\boldsymbol{k},n-\ell,\sigma_4}).
\end{aligned} \tag{G.2}
$$

Appendix H

Gauge transformation

Under the gauge transformation $A_\mu(\boldsymbol{q}) \to A_\mu(\boldsymbol{q}) + iq_\mu\Lambda(\boldsymbol{q})$, where $\Lambda(\boldsymbol{q})$ is the gauge degree of freedom, the change in the effective Hamiltonian linear in Λ is given by

$$\delta H_{\text{eff}} = -i\sum_{\boldsymbol{q}} \Lambda(\boldsymbol{q}) \times \begin{bmatrix} g_1(\boldsymbol{\mathcal{A}}_{\text{R}}\cdot\boldsymbol{q})[\boldsymbol{q}\cdot\boldsymbol{A}(-\boldsymbol{q}) - \boldsymbol{q}\cdot\boldsymbol{A}(-\boldsymbol{q})] \\ +g_2\begin{bmatrix}(\boldsymbol{\mathcal{A}}_{\text{R}}\cdot\boldsymbol{A}(-\boldsymbol{q}))\boldsymbol{q}^2 + (\boldsymbol{q}\cdot\boldsymbol{A}(-\boldsymbol{q}))(\boldsymbol{\mathcal{A}}_{\text{R}}\cdot\boldsymbol{q}) \\ -(\boldsymbol{\mathcal{A}}_{\text{R}}\cdot\boldsymbol{q})(\boldsymbol{q}\cdot\boldsymbol{A}(-\boldsymbol{q})) - (\boldsymbol{\mathcal{A}}_{\text{R}}\cdot\boldsymbol{A}(-\boldsymbol{q}))\boldsymbol{q}^2\end{bmatrix} \\ +g_3[\boldsymbol{A}(-\boldsymbol{q})\cdot(\boldsymbol{\alpha}_{\text{R}}\times\boldsymbol{q})(\boldsymbol{M}^\perp\cdot\boldsymbol{q}) - (\boldsymbol{M}^\perp\cdot\boldsymbol{q})\boldsymbol{A}(-\boldsymbol{q})\cdot(\boldsymbol{\alpha}_{\text{R}}\times\boldsymbol{q})] \end{bmatrix}. \quad \text{(H.1)}$$

Appendix I

Derivation of Eqs. (3.19), (3.20), and (3.21)

This section shows the detailed derivation of Eqs. (3.19), (3.20), and (3.21) from Eq. (3.17) as a same manner in Appendix F. By use of Eq. (F.4) and

$$\mathrm{tr}[\sigma_\alpha\sigma_i\sigma_\beta\sigma_j\sigma_\gamma] = 2i(\delta_{\alpha i}\epsilon_{\beta j\gamma} + \delta_{j\gamma}\epsilon_{\alpha i\beta} + \delta_{\beta j}\epsilon_{\alpha i\gamma} - \delta_{\beta\gamma}\epsilon_{\alpha ij}), \tag{I.1}$$

the result up to the linear order in $\boldsymbol{q}$ thus reads

$$\begin{aligned}\chi^{\mu\nu}_{jj}(\boldsymbol{q}, i\Omega_\ell) \simeq \chi^{\mu\nu}_{jj}(\boldsymbol{q}=0, i\Omega_\ell) - \frac{(-i)e^2\lambda^2}{\beta V}\sum_{n,\boldsymbol{k}}\sum_{\rho} \\ \times\left\{\begin{array}{c} -\sum_i \frac{1}{\lambda m}\gamma^\rho_{\boldsymbol{q}}\hat{\gamma}^i_{\boldsymbol{k}}(\epsilon_{\mu i\rho}k_\nu - k_\mu\epsilon_{\nu i\rho})(h^2_{\boldsymbol{k},n} - j^2_{\boldsymbol{k},n})(j_{\boldsymbol{k},n+\ell} + j_{\boldsymbol{k},n-\ell}) \\ -\frac{k_\rho q_\rho}{m}\sum_i \hat{\gamma}^i_{\boldsymbol{k}}\epsilon_{\mu\nu i}(h^2_{\boldsymbol{k},n} + j^2_{\boldsymbol{k},n})(j_{\boldsymbol{k},n+\ell} + j_{\boldsymbol{k},n-\ell}) \\ +\gamma^\rho_{\boldsymbol{q}}\left[\begin{array}{c}\epsilon_{\mu\nu\rho}(h^2_{\boldsymbol{k},n} + j^2_{\boldsymbol{k},n})(h_{\boldsymbol{k},n+\ell} + h_{\boldsymbol{k},n-\ell}) \\ +2j^2_{\boldsymbol{k},n}\sum_{mn'op}\epsilon_{\rho mn'}\epsilon_{n'op}\epsilon_{\mu\nu\rho}\hat{\gamma}^m_{\boldsymbol{k}}\hat{\gamma}^o_{\boldsymbol{k}}(h_{\boldsymbol{k},n+\ell} + h_{\boldsymbol{k},n-\ell}) \\ +2\sum_i \hat{\gamma}^i_{\boldsymbol{k}}\hat{\gamma}^\rho_{\boldsymbol{k}}\epsilon_{\mu i\nu}h_{\boldsymbol{k},n}j_{\boldsymbol{k},n}(j_{\boldsymbol{k},n+\ell} + j_{\boldsymbol{k},n-\ell})\end{array}\right]\end{array}\right\},\end{aligned} \tag{I.2}$$

where $\hat{\boldsymbol{\gamma}}_{\boldsymbol{k}} \equiv \boldsymbol{\gamma}_{\boldsymbol{k}}/|\boldsymbol{\gamma}_{\boldsymbol{k}}|$, $\boldsymbol{\gamma}_{\boldsymbol{q}} \equiv -\lambda\boldsymbol{q}$, and $h_{\boldsymbol{k},n}$ and $j_{\boldsymbol{k},n}$ are defined as

$$\begin{aligned} h_{\boldsymbol{k},n} &\equiv \frac{1}{2}\sum_{\sigma=\pm}\mathrm{g}_{\boldsymbol{k},n,\sigma}, \\ j_{\boldsymbol{k},n} &\equiv \frac{1}{2}\sum_{\sigma=\pm}\sigma\mathrm{g}_{\boldsymbol{k},n,\sigma}, \end{aligned} \tag{I.3}$$

where $\sigma = \pm$ is the diagonalized spin index. Using a rotational symmetry in k-space, i.e., $k_\mu k_\nu = \frac{\boldsymbol{k}^2}{3}\delta_{\mu\nu}$ and Eq. (I.3), the result of Eq. (I.2) is summarized in Eqs. (3.19), (3.20), and (3.21).

References

[1] J. D. Jackson, *Classical Electrodynamics*, 3rd ed. (Wiley, New York, 1998).

[2] G. Tatara, H. Kohno, and J. Shibata, Phys. Rep. **468**, 213 (2008).

[3] J. C. Slonczewski, J. Magn. Magn. Mater. **159**, L1 (1996).

[4] L. Berger, Phys. Rev. B **54**, 9353 (1996).

[5] L. Berger, Phys. Rev. B **33**, 1572 (1986).

[6] E. I. Rashba, Sov. Phys. Solid State **2**, 1109 (1960).

[7] K. Obata and G. Tatara, Phys. Rev. B **77**, 214429 (2008).

[8] A. Manchon and S. Zhang, Phys. Rev. B **78**, 212405 (2008).

[9] I. M. Miron, G. Gaudin, S. Auffret, B. Rodmacq, A. Schuhl, S. Pizzini, J. Vogel, and P. Gambardella, Nat. Mater. **9**, 230 (2010).

[10] G. Tatara, *Proceedings of Symmetry and Structural Properties of Condensed Matter (SSPCM) 2016* (see also arXiv:1612.09019) .

[11] G. Tatara, H. Saarikoski, and C. Mitsumata, Appl. Phys. Express **9**, 103002 (2016).

[12] K. Taguchi and G. Tatara, J. Phys. Conf. Series **400**, 042055 (2012).

[13] A. Qaiumzadeh and M. Titov, Phys. Rev. B **94**, 014425 (2016).

[14] J. J. Sakurai, *Advanced Quantum Mechanics* (Addison Wesley, 1967).

[15] C. R. Ast, J. Henk, A. Ernst, L. Moreschini, M. C. Falub, D. Pacilé, P. Bruno, K. Kern, and M. Grioni, Phys. Rev. Lett. **98**, 186807 (2007).

[16] K. Ishizaka, M. S. Bahramy, H. Murakawa, M. Sakano, T. Shimojima, T. Sonobe, K. Koizumi, S. Shin, H. Miyahara, A. Kimura, K. Miyamoto, T. Okuda, H. Namatame, M. Taniguchi, R. Arita, N. Nagaosa, K. Kobayashi, Y. Murakami, R. Kumai, Y. Kaneko, Y. Onose, and Y. Tokura, Nat. Mater. **10**, 521 (2011).

[17] V. M. Edelstein, Solid State Commun. **73**, 233 (1990).

[18] J. Puebla, F. Auvray, M. Xu, B. Rana, A. Albouy, H. Tsai, K. Kondou, G. Tatara, and Y. Otani, Appl. Phys. Lett. **111**, 092402 (2017).

[19] K. Shen, G. Vignale, and R. Raimondi, Phys. Rev. Lett. **112**, 096601 (2014).

[20] J. C. R. Sánchez, L. Vila, G. Desfonds, S. Gambarelli, J. P. Attané, J. M. De Teresa, C. Magén, and A. Fert, Nat Commun **4**, 2944 (2013).

[21] J. Shibata, A. Takeuchi, H. Kohno, and G. Tatara, J. Phys. Soc. Jpn. **85**, 033701 (2016).

[22] J. Shibata, A. Takeuchi, H. Kohno, and G. Tatara, arXiv:1709.03689.

[23] E. E. Narimanov and A. V. Kildishev, Nat Photon **9**, 214 (2015).

[24] J. S. Lee, G. A. H. Schober, M. S. Bahramy, H. Murakawa, Y. Onose, R. Arita, N. Nagaosa, and Y. Tokura, Phys. Rev. Lett. **107**, 117401 (2011).

[25] L. Demkó, G. A. H. Schober, V. Kocsis, M. S. Bahramy, H. Murakawa, J. S. Lee, I. Kézsmárki, R. Arita, N. Nagaosa, and Y. Tokura, Phys. Rev. Lett. **109**, 167401 (2012).

[26] K.-W. Kim, J.-H. Moon, K.-J. Lee, and H.-W. Lee, Phys. Rev. Lett. **108**, 217202 (2012).

[27] N. Nakabayashi and G. Tatara, New J. Phys. **16**, 015016 (2014).

[28] A. Takeuchi and G. Tatara, J. Phys. Soc. Jpn. **81**, 033705 (2012).

[29] S. Hayami, H. Kusunose, and Y. Motome, Phys. Rev. B **90**, 024432 (2014).

[30] K. Sawada and N. Nagaosa, Phys. Rev. Lett. **95**, 237402 (2005).

[31] H. Kawaguchi and G. Tatara, Phys. Rev. B **94**, 235148 (2016).

[32] G. Tatara and N. Nakabayashi, J. Appl. Phys. **115**, 172609 (2014).

[33] J. J. Sakurai, *Modern Quantum Mechanics*, Revised ed. (Addison Wesley, Reading, MA, 1993) p. 61.

[34] G. Tatara, N. Nakabayashi, and K.-J. Lee, Phys. Rev. B **87**, 054403 (2013).

[35] D. Xiao, M.-C. Chang, and Q. Niu, Rev. Mod. Phys. **82**, 1959 (2010).

[36] G. E. Volovik, J. Phys. C: Solid State Phys. **20**, L83 (1987).

[37] M. Lee, W. Kang, Y. Onose, Y. Tokura, and N. P. Ong, Phys. Rev. Lett. **102**, 186601 (2009).

[38] N. Nagaosa, J. Shinava, S. Onoda, A. H. Macdonald, and N. P. Ong, Rev. Mod. Phys. **82**, 1539 (2010).

[39] K. Nakazawa and H. Kohno, J. Phys. Soc. Jpn. **83**, 073707 (2014).

[40] K. Nakazawa, M. Bibes, and H. Kohno, arXiv:1711.08366v1.

[41] S. A. Yang, G. S. D. Beach, C. Knutson, D. Xiao, Q. Niu, M. Tsoi, and J. L. Erskine, Phys. Rev. Lett. **102**, 067201 (2009).

[42] K. Tanabe, D. Chiba, J. Ohe, S. Kasai, H. Kohno, S. E. Barnes, S. Maekawa, K. Kobayashi, and T. Ono, Nat. Commun **3**, 845 (2012).

[43] T. Schulz, R. Ritz, A. Bauer, M. Halder, M. Wagner, C. Franz, C. Pfleiderer, K. Everschor, M. Garst, and A. Rosch, Nat. Phys. **8**, 301 (2012).

[44] Y. B. Bazaliy, B. A. Jones, and S.-C. Zhang, Phys. Rev. B **57**, R3213 (1998).

[45] G. Tatara and S. Mizukami, Phys. Rev. B **96**, 064423 (2017).

[46] G. Tatara, A. Takeuchi, N. Nakabayashi, and K. Taguchi, J. Korean Phys. Soc. **61**, 1331 (2012).

[47] A. Stern, Phys. Rev. Lett. **68**, 1022 (1992).

[48] S. E. Barnes and S. Maekawa, Phys. Rev. Lett. **98**, 246601 (2007).

[49] S. A. Yang, G. S. D. Beach, C. Knutson, D. Xiao, Z. Zhang, M. Tsoi, Q. Niu, A. H. MacDonald, and J. L. Erskine, Phys. Rev. B **82**, 054410 (2010).

[50] H. Kawaguchi and G. Tatara, J. Phys. Soc. Jpn. **83**, 074710 (2014).

[51] H. Kohno, S. Kawabata, T. Noguchi, S. Ueta, J. Shibata, and G. Tatara, in *Proceedings of ISQM-Tokyo '08*, pp.111-117, Eds. S. Ishioka and K. Fujikawa, (World Scientific, Singapore, 2009) (see also arXiv:0912.1676) .

[52] V. Vlaminck and M. Bailleul, Science **322**, 410 (2008).

[53] Y. Yamane, J. Ieda, and J. Sinova, Phys. Rev. B **94**, 054409 (2016).

[54] K. Taguchi, J.-I. Ohe, and G. Tatara, Phys. Rev. Lett. **109**, 127204 (2012).

[55] R. A. Duine, Phys. Rev. B **77**, 014409 (2008).

[56] M. E. Lucassen, G. C. F. L. Kruis, R. Lavrijsen, H. J. M. Swagten, B. Koopmans, and R. A. Duine, Phys. Rev. B **84**, 014414 (2011).

[57] J. Shibata and H. Kohno, Phys. Rev. Lett. **102**, 086603 (2009).

[58] J. Shibata and H. Kohno, Phys. Rev. B **84**, 184408 (2011).

[59] E. Saitoh, M. Ueda, H. Miyajima, and G. Tatara, Appl. Phys. Lett. **88**, 182509 (2006).

[60] Y. Tserkovnyak, A. Brataas, and G. E. W. Bauer, Phys. Rev. Lett. **88**, 117601 (2002).

[61] L. D. Landau and E. M. Lifshitz, *Electrodynamics of Continuous Media*, 2nd ed. (Pergamon, Oxford, 1984).

[62] E. U. Condon, Rev. Mod. Phys. **9**, 432 (1937).

[63] H. Nakano and H. Kimura, J. Phys. Soc. Jpn. **27**, 519 (1969).

[64] K. V. Samokhin, Phys. Rev. B **76**, 094516 (2007).

[65] V. P. Mineev and Yu. Yoshioka, Phys. Rev. B **81**, 094525 (2010).

[66] V. P. Mineev, Phys. Rev. B **88**, 134514 (2013).

[67] J. Ma and D. A. Pesin, Phys. Rev. B **92**, 235205 (2015).

[68] T. Yoda, T. Yokoyama, and S. Murakami, Sci. Rep. **5**, 12024 (2015).

[69] L. Barron, Chem. Phys. Lett. **123**, 423 (1986).

[70] A. A. Zyuzin and A. A. Burkov, Phys. Rev. B **86**, 115133 (2012).

[71] P. Goswami and S. Tewari, Phys. Rev. B **88**, 245107 (2013).

[72] M. M. Vazifeh and M. Franz, Phys. Rev. Lett. **111**, 027201 (2013).

[73] N. A. Spaldin, M. Fiebig, and M. Mostovoy, J. Phys.: Condens. Matter **20**, 434203 (2008).

[74] H. Kawaguchi and G. Tatara, submittied to J. Phys. Soc. Jpn (see also arXiv:1801.10329).

[75] L. D. Landau and E. M. Lifshitz, *The Classical Theory of Fields*, 2nd ed. (Pergamon, Oxford, 1971).

[76] X.-L. Qi, T. L. Hughes, and S.-C. Zhang, Phys. Rev. B **78**, 195424 (2008).

[77] X.-L. Qi and S.-C. Zhang, Rev. Mod. Phys. **83**, 1057 (2011).

[78] U. Leonhardt and P. Piwnicki, Phys. Rev. A **60**, 4301 (1999).

[79] N. T. Phuc, G. Tatara, Y. Kawaguchi, and M. Ueda, Nat Commun **6**, 8135 (2015).

[80] I. Dzyaloshinsky, J. Phys. Chem. Solids **4**, 241 (1958).

[81] T. Moriya, Phys. Rev. **120**, 91 (1960).

[82] T. Kikuchi, T. Koretsune, R. Arita, and G. Tatara, Phys. Rev. Lett. **116**, 247201 (2016).

[83] S. Seki, Y. Okamura, K. Kondou, K. Shibata, M. Kubota, R. Takagi, F. Kagawa, M. Kawasaki, G. Tatara, Y. Otani, and Y. Tokura, Phys. Rev. B **93**, 235131 (2016).

[84] N. B. Baranova, Yu. V. Bogdanov, and B. Ya. Zei'dovich, Sov. Phys. Usp. **20**, 870 (1977).

[85] C. Train, R. Gheorghe, V. Krstic, L.-M. Chamoreau, N. S. Ovanesyan, G. L. J. A. Rikken, M. Gruselle, and M. Verdaguer, Nat Mater **7**, 729 (2008).

[86] B. Sakita, *Quantum theory of many-variable systems and fields* (World Scientific, Singapore, 1985).

[87] A. A. Abrikosov, L. P. Gorkov, and I. E. Dzialoshinskii, *Methods of Quantum Field Theory in Statistical Physics* (Dover, New York, 1975).

[88] A. Altland and B. Simons, *Condensed Matter Field Theory*, 2nd ed. (Cambridge University Press, New York, 2006).

[89] A. A. Burkov and L. Balents, Phys. Rev. Lett. **107**, 127205 (2011).

[90] K. Taguchi, T. Imaeda, M. Sato, and Y. Tanaka, Phys. Rev. B **93**, 201202(R) (2016).

[91] K. Fujikawa and H. Suzuki, *Path Integrals and Quantum Anomalies* (Oxford University Press, Oxford, 2004).

[92] M. Kargarian, M. Randeria, and N. Trivedi, Sci. Rep. **5**, 12683 (2015).

[93] Adolfo G. Grushin, Phys. Rev. D **86**, 045001 (2012).

[94] D. M. Lipkin, J. Math. Phys. **5**, 696 (1964).

[95] I. Proskurin, A. S. Ovchinnikov, P. Nosov, and J. i. Kishine, New J. Phys. **19**, 063021 (2017).

[96] Y. Tang and A. E. Cohen, Phys. Rev. Lett. **104**, 163901 (2010).

[97] K. Y. Bliokh and F. Nori, Phys. Rev. A **83**, 021803(R) (2011).

[98] K. Y. Bliokh and F. Nori, Phys. Rep. **592**, 1 (2015).

[99] A. O. Caldeira and A. J. Leggett, Phys. Rev. Lett. **46**, 211 (1981).

[100] H. Haug and A. P. Jauho, *Quantum Kinetics in Transport and Optics of Semi-conductors* (Springer-Verlag, 1998).

[101] R. Kubo, J. Phys. Soc. Jpn. **12**, 570 (1957).

[102] D. C. Langreth, in *NATO Advanced Study Institute Series* B**17**, pp.3-32, Eds. J. T. Devreese and E. van Doren, (Plenum, NewYork/London, 1976) .

Acknowledgments

First of all, I would like to thank Dr. G. Tatara for his invaluable supports, continuous guidance, and stimulating discussions through the difficult times of the corse of my study. I am also indebted to my supervisor, Prof. H. Mori, for his various supports in Tokyo metropolitan university.

In Chapter 2, I am deeply grateful to Prof. J. Shibata, Prof. H. Kohno, Prof. S. Murakami, Dr. S. Seki, Dr. A. Takeuchi, Dr. T. Kikuchi, Dr. A. Shitade, and Dr. K. Taguchi for helpful discussions and comments. In Chapter 3, I am also grateful to Dr. A. Shitade, Assoc. Prof. J.-i. Ohe, and Prof. J. i. Kishine for fruitful comments. I would like to thank Prof. H. Fukuyama, Mr. K. Yokoyama, Dr. H. T. Ueda, Dr. Y. Hashizume, and Dr. D. Ootsuki, who clearly gave answers to my stupid questions.

I was financially supported by RIKEN Junior Associate Program. I would like to appreciate all the former and present members of the condensed matter theory group in TMU and the spin physics theory research team in RIKEN for presenting the grateful workplace. I want to express to all my friends for their helpful communications. Especially, I would like to offer my special thanks to Mr. K. Yoshida, Mr. T. Agatsuma, and Mr. K. Nakazawa for giving an enjoyable time to my study life. Finally, special thanks to my family for their supports and encouragements. I dedicate my thesis to them.

List of Publications

Refereed papers

- **Hideo Kawaguchi** and Gen Tatara, "*Effective Hamiltonian approach to optical activity in Weyl spin-orbit system*", submitted to Journal of the Physical Society of Japan (see also arXiv:1801.10329).
- **Hideo Kawaguchi** and Gen Tatara, "*Effective Hamiltonian theory for nonreciprocal light propagation in magnetic Rashba conductor*", Physical Review B, **94**, 235148 (2016).
- **Hideo Kawaguchi** and Gen Tatara, "*Coupling Theory of Emergent Spin Electromagnetic Field and Electromagnetic Field*", Journal of the Physical Society of Japan, **83**, 074710 (2014).

List of Presentations

International Conferences (Poster)

- **Hideo Kawaguchi** and Gen Tatara, "*Effective Hamiltonian approach to optical chirality and optical activity induced by Weyl spin-orbit interaction*", American Physics of Science March Meeting, G60, Los Angeles, CA, USA (March 2018).
- **Hideo Kawaguchi** and Gen Tatara, "*Effective Hamiltonian approach to optical chirality in Weyl spin-orbit system*", SpinTECK IX, International school and conference 2017, B-100, Fukuoka, Japan (June 2017).
- **Hideo Kawaguchi** and Gen Tatara, "*Effective Hamiltonian theory for electromagnetic cross-correlation effect in spin-orbit systems*", Status Meeting on Nano Spin conversion 2017, PF-11, Tokyo, Japan (March 2017).
- **Hideo Kawaguchi** and Gen Tatara, "*Effective Hamiltonian theory for nonreciprocal light propagation in magnetic Rashba conductor*", International workshop on nano-spin conversion science & quantum spin dynamics, N-26, Tokyo, Japan (October 2016).
- **Hideo Kawaguchi** and Gen Tatara, "*Effective Hamiltonian approach to nonreciprocal directional dichroism in magnetic Rashba conductor*", 9th International Conference on Physics and Applications of Spin-Related Phenomena in Solid, P2-19, Kobe, Japan (August 2016).
- **Hideo Kawaguchi** and Gen Tatara, "*Coupling Theory of Emergent Spin Electromagnetic Field and Electromagnetic Field*", Asia-Pacific Workshop (APW)-CEMS Joint Workshop "Highlights of modern condensed matter physics", P25, Saitama, Japan (January 2016).
- **Hideo Kawaguchi** and Gen Tatara, "*Novel coupling between spin and electromagnetic field in a ferromagnetic metal with Rashba spin-orbit interaction*", New Perspectives in Spintronics and Mesoscopic Physics, P16, Kashiwa, Japan (June 2015).
- **Hideo Kawaguchi** and Gen Tatara, "*Coupling between spin electromagnetic field and electromagnetic wave*", FIRST-QS2Cl Workshop on "Emergent Phenomena of Correlated Materials", P51, Tokyo, Japan (November 2013).
- **Hideo Kawaguchi** and Gen Tatara, "*Coupling between spin electromagnetic field and electromagnetic wave*", RIKEN-ICCAS-IOP-PKU-

Tsinghua Joint on Symposium on Materials Science, Saitama, Japan (November 2013).

Domestic Conferences (Oral & Poster)

- 川口秀雄、多々良源、「有効ハミルトニアンの方法によるワイル型スピン軌道相互作用系の電磁応答現象の解析」、日本物理学会 (年次大会)、19pC24-1、大阪大学 (豊中キャンパス)、2017 年 3 月 (口頭)
- 川口秀雄、多々良源、「ラシュバ型スピン軌道相互作用系における特異な電磁特性 III」、日本物理学会 (秋季大会)、13pPSA-36、金沢大学 (角間キャンパス)、2016 年 9 月 (ポスター)
- 川口秀雄、多々良源、「ラシュバ型スピン軌道相互作用系における特異な電磁特性 II」、日本物理学会 (年次大会)、20pAU-7、東北学院大学 (泉キャンパス)、2016 年 3 月 (口頭)
- 川口秀雄、多々良源、「ラシュバ型スピン軌道相互作用系における特異な電磁特性」、日本物理学会 (秋季大会)、16pPSA-39、関西大学 (千里山キャンパス)、2015 年 9 月 (ポスター)
- 川口秀雄、多々良源、「ラシュバ型スピン軌道相互作用系の有効作用と磁化ダイナミクスの解析」、日本物理学会 (秋季大会)、7aBF-2、中部大学 (春日井キャンパス)、2014 年 9 月 (口頭)
- 川口秀雄、多々良源、「スピン電磁場と電磁波の結合理論 II」、日本物理学会 (年次大会)、28aAF-8、東海大学 (湘南キャンパス)、2014 年 3 月 (口頭)
- 川口秀雄、多々良源、「スピン電磁場と電磁波の結合理論」、日本物理学会 (秋季大会)、27pKF-11、徳島大学 (三島キャンパス)、2013 年 9 月 (口頭)